THE ROLE OF THE GRAM-NEGATIVE CELL ENVELOPE IN THE PATHOGENESIS AND TREATMENT OF PNEUMONIA

By

Christiaan Diederik Mathijs Wijers

Dissertation

Submitted to the Faculty of the

Graduate School of Vanderbilt University

In partial fulfillment of the requirements

For the degree of

DOCTOR OF PHILOSOPHY

In

Microbe-Host Interactions

May 31st, 20222

Nashville, Tennessee

Approved:

Maria Hadjifrangiskou, PhD

Eric Skaar, PhD, MPH

Stokes Peebles, MD

Brian Bachmann, PhD

Michael Noto, MD, PhD

DEDICATION

To my son Mathijs: may you always be inspired to imagine, discover, explore, and create.

ACKNOWLEDGEMENTS

First and foremost, I would like to express my gratitude to my thesis advisor, Dr. Michael Noto, for his wisdom, guidance, and support throughout my graduate school training. You have contributed tremendously to my development as an aspiring physician-scientist by teaching me how to ask the important questions, formulate hypotheses, and communicate my findings. Over the course of my time in the Noto laboratory, I have learned a great deal from you about scientific rigor and written communication in particular. I would like to thank you for helping me design carefully controlled experiments, approaching any given scientific problem from at least three separate angles, and for reading and critiquing countless pieces of writing. It has been a privilege and a pleasure working in your laboratory, and I sincerely hope that our mentor-mentee relationship continues well beyond my graduation from this program.

Next, I would like to thank my thesis committee: Dr. Maria Hadjifrangiskou, Dr. Stokes Peebles, Dr. Eric Skaar, and Dr. Brian Bachmann. I have learned a great deal from you all in terms of how to keep track of the bigger picture, and how to place the significance of my work in the context of what is already known. I would also like to thank you for continuing to encourage me to further my knowledge, and for not withholding the tough questions, for it is outside the borders of our comfort zone where we grow most profoundly. Lastly, I would like to thank you for making the transition of our laboratory to Emory University as smooth as possible. All of you reached out to me offering your support in terms of time and resources, and I would not have been able to complete this work without it. Similarly, I would like to thank Dr. Dawn Newcomb and the people of her laboratory for providing me with space and equipment to continue my work at Vanderbilt University, and for your company.

I would also like to thank my colleagues of the Noto laboratory, both current and former. Thank you, Dr. Ly Pham, for teaching me everything you know about cell culture techniques and for laying down part of the foundation of what has become my dissertation research. Thank you, Alex Eddie and Jeromy Dooyema, for your unyielding support of my work, and for taking care of much of the logistical

aspects of my research. You have saved me oceans of time, and for that I am grateful. Thank you, Dr. Padmini Komalavilas, for brightening my days with your smile and our conversations, and for inspiring me with your drive and intelligence. I have seldom come across someone with such talent and zest for laboratory science, and I will count my lucky stars should I be able to channel even a fraction of that throughout my future career.

Of course, none of this work could have been completed without the support of my loving family – the one I was born into as well as the one I built here in Nashville. Thank you to my dad for teaching me how to channel and celebrate one's curiosity, and for setting the best example of what it means to be a life-long learner; thank you to my mom for teaching me diligence and professionalism, and for taking care of a lot of bureaucracy on my behalf while I am an entire ocean away; and thank you to my sister, Fleur, for being a standout godmother to my son. Further, although I fear that words cannot express how truly grateful I am, I would like to thank my wife Alissa Cutrone: thank you for your emotional support, your proof-reading, and for putting up with me spending many nights and weekends in the laboratory. You are truly the most caring person I know, and you continue to make sure that I do not lose sight of the human sides of science and medicine. Additionally, I would like to thank my son, Mathijs, for being an inspiration and for making all of my worries melt away after a long day with a simple smile. Finally, I would like to thank the medical scientist training program at Vanderbilt University, both its leadership team and my colleagues, as well as my friends both near and far: you have been a tremendous source of support, and at times a much-needed distraction from academic life.

TABLE OF CONTENTS

LIST OF TABLES

LIST OF FIGURES

LIST OF ABBREVIATIONS

A. baumannii:	*Acinetobacter baumannii*
Ab 17978 UN:	*Acinetobacter baumannii* strain ATCC 17978 University of Nebraska variant
Ab 17978 VU:	*Acinetobacter baumannii* strain ATCC 17978 Vanderbilt University variant
AbaAL44:	*Acinetobacter baumannii* accessory locus 44 kb
AG:	aminoglycoside
ALI:	acute lung injury
ANOVA:	analysis of variance
ARDS:	acute respiratory distress syndrome
ATCC:	American type culture collection
BALF:	bronchoalveolar lavage fluid
BCA:	bicinchoninic acid
BMDM:	bone marrow-derived macrophage
CAP:	community-acquired pneumonia
CCCP:	Carbonyl cyanide m-chlorophenyl hydrazone
CDC:	centers for disease control and prevention
CF:	cystic fibrosis
CFU:	colony-forming unit
CL:	cardiolipin
cls:	cardiolipin synthase
DAMP:	damage-associated molecular pattern
DMEM:	Dulbecco's modified Eagle medium
E. coli:	*Escherichia coli*
ELISA:	enzyme-linked immunosorbent assay
EPIC III:	Extended Prevalence of Infection in Intensive Care III
EV:	empty vector
FBS:	fetal bovine serum
GlcNAc:	N-acetylglucosamine
Gm:	gentamicin
h.p.i.:	hours post-infection
H&E:	hematoxylin & eosin
HAP:	hospital-acquired pneumonia
HCAP:	healthcare-associated pneumonia
ICU:	intensive care unit
IDSA:	infectious disease society of America
IFNγ:	interferon gamma
IL:	interleukin
IM:	inner membrane
IPTG:	isopropyl β-d-1-thiogalactopyranoside
IS:	insertion sequence
K. pneumoniae:	*Klebsiella pneumoniae*
KC:	keratinocytes-derived chemokine
Km:	kanamycin
LB:	lysogeny broth
LBA:	LB agar
LC:	L929 cell conditioned
LC-MS:	liquid chromatography coupled with mass spectrometry
LC-MS/MS:	liquid chromatography coupled with tandem mass spectrometry
LOS:	lipo-oligosaccharide

LPS:	lipopolysaccharide
MDR:	multi-drug resistant
MFS:	major facilitator superfamily
MIC:	minimum inhibitory concentration
MIP-2:	macrophage inflammatory protein 2
Mla:	maintenance of lipid asymmetry
MOI:	multiplicity of infection
MRSA:	methicillin-resistant *Staphylococcus aureus*
MSSA:	methicillin-susceptible *Staphylococcus aureus*
MurNAc:	N-actylmuramic acid
NAO:	nonyl acridine orange
NF-κB:	Nuclear factor kappa B
NLRC4:	Nods-Like receptor family, CARD domain containing 4
NLRP3:	NLR family pyrin domain containing 3
NOD:	nucleotide-binding oligomerization domain-containing protein
OD_{600}:	optical density at 600 nm
OM:	outer membrane
OMP:	outer membrane protein
OMV:	outer membrane vesicle
P. aeruginosa:	*Pseudomonas aeruginosa*
P/S:	penicillin/streptomycin
PAMP:	pathogen-associated molecular pattern
PBMC:	peripheral blood mononuclear cell
PBS:	phosphate-buffered saline
PCR:	polymerase chain reaction
PE: p	hosphatidylethanolamine
PetN:	phosphoethanolamine
PG:	phosphatidylglycerol
PMF:	proton motive force
PRR:	pathogen recognition receptor
^{R}:	resistant
RND:	resistance nodulation-division
RPMI:	Roswell Park Memorial Institute medium
RPMI/H:	RPMI/Hepes medium
RT-qPCR:	reverse transcription quantitative PCR
^{S}:	susceptible
S. aureus:	*Staphylococcus aureus*
S. pneumoniae:	*Streptococcus pneumoniae*
SEM:	scanning electron microscopy
SNP:	single nucleotide polymorphism
SP:	surfactant protein
spp.:	species pluralis
T2SS:	type 2 secretion system
T3SS:	type 3 secretion system
T6SS:	type 6 secretion system
TGF-β:	transforming growth factor beta
TLR:	toll-like receptor
TMS:	Tris minimal succinate
Tn:	transposon
TNF-α:	tumor necrosis factor alpha
UIC:	University of Illinois at Chicago

uppS:	undecaprenyl pyrophosphate synthase
VAP:	ventilator-associated pneumonia
VUMC:	Vanderbilt University Medical Center
WT:	wild-type
XDR:	extensively drug-resistant

CHAPTER I

INTRODUCTION

Portions of this Chapter have been adapted from:

(a): **Wijers CDM**, Pham L, Skaar EP, Palmer LD, and Noto MJ. Gram-negative bacteria act as a reservoir for aminoglycoside antibiotics that synergize with host factors to enhance bacterial killing in a mouse model of pneumonia. At the time of writing, this manuscript is undergoing peer review and being considered for publication.

(b): Hood-Pishchany MI, Pham L, **Wijers CD**, Burns WJ, Boyd KL, Palmer LD, Skaar EP, and Noto MJ. 2020. Broad-spectrum suppression of bacterial pneumonia by aminoglycoside-propagated *Acinetobacter baumannii*. PLoS Pathog 16(3): e1008374.

(c): **Wijers CDM**, Pham L, Menon S, Boyd KL, Noel HR, Skaar EP, Gaddy JA, Palmer LD, and Noto MJ. 2021. Identification of Two Variants of *Acinetobacter baumannii* Strain ATCC 17978 with Distinct Genotypes and Phenotypes. Infect Immun 89(12): e0045421.

1.1 Pneumonia as a leading cause of morbidity and mortality

Pneumonia is an infection that inflames the air sacs in the lungs, causing them to fill with fluid, pus, or blood. When severe, this can lead to respiratory failure, systemic inflammation, and death. In the United States alone, pneumonia was responsible for 1.5 million emergency room visits in 2018 and 47,601 deaths in 2020 (1). Globally, pneumonia remains the single largest infectious cause of death for children under the age of five, and is among the top ten causes of death in both the developed as well as the developing world (2, 3). Despite a significant decrease in both incidence and associated mortality since the turn of the millennium (4), pneumonia killed 740,180 children less than five years old in 2019 alone, which accounted for 14% of deaths in this age group (2). The burden of (childhood) pneumonia is particularly large in the developing world, with India, Nigeria, Indonesia, Pakistan, and China accounting for more than 54% of clinical pneumonia and severe pneumonia cases in 2015 (4). Given the prevalence, morbidity, and mortality caused by pneumonia on a global scale, an increased understanding of the molecular factors contributing to pneumonia pathogenesis as well as the development of novel therapeutic strategies have the potential to dramatically improve human health around the globe.

Classification, microbiology, and epidemiology

Conventionally, pneumonia is subdivided into separate categories: hospital-acquired pneumonia (HAP), ventilator-associated pneumonia (VAP), and community-acquired pneumonia (CAP) (5). HAP requires that the infection was acquired after at least 48 hours of hospitalization, whereas VAP is a subcategory of HAP associated with mechanically ventilated patients (5). CAP is pneumonia that is acquired outside of the hospital or healthcare setting (5). The term healthcare-associated pneumonia (HCAP), which was defined as an infection that is acquired in lower acuity healthcare settings such as nursing homes (5), was determined to be of minimal value in clinical practice and as such was removed from the Infectious Disease Society of America (IDSA) guidelines in 2016 (6, 7). Instead, patients who previously would have qualified as having "HCAP" are currently considered as having "CAP" for treatment purposes (7). CAP, HAP, and VAP may be caused by bacteria, viruses or fungi. While the proportion of CAP cases caused by bacteria has steadily declined over the last century or so, the relative incidence of viral CAP has increased (8). This is particularly true for the United States, as bacteria are still the most commonly identified etiologic agent of CAP in Europe, China, and India (9). Examples of viral causes of CAP include influenza, rhinovirus, and – especially as of late – coronavirus. In terms of bacterial CAP, *Streptococcus pneumoniae* remains the most common bacterial etiology of CAP (8-10). Other bacterial causes of CAP include *Haemophilus influenzae* and *Staphylococcus aureus* (8).

In contrast to CAP, HAP and VAP are most commonly caused by bacterial pathogens. Frequent etiologic agents include Gram-negative bacteria such as *Pseudomonas aeruginosa*, *Klebsiella pneumoniae*, enteric Gram-negative bacilli, *Acinetobacter baumannii* (see **Chapter I section 1.4 - *Acinetobacter baumannii* as a human pathogen**), as well as the Gram-positive pathogen *S. aureus* (11, 12). Pneumonia caused by either *P. aeruginosa* or *A. baumannii* is particularly common in mechanically ventilated patients (i.e. those with VAP) (11, 13). As such, both of these organisms are of grave concern to intensive care units. Although less common than in CAP, HAP may also be caused by (respiratory) viruses such as influenza, parainfluenza, and respiratory syncytial virus. For instance,

one study conducted prior to the onset of the COVID19 pandemic found that 22.5% and 8.0% of HAP cases were caused by a viral infection or a viral-bacterial co-infection, respectively (14).

Risk factors for bacterial HAP and VAP include mechanical ventilation for longer than 48 hours, prolonged hospital or ICU stay, and prior use of antibiotics (11). Prior use of antibiotics, especially broad-spectrum antimicrobials, increases the risk of HAP or VAP caused by *P. aeruginosa* or *Acinetobacter* spp. in particular (15). Both of these organisms exhibit intrinsic resistance to antimicrobials and also rapidly accumulate antibiotic resistance (16, 17). Prior exposure to antibiotics, therefore, selects for these inherently more antimicrobial-resistant organisms. Because of this selective pressure, prior exposure to antibiotics is a significant risk factor for pneumonia caused by other antimicrobial-resistant organisms as well. For example, up to 100% of patients with HAP or VAP caused by methicillin-resistant *S. aureus* (MRSA) had prior exposure to antibiotics, whereas only a minority of patients with HAP or VAP caused by methicillin-susceptible *S. aureus* (MSSA) did (18, 19). Naturally, infections caused by antimicrobial-resistant organisms necessitate the use of more aggressive and/or prolonged antibiotic therapy. Paradoxically, this also increases the risk of acquiring infection with a resistant pathogen in the first place. Because of this, antibiotic stewardship, minimizing the length of treatment, and curtailing unnecessary exposure to antibiotics are important paradigms of the most recent HAP treatment guidelines (6).

In the setting of HAP and VAP, rates of antibiotic resistance among infecting organisms are high (20), complicating treatment regimens. Because of this, mortality among patients with HAP or VAP is substantial. Globally, HAP-associated mortality is estimated at 20-30% (9), although exact mortality rates vary by region. To illustrate, HAP (non-VAP) mortality in the United States was recently reported at 13.1% (21), well below the estimated global average. Similarly, per the IDSA, VAP-associated mortality in the United States was approximately 13% (6), whereas VAP-associated mortality rates are as high as 30% in Europe and 74% in South-East Asia (22, 23). It should be noted, however, that considerable intra-region variability in terms of HAP- and VAP-associated mortality exists as well. In patients with CAP, disease severity determines the treatment setting. Therefore, mortality differs

significantly based on the treatment setting. CAP-associated mortality is <1%, up to 18%, and up to 50% for patients treated as an outpatient, patients in non-ICU hospital wards, and patients treated in ICUs, respectively (9). In addition to treatment setting, patient age influences CAP-associated mortality, which is highest in older adults (>70 years of age) (9, 24, 25).

Current treatment standards

Evidence-based treatment guidelines of bacterial pneumonia are updated on a regular basis as new evidence becomes available. Current recommendations and guidelines regarding the treatment of CAP or HAP and VAP were published by the IDSA in 2019 and 2016, respectively (6, 26). Briefly, empiric treatment of CAP in adults without comorbidities or risk factors for *P. aeruginosa* or MRSA consists of a single antimicrobial agent such as amoxicillin (26). For HAP and VAP, empiric treatment includes an anti-staphylococcal agent (e.g. cefepime for MSSA or vancomycin for MRSA) and an anti-pseudomonal agent (e.g. a cephalosporin) (6). Aminoglycosides (AGs) are a class of polycationic antimicrobials that inhibit bacterial peptide synthesis by binding to the 30S ribosomal subunit, resulting in cell death (27). AGs have good activity against Gram-negative pathogens such as *P. aeruginosa* (28, 29). However, for patients with HAP or VAP due to *P. aeruginosa*, systemic treatment with an AG alone is not recommended (6). Systemically administered AGs have poor lung penetration, requiring high peak serum concentrations in order to achieve biologically active concentrations inside the lungs (30, 31). This, in turn, increases the risk of ototoxicity and nephrotoxicity, two serious side effects associated with AG use (32, 33). Nonetheless, inhaled (nebulized) AGs are suggested in the treatment of HAP and VAP caused by MDR, Gram-negative pathogens that are susceptible to AGs (6, 34). Inhaled AGs are also used to treat bacterial lung infections in patients with cystic fibrosis (CF) (35). *P. aeruginosa* is a common cause of CF pulmonary infections, and nebulized tobramycin results in increased pulmonary function, decreased bacterial density, and decreased risk of hospitalization (36-38). Moreover, treatment with inhaled tobramycin leads to improvements in pulmonary function even when infecting *P. aeruginosa* isolates have increased minimum inhibitory concentration (MIC) values for tobramycin (≥ 8

mg/L), and may therefore be resistant to treatment (37). Collectively, these data raise the hypothesis that AG antibiotics may be more effective inside the lung, particularly when they are administered directly to the lung. A more thorough mechanistic understanding of this phenomenon, therefore, may expand the clinical utility of AG antibiotics.

Pneumonia is a pathology that poses a significant burden to ICUs, hospital wards, and communities throughout the world. Antibiotic resistance among infecting organisms is already substantial, particularly in the setting of HAP and VAP (20), necessitating complex treatment algorithms that take into account multiple risk factors for acquiring an MDR infection (6, 26). Considering the increasing prevalence of MDR organisms (39), this is unlikely to change. Thus, the discovery of novel therapeutic targets and the development of new treatment modalities may help curb the threat of MDR organisms and thereby ameliorate the global impact of pneumonia. Further, to optimize the chances of accomplishing this goal, it is imperative that the clinical utility of currently available treatment options is maximized.

1.2 Molecular drivers of pneumonia pathogenesis

The pathophysiology of bacterial pneumonia is characterized by colonization of the lower respiratory tract by pathogenic bacteria, where they evade, degrade, or otherwise overwhelm endogenous host defenses. The resulting inflammatory response, in combination with cytotoxic factors elaborated by some pathogenic bacteria, compromise the integrity of the respiratory epithelium. This leads to extravasation of fluid, pus, and/or blood into the alveolar air spaces, impeding effective gas exchange (40). As such, both pathogen-derived factors as well as the host response to infection contribute to lung injury, morbidity, and mortality in pneumonia. A more thorough mechanistic understanding of the molecular interactions at the host-microbe interface may uncover novel targets for antimicrobials or immune modulation. These, in turn, may help minimize lung injury and improve clinical outcome for patients with pneumonia.

Colonization of the respiratory epithelium and establishment of infection

One of the first steps of establishing pneumonic infection is the colonization of the host respiratory epithelium by pathogenic bacteria. To do this, bacterial pathogens produce virulence factors that promote attachment to host cells. Common strategies employed by pathogenic bacteria include the expression of proteins that bind to host cell surface molecules or the elaboration of pili: hair-like surface appendages that facilitate bacterial attachment to surfaces such as epithelial cells. For instance, *S. aureus*, a Gram-positive cause of pneumonia, produces fibronectin binding proteins that mediate bacterial attachment to host cells (41). Specifically, *S. aureus* fibronectin binding proteins bind to fibronectin, which in turn binds to fibronectin receptor integrin ($\alpha5)\beta1$ molecules on host cells (42). This mechanism promotes bacterial invasion of host cells, further contributing to the establishment of infection (42, 43). The Gram-negative, opportunistic pathogen *P. aeruginosa*, expresses numerous pili on its cell surface promoting attachment to respiratory epithelial cells (44). Adhesion of *P. aeruginosa* pili to hydrophobic surfaces, such as cell membranes, is strong enough to withstand physiological shear forces, indicating that pili constitute an important virulence factor for colonization of the host respiratory system (45). Once bacterial attachment to the respiratory epithelium is accomplished, airway clearance of the pathogen through cough and the mucociliary apparatus must be impeded in order to achieve stable colonization. *S. pneumoniae*, another Gram-positive pathogen and the leading bacterial cause of pneumonia, is notorious for its polysaccharide capsule. This polysaccharide capsule promotes airway colonization through the inhibition of mucus-mediated bacterial clearance from the airways (46, 47).

After an infection is established, bacteria must sequester nutrients from the host in order to survive and propagate. Several pathogenic bacteria secrete proteins that are toxic to host cells, culminating in host cell lysis and the liberation of nutrients for bacteria. Through their direct cytotoxic effects, these proteins incite or exacerbate damage to the respiratory system and thereby contribute to pneumonia pathogenesis. *S. pneumoniae*, for example, produces pneumolysin. This toxin causes lysis of host cells through membrane pore formation (46, 48). Inside host cells, pneumolysin also induces

DNA double strand breaks, which result in cell cycle arrest and host cell apoptosis (49). As a consequence of its cytotoxic properties, *S. pneumoniae* pneumolysin increases capillary permeability in the lungs, thereby promoting lung edema and contributing to acute lung injury in experimental pneumonia (50, 51). Analogous to *S. pneumoniae* pneumolysin, *S. aureus* produces pore-forming α-toxin, which is capable of lysing a wide range of host cells and also inducing T-lymphocyte apoptosis (52). Like pneumolysin, *S. aureus* α-toxin promotes lung injury and pulmonary edema in experimental pneumonia (53), and increased expression of *S. aureus* α-toxin is associated with enhanced mortality in a mouse model of pneumonia (54). *P. aeruginosa* also secretes several proteins with cytotoxic properties. Two examples that have been implicated in pneumonia pathogenesis are exotoxin A, which is elaborated by the pathogen's type 2 secretion system (T2SS), and ExoU, which is elaborated by its type 3 secretion system (T3SS). Exotoxin A exerts its effects inside host cells, where it inactivates eukaryotic elongation factor-2 on host ribosomes through ADP-ribosylation. This impedes host cell protein synthesis, which is followed by the induction of apoptosis (55). In a mouse model of *P. aeruginosa* pneumonia, presence of the T2SS – the bacterial machinery implicated in Exotoxin A secretion – contributes to mortality (56). ExoU, on the other hand, lyses host cells through its phospholipase A_2 activity, and contributes to lung epithelial injury in a model of pneumonia (57-59). Moreover, ExoU secretion is associated with severe disease in adults with VAP caused by *P. aeruginosa* (60). Collectively, these findings suggest that some of the major causative agents of bacterial pneumonia elaborate virulence factors that damage host tissues and cells directly, thereby liberating nutrients. Some of these toxins are associated with poorer clinical outcomes in human patients.

During pneumonic infection, pathogenic bacteria must sequester micronutrients such as metals. To accomplish this, pathogenic organisms capable of causing pneumonia produce metal scavenging molecules and/or receptors to acquire essential nutrient metals from metal-host protein complexes. For instance, *S. aureus* preferentially acquires iron from heme (61), which is accomplished through the Isd

system (62). Siderophore molecules such as staphyloferrin A and B, which scavenge iron complexed to host proteins, constitute an additional iron acquisition mechanism for this pathogen (62). Similarly, *K. pneumoniae*, secretes siderophores such as enterobactin and yersiniabactin to obtain iron from its host environment (63). In a mouse model of pneumonia, *K. pneumoniae* siderophores were demonstrated to contribute to mortality and extrapulmonary dissemination (63, 64), and increased siderophore expression is associated with an outbreak strain of this pathogen (65). Other metals required by pathogenic bacteria over the course of pneumonic infection include zinc, manganese, and copper. Although such nutrient metals are required for bacterial physiology, they are toxic to bacteria in high concentrations. Therefore, pathogenic bacteria must maintain a homeostatic balance between metal starvation and metal toxicity (66).

Bacterial evasion and degradation of host defenses

The processes described above – colonization of the respiratory epithelium and pathogen-induced damage to host cells – alert the host of an invading pathogen. To combat the invading pathogen, the host mounts an immune response. This response is comprised of host defenses that are constitutively present in the lungs, such as pulmonary surfactant, as well as host defenses that must be recruited to the site of infection, such as neutrophils. Bacterial pathogens have evolved multiple virulence factors to counteract these host defenses through evasion or active degradation. In doing so, bacterial pathogens impede their immune-mediated clearance, prolong infection, and further contribute to pneumonia pathogenesis.

One strategy that bacterial pathogens employ to evade components of the immune system is to produce a physical barrier that acts as a shield, such as a thick polysaccharide capsule. For instance, *S. pneumoniae* produces a capsule that protects bacterial cells from complement activity and phagocytosis (67). *K. pneumoniae* produces a polysaccharide capsule with similar functions. Similar to the *S. pneumoniae* capsule, the capsule elaborated by *K. pneumoniae* inhibits phagocytosis of bacteria by polymorphonuclear leukocytes and impedes deposition of complement proteins on the bacterial cell

surface (68, 69). Finally, the Gram-negative, nosocomial pathogen *A. baumannii* also produces such a polysaccharide capsule (70). This pathogen is discussed in detail in **Chapter I, section 1.4 - *Acinetobacter baumannii* as a human pathogen**.

Another strategy that pathogenic bacteria utilize to evade the immune system is to secrete effectors that actively degrade or interfere with components of the immune system. Two of the first lines of host defense in the setting of a bacterial respiratory infection are the mucosal epithelial barrier and pulmonary surfactant that lines this epithelium in the distal airways. Pulmonary surfactant is predominately comprised of lipids, which act as a molecular detergent (71), and contains surfactant proteins with antibacterial properties (72, 73). Further, pulmonary surfactant increases bacterial susceptibility to AG antibiotics (74). As discussed above, nebulized AG antibiotics may be administered directly to the lungs through inhalation in the treatment suggested for HAP and VAP (6, 34). These findings, therefore, raise the possibility that pulmonary surfactant – in addition to its innate antibacterial properties – may promote bacterial clearance from the lungs through synergy with AG antibiotics (addressed in detail in **Chapter II**). The nosocomial and CF-associated pathogen *P. aeruginosa* has evolved mechanisms to actively interfere with the mucosal barrier function as well as the antibacterial properties of pulmonary surfactant. Specifically, *P. aeruginosa* secretes a serine protease – protease IV – that cleaves surfactant proteins and IL-22. IL-22 is crucial for maintaining lung mucosal barrier integrity (75, 76). Similarly, *S. aureus* produces a hydrolyzing enzyme – staphopain A – that degrades surfactant protein A, which has antibacterial properties (72). In doing so, *S. aureus* impairs innate immune-mediated bacterial clearance from the airways and increases bacterial attachment to the respiratory epithelium (77). Bacterial access to and subsequent degradation of the respiratory mucosal barrier lead to lung injury and therefore comprise critical steps in the pathogenesis of bacterial pneumonia.

In terms of the cellular components that contribute to effective immune-mediated clearance of bacterial pathogens from the respiratory system, neutrophils are indispensable. Functional recruitment of neutrophils to the lungs is strongly implicated in protecting the host from pneumonia caused by *S.*

pneumoniae, *K. pneumoniae*, and *S. aureus* in animal models (78-80). As such, pathogenic bacteria have evolved mechanisms to evade or actively interfere with neutrophil function. As discussed above, a polysaccharide capsule may protect from phagocytosis by neutrophils, such as is the case for *K. pneumoniae* (68). Similarly, *P. aeruginosa* produces the extracellular polysaccharide Psl. Psl is implicated in *P. aeruginosa* biofilm formation (81), and also inhibits bacterial detection by neutrophils in the lung vasculature (82). Additionally, the *P. aeruginosa* T3SS, previously discussed as the machinery responsible for ExoU secretion, prevents acidification of the neutrophilic phagolysosome upon phagocytosis, thereby inhibiting intracellular killing of bacteria by neutrophils (82). Intriguingly, a bispecific antibody that simultaneously targets Psl and the T3SS enhanced neutrophilic detection and processing of *P. aeruginosa*, and significantly improved survival in an animal model (82). This finding further underscores the importance of neutrophils in effectively protecting the host against this pathogen. Finally, *S. aureus* possesses an impressive arsenal of factors that enable this pathogen to evade or interfere with almost every aspect of neutrophil biology, including detection, intracellular killing, and neutrophil extracellular traps (83).

While neutrophils must be recruited to the lung upon pneumonic infection, alveolar macrophages are constitutively present and are, therefore, the resident phagocytes in the lung. In animal models of bacterial pneumonia, alveolar macrophages clear bacterial pathogens from the respiratory system prior to the onset of fulminant pneumonia. In order to effectively kill engulfed bacteria, alveolar macrophage apoptosis must be induced (84, 85). However, the capacity for alveolar macrophages to kill bacteria is finite, and even in immunocompetent animals, the bacterial inoculum can be increased to a point where these resident phagocytes become overwhelmed and neutrophils become critical to achieve bacterial clearance (84, 85). Alveolar macrophages play a role in recruiting neutrophils to the lungs during the early stages of pneumonic infection (86). The importance of alveolar macrophages in bacterial airway clearance is underscored by the fact that patients with chronic obstructive pulmonary disease have dysfunctional alveolar macrophages, leading to persistent bacterial airway colonization and disease exacerbations (87). Bacterial pathogens have evolved virulence factors to counteract this aspect of

host defense and impede bacterial clearance from the respiratory system. For example, the *P. aeruginosa* metalloprotease LasB, which is secreted by the T2SS, interferes with alveolar macrophage bactericidal activity by downregulating reactive oxygen species production (88).

As illustrated above, the host defenses in the lung are comprised of several components that aim to prevent bacterial colonization altogether or prevent the progression of bacterial colonization to fulminant pneumonic infection. Bacterial pathogens, in turn, have evolved several strategies to evade, degrade, or interfere with these host defenses. If, through these mechanisms, host defenses become overwhelmed, bacterial infection persists, airway inflammation progresses, and the pathogenesis of pneumonia proceeds.

Dysregulation of the immune response to bacterial infection

An effective and well-regulated immune response is critical to clearing pneumonic infection caused by bacterial pathogens. Under homeostatic conditions, the immune system uses pathogen recognition receptors (PRRs) to detect pathogen associated molecular patterns (PAMPs) of invading pathogens. An example of a well-characterized interaction between a PAMP and a PRR is the recognition of the Gram-negative glycolipid lipopolysaccharide (LPS) by toll-like receptor (TLR) 4 on immune cells. Stimulation of TLR4 by LPS engages an intracellular signaling cascade culminating in the production of pro-inflammatory cytokines (89). The role of LPS and other bacterial lipids in pneumonia pathogenesis is discussed in detail in **Chapter I, section 1.3 – The cell envelope of Gram-negative bacteria**. During pneumonic infection, however, the immune response to infection can become dysregulated or overactivated. Such a dysregulated or overactive immune response fails to clear the infection and actively contributes to pneumonia pathogenesis and lung injury. This process often starts with the invading pathogen itself, as bacterial pathogens have evolved mechanisms to incite immune dysregulation or overactivation.

The Nods-Like receptor family, CARD domain containing 4 (NLRC4) inflammasome plays an important role in host defense against intracellular pathogens such as *Legionella pneumophila*, an

uncommon cause of pneumonia (90). However, the NLRC4 inflammasome is also activated by *P. aeruginosa*, a predominately extracellular pathogen. Paradoxically, alveolar macrophage NLRC4 inflammasome activation by *P. aeruginosa* decreased bacterial clearance and increased mortality in a mouse model of pneumonia (91). Mechanistically, this is thought to occur through expression of IL-18, which is induced by NLRC4 inflammasome activation. IL-18, in turn, decreased expression of antimicrobial peptides in the lung, thereby increasing *P. aeruginosa* burdens. Further, NLRC4-mediated expression of IL-18 led to excessive recruitment of neutrophils to the lung, which exacerbated lung injury (92).

Similarly, activation of the NLR family pyrin domain containing 3 (NLRP3) inflammasome is primed by the binding of bacterial LPS to TLR4 on host cells such as macrophages (93). Activation of NLRP3 leads to the production of pro-inflammatory cytokines IL-1β and IL-18, which are important in mediating the host immune response to invading microbes (94). For instance, IL-1β and IL-18 have been demonstrated to promote neutrophil recruitment to the lungs and neutrophil activation, respectively (95, 96). As discussed previously, neutrophils are critical in host defense against bacterial pneumonia. However, excessive neutrophil recruitment to the lungs in the setting of bacterial pneumonia may exacerbate lung injury, as opposed to ameliorate pathogen-induced lung injury. In fact, activation of the NLRP3 inflammasome or, as discussed above, the NLRC4 inflammasome, may cause excessive neutrophil recruitment to the lungs (92, 97). Inside the lungs, neutrophils can contribute to organ injury through the release of cytotoxic enzymes and the activation of oxidative stress pathways (98). In a mouse model of LPS-induced acute lung injury (ALI), NLRP3 inflammasome activation resulted in increased recruitment of leukocytes to the lungs and increased mortality (97). In critically ill human patients, elevated levels of IL-18 – a product of NLRP3 and NLRC4 inflammasome activation – were associated with increased disease severity (such as those with Acute Respiratory Distress Syndrome [ARDS]) and mortality (99). Thus, excessive inflammasome activation by bacterial products can result in neutrophil-mediated ALI, thereby exacerbating pneumonia pathogenesis.

Dysregulation of the immune response may also be caused by the reveal of host-derived molecules, so-called damage-associated molecular patterns (DAMPs), to components of the immune system. Under homeostatic conditions, DAMPs are confined to specific subcellular locations not accessible to the immune system. During bacterial pneumonia, however, damaged and dying host cells may release DAMPS from their subcellular locations and render them detectable by immune components. Apoptosis, a form of regulated cell death, may be induced in host cells such as respiratory epithelial cells and immune cells by *P. aeruginosa*, *S. pneumoniae*, and *S. aureus* (100). During apoptosis, the DAMP cardiolipin (CL), a tetra-acylated lipid normally confined to the inner mitochondrial membrane, translocates to the outer mitochondrial membrane (101). Once in the outer mitochondrial membrane, CL may become accessible to components of the NLRP3 inflammasome. Mitochondrial CL has been demonstrated to bind NLRP3 directly, causing inflammasome activation (102). (Over)activation of the NLRP3 inflammasome may result in neutrophil-mediated ALI, as discussed above. As the process of apoptosis progresses, mitochondrial CL inserts into the host cell membrane (103). From there, it may be released extracellularly into lung fluid (104). Lung fluid mitochondrial CL concentrations were elevated in both experimental bacterial pneumonia and human patients. Further, release of mitochondrial CL into lung fluid reduced epithelial barrier integrity and worsened lung mechanics in a mouse model of bacterial pneumonia (104). Mitochondrial CL, therefore, is an intriguing example of how host-derived DAMPs can induce and sustain inflammation and lung injury during pneumonia pathogenesis. CL is also a constituent of bacterial membranes (see **Chapter I, section 1.3 – The cell envelope of Gram-negative bacteria**). However, to what extent bacterial CL contributes to inflammation and lung injury in the setting of bacterial pneumonia remains to be elucidated. Preliminary studies aimed at interrogating this question are discussed in **Chapter IV**.

The molecular interactions at the host-microbe interface in bacterial pneumonia are complex and multi-faceted. Fulminant bacterial pneumonia is uncommon in immunocompetent adults (9), suggesting that endogenous host defenses prevent pathogenic bacteria from gaining a foothold in the

lower respiratory tract in most instances. Even when bacterial colonization progresses to infection, uncontrolled or unrelenting inflammation is uncommon, as evidenced by the fact that the majority of bacterial pneumonia cases is comprised of CAP that can be treated exclusively in the outpatient setting (9). A more thorough, mechanistic understanding of what makes some hosts more susceptible to developing a maladaptive immune response to bacterial pneumonia, as well as of the bacterial attributes that elicit such a response, may lead to the development of therapeutic strategies that boost a well-regulated, robust immune response. In doing so, effective immune-mediated bacterial clearance will be encouraged, and excessive inflammation and lung damage will be ameliorated or even prevented altogether.

1.3 The Gram-negative cell envelope

The cell envelope of Gram-negative bacteria consists of three distinct layers: a lipid inner membrane (IM), the periplasm, and a lipid outer membrane (OM). In Gram-negative bacteria, a cell wall comprised of a thin layer of peptidoglycan is contained within the periplasm (105). Embedded in each layer are bacterial factors such as proteins that play key roles in bacterial physiology and pathogenesis. Additionally, each layer of the Gram-negative cell envelope encompasses PAMPs that can be detected by host PRRs, thereby inciting an inflammatory response. As such, the Gram-negative cell envelope is a key determinant of pathogenesis in bacterial pneumonia.

Outer membrane

The lipid OM is a unique feature of Gram-negative bacteria. It is a lipid bilayer comprised of an inner leaflet and an outer leaflet. Under homeostatic conditions, the OM outer leaflet of the model Gram-negative organism *Escherichia coli* is comprised of a monolayer of LPS (106). The OM outer leaflet of some Gram-negative bacteria, such as the nosocomial pathogen *A. baumannii*, is comprised of lipo-oligosaccharide (LOS) instead, which is similar to LPS except that it lacks the O antigen component (107). In *E. coli*, LPS was demonstrated to enhance OM rigidity, which in turn contributed to the strength

of bacterial cells in general (108). This suggests that LPS is critical to the structural integrity of Gram-negative bacterial cells. Indeed, the presence of either LPS or LOS is essential to survival for most Gram-negative bacteria. Some species, however, including the human pathogen *A. baumannii*, can survive in the absence of LPS/LOS due to structural support from the underlying peptidoglycan layer (109). Therefore, under certain environmental conditions, expressing an OM without LPS/LOS may provide a fitness advantage to some Gram-negative pathogens (Also, see **Chapter I, section 1.4 – *Acinetobacter baumannii* as a human pathogen**).

LPS also contributes to the pathogenesis of Gram-negative bacteria during infection, as it protects cells from complement deposition as well as the effects of antimicrobial peptides (110-112). As discussed previously, LPS is a PAMP that is recognized by TLR4 (a PRR) on host cells. This interaction provides the priming signal of NLRP3 inflammasome activation, which is completed after a second signal is received (93). NLRP3 inflammasome activation results in the secretion of mature IL-1β and IL-18, and overactivation of this inflammasome is implicated in pneumonia pathogenesis (see **Chapter I, section 1.2 - Molecular drivers of pneumonia pathogenesis**). In addition, engagement of TLR4 by LPS initiates an intracellular signaling cascade that culminates in the activation of the NF-κB transcription factor and the expression of pro-inflammatory cytokines such as TNF-α and IL-6 (89, 113). Bacteria can take advantage of this interaction by adjusting LPS composition and/or expression to modulate pathogenesis. For instance, *Yersinia pestis* hypo-acylates LPS in a temperature-dependent manner. Hypo-acylated LPS is less stimulatory to human TLR4 and therefore helps this pathogen to avoid immune recognition (114). By contrast, over the course of chronic respiratory infection in patients with CF, *P. aeruginosa* synthesizes specific forms of LPS that increase bacterial resistance to host-derived antimicrobial peptides and induce an enhanced inflammatory response (115). Thus, Gram-negative LPS is considered a key immune regulatory molecule.

The vast majority of the inner leaflet of the OM is comprised of phosphatidylethanolamine (PE), whereas a small minority (<9%) is composed of the anionic lipids phosphatidylglycerol (PG) and CL (106). Although a relatively minor component of the Gram-negative OM, CL plays important roles in

both bacterial physiology and pathogenesis. CL tends to localize at the cell poles and septal planes, and is implicated in respiration and cell division (116-119). Further, CL promotes bacterial resistance to cell envelope stressors such as osmotic and surfactant stress (120-122). This is relevant to pneumonia pathogenesis as pulmonary surfactant is abundant in the fluid lining the distal airways and alveolar spaces, and Gram-negative pathogens such as *A. baumannii* have been demonstrated to encounter surfactant upon pneumonic infection in a mouse model (123, 124). Additionally, CL plays a role in immune signaling. As discussed previously, mitochondrial CL is a direct agonist of the NLRP3 inflammasome (102). It is plausible that bacterial CL activates the NLRP3 inflammasome in a similar manner, although this remains to be investigated. Further, CL differentially activates TLR4-mediated inflammatory signaling depending on acyl chain saturation. Unsaturated CL blocks LPS-mediated activation of TLR4, whereas saturated CL mimics LPS and can serve as a TLR4 agonist. As such, saturated CL increases the production of TLR4-mediated pro-inflammatory cytokines while unsaturated CL has the opposite effect (125). This suggests that, like LPS, bacterial CL may contribute to inflammation and lung injury in pneumonia.

Proteins are embedded within the lipid bilayer of the Gram-negative OM. Gram-negative, integral OM proteins can be crudely divided into two classes: lipoproteins and β-barrel proteins (105). Lipoproteins are globular proteins that are anchored to the inner leaflet of the OM by a lipid moiety and are involved in a variety of functions, including cell envelope stress sensing and OM biogenesis (105, 126). Additionally, lipoproteins contribute to the structural integrity of the Gram-negative cell envelope by anchoring the OM to the thin layer of peptidoglycan underneath (126). On the other hand, β-barrel proteins are integral OM proteins that take on a cylindrical shape and are frequently implicated as virulence factors (105). For instance, in *P. aeruginosa*, the OM protein OprF is involved in virulence through modulation of the quorum sensing network and T3SS-mediated toxin secretion (127). Expression of such proteins is not always advantageous to pathogenic bacteria, however, as illustrated by the reduced expression of the OM protein OprH in CF-associated clinical isolates of *P. aeruginosa*. OprH serves as a ligand for surfactant protein A, and this interaction promotes phagocytic killing of *P.*

aeruginosa in the CF lung (128). This finding indicates that, while the Gram-negative OM shields bacteria from environmental stressors such as complement and antimicrobial peptides, it may also serve as a target for novel therapeutics.

Periplasm

Inside the OM is an aqueous cellular compartment called the periplasm, which is limited by the bacterial IM on its opposite border. Within the periplasm, there is a thin layer of peptidoglycan, which is anchored to the OM by lipoproteins (126). Peptidoglycan consists of monomers composed of N-acetylglucosamine (GlcNAc) and N-acetylmuramic acid (MurNAc), strands of which are crosslinked by pentapeptide side chains (105). Peptidoglycan is essential to the structure and function of most bacterial species, and is therefore a common target for antibiotics. For instance, β-lactam antibiotics target the enzymes that catalyze peptidoglycan crosslinking (105). Additionally, peptidoglycan fragments are considered PAMPs, as they can be sensed by the PRRs nucleotide-binding oligomerization domain-containing protein (NOD)1 and NOD2, among other receptors. Similar to TLR4 engagement by LPS, activation of NOD1 or NOD2 activates intracellular signaling cascades culminating in the activation of either the NF-κB or the AP-1 transcription factors. Activation of either of these transcription factors leads to the expression of pro-inflammatory cytokines such as TNF-α and IL-6. Of note, NOD1 and NOD2 are located within the cytosol of host cells and, as such, must detect peptidoglycan from bacteria that have entered the host cell cytosol or have been degraded (129).

Smaller bacterial proteins can freely diffuse through the periplasmic peptidoglycan layer. By contrast, larger bacterial nanomachines that span the IM, periplasm, and OM must locally degrade the peptidoglycan layer in order to traverse it. The Gram-negative T3SS, previously discussed in the context of *P. aeruginosa* exotoxin secretion, is an example of such a nanomachine. Many Gram-negative bacteria encode a T3SS-specific enzyme such as a lytic transglycosylase that creates local defects in the peptidoglycan layer for the periplasmic components of the T3SS to fit through (130). Efflux pumps that expel noxious agents, such as antibiotics, from the bacterial cytosol also span all

three layers of the Gram-negative cell envelope (131). *A. baumannii* is notorious for its antibiotic efflux pumps, which contribute to this pathogen's propensity for antibiotic resistance. Antibiotic efflux pumps will be discussed in the context of this pathogen in **Chapter I, section 1.4 – *Acinetobacter baumannii* as a human pathogen**. Bacterial products that are not part of multi-membrane spanning protein complexes but must nonetheless cross the periplasm, such as integral OM proteins, require chaperones to do so. Characterized chaperone proteins include SurA, Skp, and DegP, all of which share some functional redundancy (105). In *P. aeruginosa*, SurA may serve as a potential therapeutic target, as a MDR clinical isolate in which SurA was depleted became sensitized to multiple antibiotics (132). Therefore, like the OM, the Gram-negative periplasm is home to several targets of potential therapeutic interest.

Inner membrane

The internal border of the periplasm is limited by the IM, which is analogous to the eukaryotic plasma membrane. Like the OM, the IM is comprised of a bilayer of two lipid leaflets: a periplasmic leaflet and a cytoplasmic leaflet. The lipid composition of the Gram-negative IM is an active area of research, as the exact lipid composition of the IM is dynamic and changes depending on the state of the cell (133). Like the periplasmic leaflet of the OM, however, the majority of the IM is comprised of PE. Compared to the OM, a larger fraction of the IM is comprised of the anionic lipids CL and PG, which tend to cluster in the periplasmic leaflet (106, 133). Many membrane-associated functions of bacteria occur at the IM, including energy production and lipid synthesis. Lipid distribution around protein complexes involved in these processes is not random, but rather shows a predilection for specific types of lipid. For instance, several respiratory complexes involved in bacterial energy production associate with the anionic lipid CL (118, 134), which is also implicated in the transport of LPS to the OM (135). The importance of CL in Gram-negative physiology is further evidenced by the fact that *E. coli* encodes three enzymes that catalyze the synthesis of CL – CL synthase (Cls)A, ClsB, and ClsC – despite CL being one of the least prevalent lipids in this organism (136). In bacterial pathogenesis, the role of CL

can be considered dichotomous. As discussed earlier, CL contributes to bacterial cell envelope stress resistance and can attenuate TLR4-mediated immune signaling depending on the acyl chain saturation state (121, 122, 125). However, CL may also promote phagocytic uptake of bacteria by macrophages through the CD36 scavenger receptor (137). PG, another phospholipid present in the Gram-negative IM, may also be involved in immune signaling. Bacterial PG can be recognized by human T cell receptors. Intriguingly, such T cell receptors cannot distinguish between mammalian and bacterial PG. PG, therefore, is considered a dual self and foreign antigen (138).

Because of its involvement in many functions integral to bacterial physiology and pathogenesis, the IM is home to a wide variety of proteins and protein complexes, including those responsible for energy production, lipid biosynthesis, and protein secretion (105). Since all proteins are synthesized in the bacterial cytosol, proteins destined for the OM must cross the IM into the periplasm. This is accomplished by the SecY protein complex, which delivers proteins destined for the OM to the previously discussed chaperones inside the periplasm (139). Similarly, all phospholipids and LPS are synthesized in the IM, specifically at its inner leaflet. While the translocation of LPS from the inner leaflet of the IM all the way to the OM outer leaflet is well characterized and involves the MsbA transporter and Lpt pathway (105), the translocation of phospholipids to the OM is elusive and less well understood (140). As discussed above, there is substantial asymmetry in terms of lipid composition both between the IM and OM, as well as between the two leaflets of each membrane. Several protein complexes have been implicated in maintaining this asymmetry. Of these, the maintenance of lipid asymmetry (Mla) system is relatively well-studied and is involved in maintaining lipid asymmetry between the two leaflets of the OM (140). Specifically, this system has been demonstrated to remove misplaced phospholipids from the OM outer leaflet and transport them towards the IM (141). The mechanism for how lipid asymmetry within the IM is maintained is currently not known (133).

Like the OM, the Gram-negative IM is home to lipoproteins. Lipoproteins destined for the IM have specific amino acid residues, whereas those that lack these residues are recognized by the LolCDE system and are translocated to the OM (105, 142). In *P. aeruginosa*, MexA, which is part of a

multi-protein efflux pump contributing to this organism's intrinsic antibiotic resistance (143), is one such lipoprotein targeted for the IM (142). Finally, other proteins embedded into the Gram-negative IM include those that are part of cell envelope-spanning protein complexes such as the previously discussed T3SS (105).

In summary, the Gram-negative cell envelope is a complex structure common to all Gram-negative bacteria that has been – and will likely continue to be – a source of extensive interrogation. Although some features of the cell envelope, such as the specific protein complexes embedded within it, are species-specific, there are many aspects that are conserved across most or even all Gram-negative bacteria. Because of this, as well as its indispensable contributions to bacterial structural integrity, physiology, and pathogenesis, the Gram-negative cell envelope is a potential therapeutic target of considerable interest. Further investigations into the interactions between novel or currently available therapeutics and the Gram-negative cell envelope, therefore, have the potential to expand treatment options for patients with Gram-negative bacterial pneumonia. Particularly if those interactions involve bacterial factors that are common to multiple Gram-negative pathogens.

1.4 *Acinetobacter baumannii* as a human pathogen

A. baumannii is a Gram-negative, nosocomial pathogen, meaning that it is most commonly associated with hospital-acquired infections. It was first recognized as a human pathogen in the 1970s, with early clinical isolates susceptible to many commonly available antibiotics (144). Since then, this pathogen has gained notoriety for its propensity to accumulate antibiotic resistance, and MDR strains are isolated at an alarming frequency. As such, the Centers for Disease Control and prevention (CDC) have listed drug-resistant *A. baumannii* as an urgent threat – the highest threat level maintained by this institution (39). Here, the epidemiology, pathogenesis, mechanisms of drug resistance, and treatment considerations are discussed in the context of pneumonia caused by *A. baumannii*.

Epidemiology

Although this pathogen is capable of colonizing and infecting a variety of organ systems, including the urinary tract and bloodstream, pneumonia is the pathology most frequently associated with *A. baumannii* infection (145). The vast majority of *A. baumannii* infections occur in the hospital setting, and critically ill as well as ventilated patients are at the highest risk of acquiring *A. baumannii* pneumonia (146, 147). In one large study, The Extended Prevalence of Infection in Intensive Care (EPIC III) study, the *Acinetobacter* spp. infection rate among ICU patients in North-America was 1.0% (148). Of note, *A. baumannii* is the most common etiology of *Acinetobacter* spp. infections (145). A survey in France indicated that the prevalence of *A. baumannii* infection was 0.075% among 305,656 patients (ICU and non-ICU patients) (146). Prevalence of hospital-associated *A. baumannii* infections varies by geographical region. For instance, the EPIC III study indicated that the *Acinetobacter* spp. infection rate among ICU patients was 3.5% in Western Europe, 15.8% in Africa, and 25.6% in Asia/Middle East, suggesting that infection rates are higher in the developing world (148). CAP comprises a small minority of *A. baumannii* pneumonia cases and predominately occurs in South-East Asia and Oceania, indicating that these types of infections are associated with tropical climates (145). Moreover, *A. baumannii* CAP tends to occur during the wet/rainy season, and the vast majority of patients have an underlying condition such as alcohol use disorder (149, 150).

While the overall prevalence of *A. baumannii* pneumonia is relatively low, clinical consequences can be severe. One study reported that the 30-day mortality rate of patients with VAP due to extensively drug-resistant (XDR) *A. baumannii* was 56.8% (151). However, because the majority of *A. baumannii* HAP/VAP cases tends to occur in patients with severe illness, it is difficult to establish to what extent these high mortality rates are a consequence of *A. baumannii* infection. In one study, in-hospital mortality was numerically higher in patients with *A. baumannii* infection compared to patients with infections caused by other microorganisms (16% vs. 13%), although this difference was not statistically significant (152). A study specifically conducted with patients with VAP found similar results: mortality among patients with *A. baumannii* VAP was 40%, whereas mortality among control patients (patients

with VAP or patients free of pneumonia) was 28.3%, and this difference was not statistically significant (153). However, it should be noted that the study populations included in these studies were relatively small, and they may not have been powered to detect a mortality difference. Aside from mortality, *A. baumannii* infection is independently associated with other negative clinical outcomes such as prolonged ICU stay and increased incidence of ARDS (152). Compared to other etiologies, *A. baumannii* CAP tends to cause severe infection with high rates of bacteremia. Mortality associated with *A. baumannii* CAP is reportedly as high as 64%. Because *A. baumannii* CAP tends to occur in patients with underlying medical conditions, it is unclear to what extent specific host factors contribute to these high mortality rates (145).

Although pneumonia caused by *A. baumannii* is relatively uncommon on a global scale, its impact on hospitals and particularly ICUs is significant. Furthermore, once *A. baumannii* is introduced into a hospital, it tends to cause prolonged colonization resulting in serial or overlapping outbreaks (154). Therefore, to better control and prevent *A. baumannii* infection outbreaks in hospital settings, and to improve clinical outcomes for patients with *A. baumannii* pneumonia, enhanced understanding of the molecular pathogenesis of this organism is imperative.

Virulence factors and pathogenesis

In general, the pathogenicity of *A. baumannii* is considered to be low. However, when infection does occur, it is frequently severe, particularly in susceptible patients (145). Contributing to its ability to cause disease, *A. baumannii* possesses a myriad of virulence factors. Some of these are similar to virulence factors previously discussed for other Gram-negative pathogens, while others appear to be more specific to *Acinetobacter* spp. A better understanding of these virulence factors and of their interactions with the host environment may lead to the development of novel therapeutic strategies to combat this pathogen.

Like other Gram-negative pathogens, *A. baumannii* elaborates a polysaccharide capsule. Its synthesis is dependent on a so-called K locus, which harbors genes involved in sugar precursor

biosynthesis and polysaccharide modification, among others (155). The *A. baumannii* polysaccharide capsule is considered a major virulence factor, and protects this pathogen from complement-mediated killing, phagocytosis, and other host-derived stressors (70, 155, 156). Congruently, in a mouse model of systemic *A. baumannii* infection, augmented capsule production resulted in increased mortality (157). In a study of over 40 *A. baumannii* clinical isolates, almost all isolates produced a polysaccharide capsule, further underscoring the importance of capsule production in *A. baumannii* virulence (158). Finally, the *A. baumannii* capsule plays a role in bacterial resistance to desiccation, another remarkable attribute of this pathogen (discussed further below) (159).

The outer leaflet of the Gram-negative OM is comprised of either LPS, which contains an O antigen, or LOS, which lacks such an O antigen. *A. baumannii* is one of the Gram-negative pathogens that produces LOS instead of LPS (160). Like LPS, LOS contributes to bacterial virulence in several ways. Through hepta-acylation of the LOS lipid A anchor, *A. baumannii* can enhance OM barrier function and increase resistance to host-derived antimicrobial peptides (161). Similar to LPS, *A. baumannii* LOS activates the TLR4 receptor on host cells (162). Activation of TLR4 by *A. baumannii* LOS increases pro-inflammatory cytokine production, promotes a sepsis-like syndrome, and dramatically increases mortality in an animal model of lethal infection (163). Strains of *A. baumannii* with increased LOS shedding during growth are more virulent, whereas LOS-deficient *A. baumannii* exhibits reduced virulence in a mouse model of systemic infection (164, 165). These findings suggest that sustained activation of TLR4-mediated inflammatory signaling by *A. baumannii* LOS promotes a maladaptive host immune response and contributes to pneumonia pathogenesis. Although *A. baumannii* LOS contributes to its virulence in animal models of infection (164), this pathogen is one of very few species that is viable in the absence of LOS (or LPS). Through exposure to high concentrations of colistin, an antibiotic that binds LPS/LOS on the Gram-negative OM, *A. baumannii* can accumulate mutations in the biosynthetic pathway of lipid A, resulting in isolates devoid of lipid A and LOS (166, 167). To compensate for the loss of LOS, *A. baumannii* overexpresses lipoproteins on the cell surface and relies on structural support from the peptidoglycan cell wall (109, 161). These findings suggest that

modifying and/or downregulating lipid A and LOS expression may provide a fitness advantage to *A. baumannii* under certain environmental conditions, including environments where colistin is present.

Outer membrane protein A (OmpA) is another *A. baumannii* virulence factor that has received considerable interest. OmpA is implicated in adhesion to host cells, biofilm formation, and resistance to complement (163). Moreover, overexpression of OmpA by *A. baumannii* is an independent risk factor of mortality in human patients infected by this pathogen (168). Further, once *A. baumannii* is introduced into a hospital, it tends to cause serial or overlapping outbreaks (154). This is mediated by this pathogen's ability to tolerate dry conditions and persist on environmental surfaces. Because desiccation tolerance in *A. baumannii* makes eliminating transmission of this pathogen within hospitals challenging, it has been an area of active investigation. Regulation of *A. baumannii* desiccation tolerance is likely multifactorial, and a role for the BfmR two-component system has been implicated (169). Production of a polysaccharide capsule is also implicated in *A. baumannii* desiccation resistance (159).

Studies of *A. baumannii* pathogenesis often rely on type strains. Type strains are descendants of the original isolates that exhibit all of the relevant phenotypic and genotypic properties cited in the original published taxonomic circumscriptions (170). Strains 17978, 19606, and AB5075 are examples of type strains used to study *A. baumannii* pathogenesis. *A. baumannii* 17978 was isolated in 1951 from an infant with meningitis and is susceptible to most antibiotics (171), *A. baumannii* 19606 was isolated in 1948 from the urine of a patient with a urinary tract infection (172), and *A. baumannii* AB5075 was isolated in 2008 from the tibia of a patient with osteomyelitis (173). Because *A. baumannii* has a propensity for modulating its genome through the acquisition or loss of genetic material, caution should be used when interpreting the clinical relevance of bacterial virulence determinants. To underscore this, the identification of two variants of the type strain *A. baumannii* ATCC 17978 with distinct genotypes and infection-associated phenotypes is described in **Chapter III**.

Mechanisms of drug resistance

When *A. baumannii* was first recognized as a human pathogen, clinical isolates were susceptible to many commonly available antibiotics. Since then, however, isolates resistant to AGs, carbapenems, and/or the last resort antibiotic colistin all have emerged (174-176). Panresistant strains of *A. baumannii* that are resistant to all clinically available antimicrobials are also encountered at an increased frequency (177, 178). The emergence of MDR and XDR isolates of *A. baumannii* can in part be explained by this pathogen's ability to incorporate or shed genetic material to modify its genome, otherwise known as genomic plasticity (144). The majority of exogenous genetic material incorporated by *A. baumannii* constitutes antibiotic resistance genes (179-181), selected for in part by the use of antimicrobials in healthcare settings (182, 183). Furthermore, many strains of *A. baumannii* harbor intrinsic, chromosomal resistance genes and expression of these genes can be upregulated under certain circumstances. For instance, insertion of the IS*Aba1* element adjacent to a blaOXA-51-like carbapenemase gene conferred resistance to carbapenem antibiotics in multiple clinical isolates of *A. baumannii* (184).

Drug efflux pumps are another mechanism of antimicrobial resistance that is frequently implicated in MDR strains of *A. baumannii*. A common type of drug efflux pump in *A. baumannii* is resistance nodulation-division (RND)-type efflux pumps. RND-type efflux pumps are multi-protein complexes that span all three layers of the Gram-negative cell envelope and are comprised of a substrate-binding IM component, a periplasmic membrane fusion protein, and an OMP (185). The RND-type efflux pump AdeABC confers resistance to aminoglycosides, β-lactams, chloramphenicol, erythromycin, and tetracyclines (186). Normally, expression of this efflux pump is under tight regulation of the AdeRS two-component system (187). However, mutations in AdeRS resulting in overexpression of the AdeABC efflux pump have been identified in several clinical, MDR isolates of *A. baumannii*, suggesting that this represents one mechanism of acquired drug resistance in this pathogen (188). Less common types of efflux pumps include major facilitator superfamily (MFS) transporters such as TetA. MFS transporters transport compounds from the cytosol across the IM to the periplasm (185).

From there, these compounds are exported out of the cell via RND-type efflux pumps. In *A. baumannii*, TetA confers resistance to tetracycline antibiotics (189).

A. baumannii resistance to the last-resort antibiotic colistin is mediated by LOS modification. As described above, colistin-resistant strains can be generated in the lab through exposure to high concentrations of colistin, resulting in isolates that are completely devoid of LOS (or LPS) (167). In colistin-resistant, clinical isolates of *A. baumannii*, resistance is mediated by modification – instead of complete loss – of LOS. Specifically, mutations in the PmrAB two-component system lead to overexpression of the PmrC phosphoethanolamine (PetN) transferase (190). Overexpression of PmrC leads to modification of the LOS lipid A anchor with a PetN moiety, thereby decreasing the overall negative charge of LOS (155, 191). Colistin is a cationic antibiotic that normally binds to the negatively charged LPS/LOS. This binding interaction between cationic colistin and anionic LPS/LOS destabilizes the bacterial OM and results in bacterial cell lysis. Lipid A modifications that decrease the overall negative charge of LOS, therefore, inhibit colistin binding to the bacterial OM (155). Like colistin, AG antibiotics are cationic and interact with the bacterial OM in a similar manner. A more thorough understanding of the molecular interactions between bacterial membranes and (poly)cationic antibiotics, and how these interactions are affected by different host environments, may help preserve or even expand their clinical utility.

Current treatment standards

Treatment of *A. baumannii* infections can be challenging, given this pathogen's propensity for acquiring antimicrobial resistance and the scarcity of available clinical data. For susceptible isolates, β-lactams are the preferred mono-therapy, particularly carbapenems (163). Addition of the β-lactamase inhibitor sulbactam to β-lactam therapy with ampicillin may provide further efficacy against MDR strains (145, 163). In addition to its ability to inhibit bacterial β-lactamase enzymes, an intriguing feature of sulbactam is that it has intrinsic antibacterial activity against *A. baumannii*. Specifically, sulbactam binds and inhibits *A. baumannii* penicillin binding proteins (192). However, as alluded to previously,

carbapenem resistance is becoming increasingly common among clinical isolates of *A. baumannii*, suggesting that monotherapy with a β-lactam antibiotic may become obsolete (39, 163). In the event that β-lactam antibiotics cannot be used, alternative therapeutic options include AG or fluoroquinolone antibiotics (145, 163). Although resistance to both AGs and fluoroquinolones is common among *A. baumannii* isolates, the AGs amikacin and tobramycin have been demonstrated to retain activity against isolates with *in vitro* resistance (145). This is also true for *P. aeruginosa* respiratory infections in patients with CF (37), suggesting that the use of AG antibiotics for the treatment of MDR, Gram-negative pneumonia may be an underexplored treatment option. For the treatment of *A. baumannii* infections, AGs are typically used in combination with other agents such as a carbapenem (145, 163).

Given the concerning antimicrobial resistance profiles of many recent clinical isolates of *A. baumannii*, colistin is employed as a last-resort antibiotic for the treatment of XDR *A. baumannii* infections. As discussed above, colistin works by binding to LOS on the *A. baumannii* OM, and while resistance to colistin does occur, it is relatively uncommon (163). One significant limitation of colistin therapy is its serious side effect profile, most notably neurotoxicity and nephrotoxicity (163). Another limitation is the relatively poor lung penetration of systemically administered colistin (193). Therefore, in the setting of *A. baumannii* pneumonia, colistin is sometimes nebulized and administered as an inhaled therapy. The data on the relative efficacy of inhaled colistin versus intravenous colistin are mixed, although inhaled colistin is associated with less systemic toxicity (163). Colistin may also be combined with other agents to improve clinical outcomes in patients with XDR *A. baumannii* infections. The combination with a carbapenem antibiotic appears to be most effective, and synergy between these two antibiotics has been demonstrated *in vitro* (194). Other colistin-based combination therapies include colistin with rifampin, and colistin with tigecycline (163).

Infections with *A. baumannii* are of growing concern in large part because of its worrisome antimicrobial resistance profile and its ability to persist on (abiotic) surfaces in hospital environments. Furthermore, because it is one of very few organisms that has been observed to be viable in the

absence of LPS or LOS, *A. baumannii* provides an interesting opportunity to study the interactions between Gram-negative pathogens and cell envelope stressors such as antibiotics or immune effector molecules.

1.5 Unknowns and gaps in the field

With the exception of LOS-deficient, colistin-resistant *A. baumannii*, which notably is laboratory-generated, Gram-negative causative agents of pneumonia elaborate a cell-envelope studded with LPS/LOS. Therefore, the Gram-negative cell envelope is an attractive therapeutic target, and compounds that target LPS/LOS are likely to have broad-spectrum activity. The development of novel LPS/LOS-targeting agents is one potential avenue worth exploring. However, the current antimicrobial armamentarium already contains at least two such classes of compounds: polymyxins (e.g. colistin) and AGs. As discussed, the AGs amikacin and tobramycin may retain activity against AG-resistant *A. baumannii* (145), and therapy with inhaled tobramycin is effective in the treatment of CF-related respiratory infections caused by *P. aeruginosa* isolates with *in vitro* resistance to tobramycin (37). While these findings suggest that AG and colistin antibiotics may be uniquely effective in the lung, the mechanisms responsible for this are incompletely understood. A better understanding of these mechanisms may preserve, revitalize, or even expand the clinical utility of these classes of antibiotics. Additionally, identification of the biochemical and biophysical properties of AGs and colistin that are responsible for their increased efficacy inside the lung may lead to the development of novel compounds with similar antimicrobial activity but without the associated neuro- and nephrotoxicity. These gaps in the field will be addressed in this thesis in **Chapter II**.

Studies of *A. baumannii* virulence and pathogenesis typically involve the use of type strains such as *A. baumannii* 17978, *A. baumannii* 19606, and *A. baumannii* AB5075. As with type strains of most other bacterial species, laboratories each maintain their own stocks with limited exchange of genetic information or biological material of wild-type, parental strains. Long-term, parallel laboratory maintenance of bacterial strains, however, may result in genetic divergence of these strains. Such

laboratory adaptation has previously been described for other bacterial species. Continuous maintenance and propagation of *P. aeruginosa* strain PAO1 in laboratories throughout the world has led to substantial genotypic differences among sublines of this strain (195), and two lineages of *Clostridioides difficile* R20291 differ based on a small number of single nucleotide genomic changes leading to distinct phenotypic differences (196). If and to what extent *A. baumannii* laboratory strains differ from each other genetically, as well as the phenotypic consequences of any such genetic differences, remains to be investigated. To what extent long-term laboratory maintenance of *A. baumannii* type strains has contributed to genetic divergence between them and (recent) clinical isolates of this pathogen also warrants further investigation. As discussed, type strains 17978 and 19606 were isolated over a half a century ago (144, 172). To study clinically relevant infection biology, it is important to determine to what extent these and other type strains overlap with clinical isolates in terms of virulence factors and pathogenesis genes. If the infection-related phenotypes of type strains do not reproduce the phenotypes of clinical isolates, the relevance of these strains in pathogenesis studies should be reconsidered. In this thesis, these gaps in knowledge are addressed in **Chapter III**.

Finally, much of the research concerning the involvement of the Gram-negative cell envelope in bacterial pneumonia is focused on proteinaceous bacterial virulence factors such as OMPs. With the notable exception of LPS/LOS, much less is known about the interactions between other bacterial components, such as sugars and lipids, and the host response to infection. How these interactions contribute to pneumonia pathogenesis and drive clinical outcomes is also incompletely understood. As detailed in **Chapter I, section 1.3 – The cell envelope of Gram-negative bacteria**, the Gram-negative cell envelope harbors several lipids aside from LPS/LOS, including the anionic lipid CL. CL plays a role in both bacterial physiology and pathogenesis, as it may help protect bacteria from host-derived cell envelope stressors such as detergent stress (122). Furthermore, bacteria synthesize multiple species of CL and pathogenic bacteria vary based on genomic *cls* gene content (197-199). These findings suggest that there may be inter- and intraspecies variability in terms of cell envelope CL content. However, this remains to be empirically verified. Bacterial CL differentially activates TLR4-mediated

immune signaling based on acyl chain saturation, and mitochondrial CL has been demonstrated to activate the NLRP3 inflammasome (102, 125). Therefore, like LPS/LOS, bacterial CL may shape the host immune response to bacterial infection. To what extent this is the case, and how this affects pneumonia pathogenesis, remains to be fully investigated. In pneumonia, the release of mitochondrial CL into the extracellular environment promotes lung injury (104). Whether the presence of bacterial CL also contributes to lung injury during pneumonia, and to what extent this is governed by variability in bacterial cell envelope CL content, has yet to be fully elucidated. In summary, the potential role of variability in bacterial cell envelope CL content as a driver of inflammation and lung injury at the host-microbe interface in pneumonia is underexplored and merits further investigation. These gaps in the field will be addressed in **Chapter IV**.

CHAPTER II

GRAM-NEGATIVE BACTERIA ACT AS A RESERVOIR FOR AMINOGLYCOSIDE ANTIBIOTICS THAT SYNERGIZE WITH HOST FACTORS TO ENHANCE BACTERIAL KILLING IN A MOUSE MODEL OF PNEUMONIA

Portions of this chapter have been adapted from:

(a): **Wijers CDM**, Pham L, Skaar EP, Palmer LD, and Noto MJ. Gram-negative bacteria act as a reservoir for aminoglycoside antibiotics that synergize with host factors to enhance bacterial killing in a mouse model of pneumonia. At the time of writing, this manuscript is undergoing peer review and being considered for publication.

2.1 Introduction

Aminoglycosides (AGs) comprise a class of antibiotics that inhibit peptide synthesis by binding to the 30S ribosomal subunit resulting in bacterial cell death (27). Despite an overall decline in AG use – in part because of side effects such as nephrotoxicity and ototoxicity (27, 32, 33) – optimized dosing strategies and the emergence of MDR pathogens have ensured continued clinical utility of AGs in certain settings (200-202). AGs are frequently used to treat bacterial lung infections in patients with CF (35). *P. aeruginosa* is a common cause of CF pulmonary infections, and nebulized tobramycin results in increased pulmonary function, decreased bacterial density, and decreased risk of hospitalization (36-38). Treatment with inhaled tobramycin leads to improvements in pulmonary function even when *P. aeruginosa* isolates have increased minimum inhibitory concentration (MIC) values for tobramycin (≥ 8 mg/L), and may therefore be resistant to treatment (37). The use of inhaled AGs is also suggested for the treatment of ventilator-associated pneumonia (VAP) and hospital acquired pneumonia (HAP) (6, 34). In adults with bacteremia, however, AGs are rarely used as monotherapy, and the addition of an AG to treatment with a beta-lactam increases the risk of adverse events without reducing the risk of mortality (203, 204). These findings raise the possibility that AGs may be more effective in the lung.

Previous work describes that exposure of the human pathogen *Acinetobacter baumannii* to an AG antibiotic *in vitro* causes alterations to the bacterium that interact with host factors to achieve broad-

spectrum suppression of pneumonia caused by multiple bacterial pathogens (205). These findings led to the hypothesis that Gram-negative bacteria bind and retain AG antibiotics, which are released in the lung and interact with antibacterial host defenses to enhance bacterial killing. The current work was undertaken to address this hypothesis, as bacterial AG-binding may have implications for the treatment of bacterial lung infections with AG antibiotics.

2.2 Materials and methods

Ethics

All animal experiments were approved by the Vanderbilt University Medical Center (VUMC) Institutional Care and Use Committee and conform to policies and guidelines established by VUMC, the Animal Welfare Act, the National Institutes of Health, and the American Veterinary Medical Association.

Bacterial strains and culture conditions

Bacterial strains and plasmids used in this Chapter are listed in **table 1**. Unless noted otherwise, bacteria were grown to exponential phase (3.5 hours) at 37°C in Lysogeny Broth (LB), and the concentrations of antibiotics used were 40 μg/mL for kanamycin and 50 μg/mL for gentamicin. Exponential-phase bacteria were pelleted by centrifugation at 4,200 × g for 6 minutes and washed twice with equal volumes of ice-cold phosphate-buffered saline (PBS) to remove unbound antibiotics. Bacteria were then resuspended and further diluted in PBS as required for each experiment. Where appropriate, bacterial cultures were chemically killed prior to washing with PBS by adding an equal volume of an ice-cold ethanol/acetone mixture (1:1) and incubating cultures on ice for 10 minutes. Bacteria were then pelleted by centrifugation as above, resuspended in the same volume of fresh ethanol/acetone, and incubated on ice for 10 minutes. Killed bacteria were then washed with and diluted in PBS as described above.

Table 1. Bacterial strains and plasmids used in this Chapter

Strain/plasmid	Description	Source	Mechanism of AG resistance	Kanamycin MIC (mg/L)	Gentamicin MIC (mg/L)	Reference
A. baumannii 17978 VU	*A. baumannii* ATCC 17978 used as wild type (WT) in experiments; Km^S, Gm^S	Noto laboratory, Vanderbilt University (Nashville, TN)	N/A	0.9	0.38 (205)	(206)
A. baumannii 17978/pMU368	WT *Ab* 17978 transformed with pMU368 plasmid conferring kanamycin resistance		*aphA-3* (AG 3'-phospho-transferase)	104.0	0.38 (205)	(205)
P. aeruginosa/pME260	*P. aeruginosa* PAO1 transformed with pME260 plasmid conferring kanamycin resistance		*aph(3')-Ia* (AG 3'-phospho-transferase)	>256	0.54	This Chapter
K. pneumoniae/pCR2.1	*K. pneumoniae* ATCC 43816 transformed with pCR2.1 plasmid conferring kanamycin resistance		*aphA-3* (AG 3'-phospho-transferase)	131.5	0.62	This Chapter
Tn5A7	*Ab* 17978 UN with Tn5 inserted into putative glycosyltransferase (*lpsB*); Km^R		*aphA-3* (AG 3'-phospho-transferase)	128 (205)	1.5 (205)	(207)
A. baumannii 17978 *Δhcp*::gm	*Ab* 17978 with *hcp* replaced by gentamicin resistance cassette; Gm^R	Dr. M. Feldman	*aacC1* (Gm 3-N-acetyl-transferase)	3.0 (205)	>256 (205)	(208)
E. coli DH5α	Standard laboratory strain; Km^S, Gm^S	Noto laboratory, Vanderbilt University (Nashville, TN)	N/A	1.25	1.25	

E. coli DH5α/pCR2.1	Standard laboratory strain transformed with pCR2.1 plasmid conferring kanamycin resistance	Noto laboratory, Vanderbilt University (Nashville, TN)	*aphA-3* (AG 3'-phospho-transferase)	>256	0.83	
P. aeruginosa PAO1	Wound isolate; Km^S, Gm^S	Dr. Andrea Battistoni (Rome, Italy)	N/A	10 (209)	0.46	(210)
K. pneumonia ATCC 43816	Serotype 2 strain; Km^S, Gm^S	Dr. R. Stokes Peebles (Nashville, TN)	N/A	N.D.	1.5	(211)
S. aureus USA300 LAC	Community-associated outbreak strain	Dr. Eric Skaar (Nashville, TN)	N/A	N.D.	1.5	(212)
pCR2.1	Cloning vector conferring kanamycin resistance		*aphA-3* (AG 3'-phospho-transferase)	N/A	N/A	(213)
pME260	*P. aeruginosa* general cloning vector conferring kanamycin resistance	ATCC	*aph(3')-Ia* (AG 3'-phospho-transferase)	N/A	N/A	(214)
pMU368	*A. baumannii* cloning vector conferring kanamycin resistance		*aphA-3* (AG 3'-phospho-transferase)	N/A	N/A	(215)

Murine infection models

Wildtype, female, eight-week-old C57BL/6 mice were purchased from Jackson Laboratories. The murine model of *A. baumannii* pneumonia was performed as previously described (216). For co-inoculation experiments involving killed, kanamycin-susceptible (Km^S) bacteria incubated with kanamycin ± carbonyl cyanide m-chlorophenylhydrazone (CCCP) or $MgSO_4$, cultures were grown until exponential phase after which kanamycin ± CCCP or $MgSO_4$ were added. Cultures were then incubated for an additional 3.5 hours, followed by killing with ethanol/acetone and washing with PBS as described above.

Mice were infected intranasally with 3×10^8 cfu of *A. baumannii* ATCC 17978VU suspended in 30 µL of PBS. *A. baumannii* ATCC 17978UN derivative, Tn5A7 (Δ*lpsB*::Tn5), reliably induces enhanced killing of co-infecting bacteria in the lung after AG exposure independent of disruption of *lpsB* (205). Therefore, Tn5A7 was used as the kanamycin-resistant (Km^R) strain for these experiments. For co-inoculation experiments, bacterial slurries (1×10^{10} cfu/mL) were mixed in a 1:1 ratio prior to intranasal challenge. As such, the total bacterial load in each challenge inoculum (3×10^8 cfu) remained consistent. In one experiment, mice received a second intranasal inoculum of gentamicin in PBS or PBS alone immediately following intranasal infection. At 36 hours post infection (h.p.i.), mice were euthanized and lungs were harvested and homogenized for bacterial enumeration.

Measurement of AG concentrations in bacterial cultures and mouse lungs

To quantify AG concentrations, bacteria were exposed to media supplemented with kanamycin or gentamicin for 3.5 hours, killed, and washed as described above. Mouse lung homogenates were centrifuged and supernatants were collected. Gentamicin and kanamycin were quantified using a competitive enzyme-linked immunoassay (ELISA) (Cell Biolabs, San Diego, CA) using the manufacturer's protocol. Additionally, kanamycin and gentamicin were quantified using liquid chromatography coupled with mass spectrometry (LC-MS) as follows. Samples were derivatized with benzoyl chloride and analyzed on a Thermo LTQ Orbitrap XL mass spectrometer by reverse phase on

an Agilent Poroshell 120 EC-C18 2.7 µM 3.0x50mm column. The gradient started at 50% A (15 mM ammonium acetate + 0.2% acetic acid in 95% water and 5% methanol) and reached 100% B (15 mM ammonium acetate + 0.2% acetic acid in 45% methanol, 45% acetonitrile, and 10% water) in 8 minutes and held for 2.5 minutes before returning to the starting conditions and re-equilibrated for 4.5 minutes.

In vitro co-incubation experiments

Exponential-phase cultures of *A. baumannii* exposed to media alone (LB) or media supplemented with kanamycin were prepared and killed as described above. For *in vitro* co-incubation with *A. baumannii* or *P. aeruginosa*, bacterial slurries (1×10^{10} cfu/mL) were mixed in a 1:1 ratio. Where appropriate, bacterial mixtures were resuspended in PBS supplemented with Triton X-100, deoxycholic acid, surfactant protein B (SP-B), SP-D, or SP-B and SP-D at the indicated concentrations. Alternatively, an equal volume of porcine surfactant (Curosurf, VUMC investigational pharmacy) was added to the bacterial suspensions for a final concentration of 50% pulmonary surfactant. Samples were incubated at 37°C with constant agitation and *A. baumannii* viability was monitored over time.

Measurement of kanamycin and gentamicin MICs

Minimum inhibitory concentrations of kanamycin and gentamicin were determined by spreading 150 µL of a stationary-phase culture of the indicated strain on an LBA plate followed by the placement of an MIC test strip (Liofilchem s.r.l.) on the agar surface. Plates were then incubated at 37° C for 16 hours. Following incubation, MICs were determined by the intersection of the zone of growth inhibition with the test strip.

Quantification and statistical analysis

Statistical analyses were performed using GraphPad Prism version 7. Mean comparisons were performed using unpaired Welch's *t*-test or one-way ANOVA adjusted for multiple comparisons as

appropriate. P values less than 0.05 were considered statistically significant. Statistical details of experiments can be found in the figure legends.

2.3 Results

Gram-negative bacteria bind and retain AG antibiotics, which can collaborate with host factors in the lung to enhance bacterial killing.

To test the hypothesis that Gram-negative bacteria bind kanamycin during *in vitro* exposure and retain it despite multiple washes, *A. baumannii*, *K. pneumoniae*, *P. aeruginosa*, and *E. coli* were exposed to medium with or without kanamycin for 3.5 hours and the concentration of kanamycin in cell pellets of chemically killed bacteria was determined using a competitive ELISA. For each species, a kanamycin-resistant and a kanamycin-susceptible strain was used. The concentration of kanamycin detected in cell pellets of killed, kanamycin-resistant bacteria ranged from approximately 27 (*K. pneumoniae*) to 60 μM (*A. baumannii*) (16 – 35 μg/mL) (**Fig. 1A**). In cell pellets of killed, kanamycin-susceptible bacteria, detected kanamycin concentrations ranged from approximately 16 (*K. pneumoniae*) to 43 μM (*P. aeruginosa*) (9 – 25 μg/mL). No kanamycin was detected in cell pellets of the Gram-positive bacterium *Staphylococcus aureus* (**Fig. 1B**). Similar data were obtained using LC-MS, although low concentrations of kanamycin were detected in cell pellets of *S. aureus* using this more sensitive method (**Fig. 1C**). These data indicate that Gram-negative bacteria bind AGs during *in vitro* exposure and retain them despite multiple washes. Further, as both kanamycin-resistant and kanamycin-susceptible bacteria are equally capable of binding and retaining AGs, these data indicate that the presence of an AG 3'-phosphotransferase kanamycin-resistance determinant is not required for this phenotype.

To determine if AGs bound to Gram-negative bacteria affect the viability of AG-naïve bacteria, unexposed *A. baumannii* was mixed with kanamycin-exposed and killed *A. baumannii* or *P. aeruginosa* *in vitro*. Co-incubation with kanamycin-exposed *A. baumannii* or *P. aeruginosa* did not impact the survival of AG-naïve *A. baumannii* in the mixed suspension (**Fig. 1D**), which is consistent with previous

observations (205). To determine if AGs bound to Gram-negative bacteria affect the viability of AG-naïve bacteria during the course of pneumonic infection, mice were inoculated with kanamycin-exposed and killed *P. aeruginosa*, *K. pneumoniae*, or *E. coli* at the time of infection with live, AG-naïve *A. baumannii*. Inoculation with kanamycin-exposed bacteria resulted in a 4-$\log_{10}$ decrease in *A. baumannii* burdens in the lungs of infected mice, whereas inoculation with kanamycin-unexposed bacteria did not (**Fig. 1E**). These findings demonstrate that the reservoir of AG bound to bacteria is insufficient to affect killing of AG-naïve bacteria *in vitro*, but that AG bound to bacteria is sufficient to affect killing of AG-naïve bacteria in the murine lung. Therefore, these findings suggest that AGs bound to Gram-negative bacteria collaborate with host factors in the lung to kill AG-naïve bacteria.

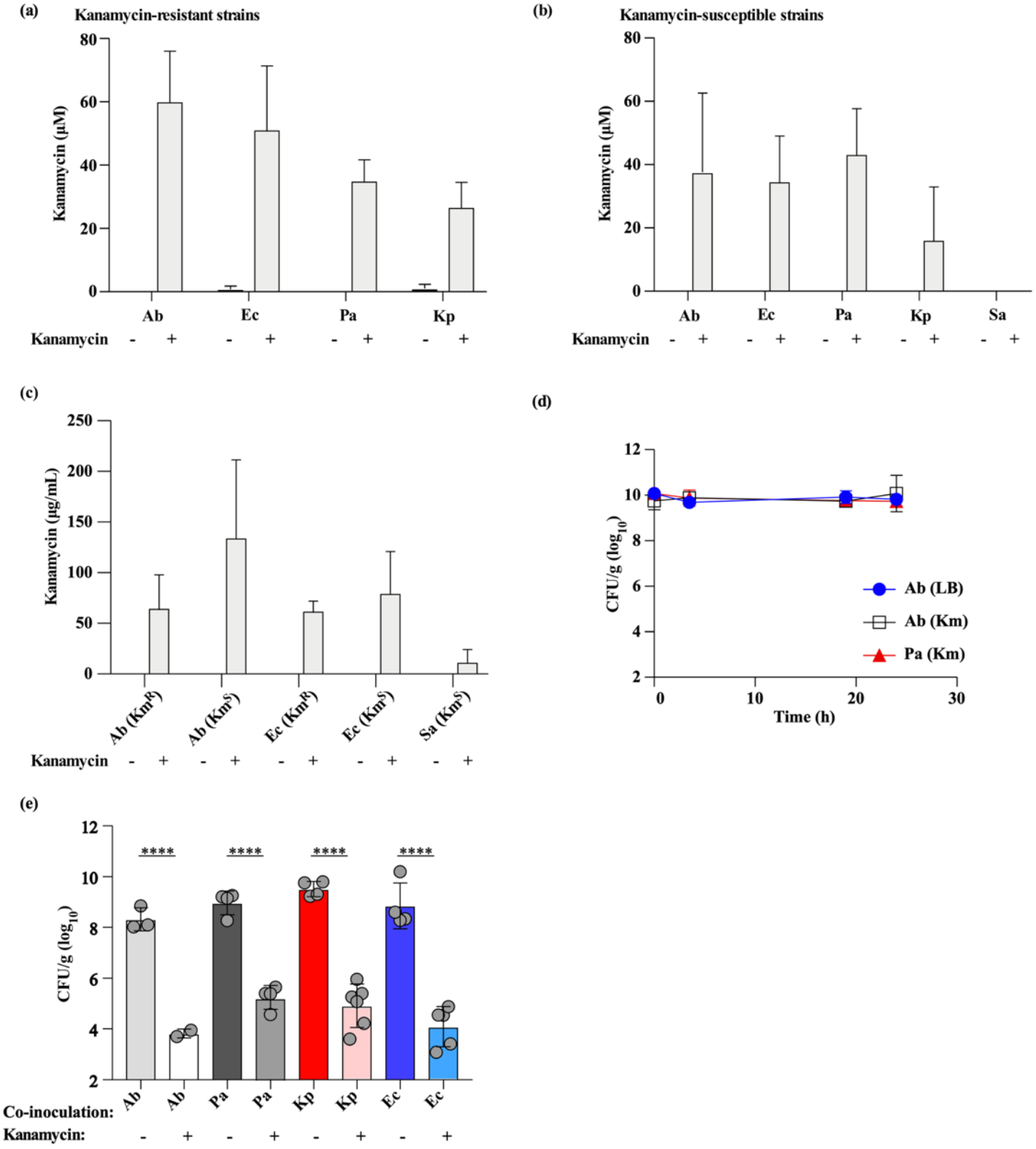
(a)
Kanamycin-resistant strains
Kanamycin (μM)
80
60
40
20
0
Ab
Ec
Pa
Kp
Kanamycin - + - + - + - +
(b)
Kanamycin-susceptible strains
Kanamycin (μM)
80
60
40
20
0
Ab
Ec
Pa
Kp
Sa
Kanamycin - + - + - + - + - +
(c)
Kanamycin (μg/mL)
250
200
150
100
50
0
Ab (KmR)
Ab (KmS)
Ec (KmR)
Ec (KmS)
Sa (KmS)
Kanamycin - + - + - + - + - +
(d)
CFU/g (log10)
12
10
8
6
4
2
0
10
20
30
Time (h)
Ab (LB)
Ab (Km)
Pa (Km)
(e)
CFU/g (log10)
12
10
8
6
4
2
****
****
****
****
Ab
Ab
Pa
Pa
Kp
Kp
Ec
Ec
Co-inoculation:
Kanamycin: - + - + - + - +

Figure 1. Gram-negative bacteria bind and retain AG antibiotics, which can collaborate with host factors in the lung to enhance bacterial killing. (a): *A. baumannii*/pMU368, *E. coli*/pCR2.1, *P. aeruginosa/*pME260, and *K. pneumoniae*/pCR2.1 (all Km^R) were grown in media alone (LB) or media supplemented with kanamycin until mid-exponential phase. (b): Mid-exponential-phase cultures of *A. baumannii*, *E. coli*, *P. aeruginosa*, *K. pneumoniae*, and *S. aureus* (all Km^S) were exposed to media alone (LB) or media supplemented with kanamycin. (a and b): After exposure, bacterial cultures were chemically killed, washed, and kanamycin in bacterial pellets was quantified using a competitive ELISA. (c): *A. baumannii*/pMU368, *A. baumannii*, *E. coli*/pCR2.1, *E. coli*, and *S. aureus* were grown in or exposed to media alone (LB) or media supplemented with kanamycin as above. Kanamycin in cell pellets of chemically killed bacteria was quantified using LC-MS. (d): Mid-exponential-phase *A. baumannii* grown in media without antibiotics (LB) was co-incubated with chemically killed *A. baumannii*, *A. baumannii*/pMU368, or *P. aeruginosa*/pME260 exposed to media alone (LB) or media supplemented with kanamycin as indicated. *A. baumannii* viability was monitored over time. (e): Mice were infected with mid-exponential-phase *A. baumannii* grown in media without antibiotics (LB) and co-inoculated with chemically killed *A. baumannii*/pMU368, *P. aeruginosa*/pME260*, K. pneumoniae*/pCR2.1, or *E. coli*/pCR2.1 exposed to media alone (LB) or media supplemented with kanamycin as indicated. At 36 h.p.i., mice were euthanized and bacterial burdens of the lungs were enumerated. (a-c): N=3 biological replicates per group, per experiment. Columns depict the mean and error bars show standard deviation (a and b) or standard error (c) of the mean. (d): N=3 biological replicates per group, per experiment. Symbols depict the mean and error bars show standard deviation of the mean. (e): Circles represent individual animals, columns depict the mean, and error bars show standard deviation of the mean. Means were compared using a one-way ANOVA adjusted for multiple comparisons. ****: $p<0.0001$; ns: not significant. Ab: *Acinetobacter baumannii*; Ec: *Escherichia coli*; Pa: *Pseudomonas aeruginosa*; Kp: *Klebsiella pneumoniae*; Sa: *Staphylococcus aureus*; Km: kanamycin.

Co-inoculation of mice with AG-bound bacteria is as effective as treatment of mice with inhaled AGs.

To test the hypothesis that Gram-negative bacteria bind and retain AGs other than kanamycin following *in vitro* exposure, Gram-negative bacteria were exposed to gentamicin, and gentamicin concentrations in bacterial cell pellets were quantified using two distinct but complementary methods. Detected gentamicin concentrations ranged from approximately 137 to 403 μM (70 – 208 μg/mL) using a competitive ELISA (**Fig. 2A**). Similar data were obtained using LC-MS (**Fig. 2B**). These data suggest that the binding and retention of AG antibiotics by Gram-negative bacteria is generalizable across multiple kinds of AGs, including kanamycin and gentamicin. However, it was previously demonstrated that this phenotype is specific to this class of antibiotics (205).

To test the hypothesis that intranasal challenge with AG-bound bacteria mimics inhalation treatment with AG solution, mice were infected with live, AG-naïve *A. baumannii* and co-inoculated with killed, gentamicin-resistant (Gm^R) *A. baumannii* exposed to media with or without gentamicin. Immediately after infection, mice were dosed intranasally with gentamicin solution or vehicle (PBS). Mice co-inoculated with gentamicin-bound *A. baumannii* and mice treated with gentamicin solution both exhibited significant reductions in the burden of AG-naïve *A. baumannii* over time. At 0, 4, and 8 h.p.i., *A. baumannii* burdens of mice co-inoculated with gentamicin-bound *A. baumannii* were significantly lower than those of mice treated with gentamicin solution (**Fig. 2C**). To test the hypothesis that AGs can be released from AG-bound bacteria inside the mouse lung, the concentration of gentamicin in lung homogenates of infected mice was measured. Gentamicin was detected in lung homogenates of infected mice treated with gentamicin solution, and in lung homogenates of infected mice co-inoculated with gentamicin-bound *A. baumannii* (**Fig. 2D**). At 0, 4, 8, and 12 h.p.i., the gentamicin concentration was significantly greater in lung homogenates of infected mice treated with gentamicin solution, despite less bacterial killing in this group (**Fig. 2C** and **D**). These data indicate that co-inoculation with AG-bound bacteria introduces AG antibiotics into the lung and achieves bacterial killing that is at least as potent as inhalation treatment with AG solution.

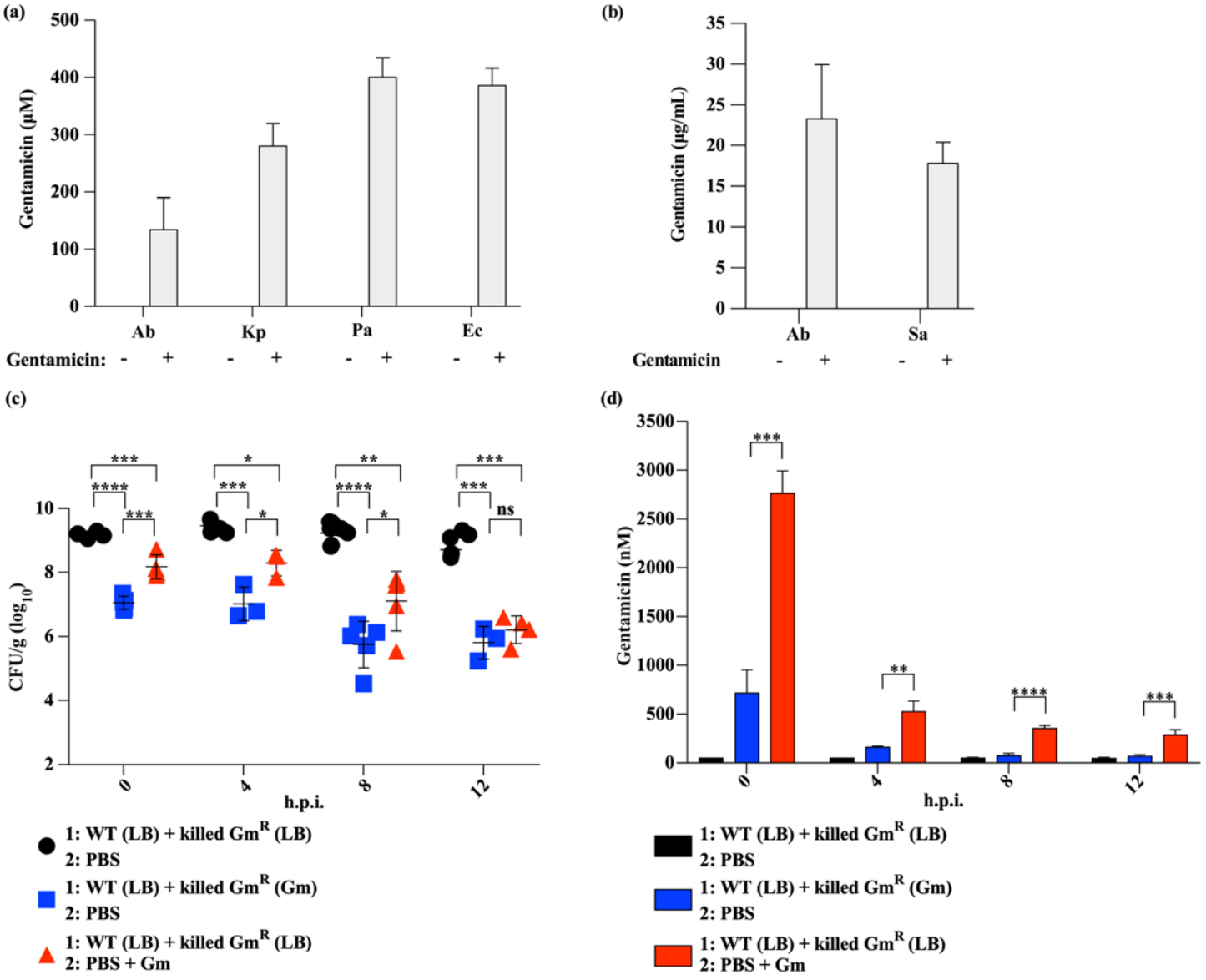
(a)
Gentamicin (μM)
500
400
300
200
100
0
Ab
Kp
Pa
Ec
Gentamicin: - + - + - + - +
(b)
Gentamicin (μg/mL)
35
30
25
20
15
10
5
0
Ab
Sa
Gentamicin - + - +
(c)
CFU/g (log10)
10
8
6
4
2
***
****
***
*
***
*
**
****
*
***
ns
0
4
8
12
h.p.i.
1: WT (LB) + killed GmR (LB)
2: PBS
1: WT (LB) + killed GmR (Gm)
2: PBS
1: WT (LB) + killed GmR (LB)
2: PBS + Gm
(d)
Gentamicin (nM)
3500
3000
2500
2000
1500
1000
500
0
***
**
****
***
0
4
8
12
h.p.i.
1: WT (LB) + killed GmR (LB)
2: PBS
1: WT (LB) + killed GmR (Gm)
2: PBS
1: WT (LB) + killed GmR (LB)
2: PBS + Gm

Figure 2. Co-inoculation of mice with AG-bound bacteria is as effective as treatment of mice with inhaled AGs. (a): *A. baumannii* Δ*hcp*::gm (Gm^R), was grown in media alone (LB) or media supplemented with gentamicin until mid-exponential phase. Mid-exponential-phase cultures of *K. pneumoniae*, *P. aeruginosa*, and *E. coli* (all Gm^S) were exposed to media alone (LB) or media supplemented with gentamicin. After exposure, bacterial cultures were chemically killed and gentamicin in bacterial pellets was quantified using a competitive ELISA. (b): *A. baumannii* Δ*hcp*::gm (Gm^R) was grown in and *S. aureus* (Gm^S) was exposed to media alone (LB) or media supplemented with gentamicin as above. Gentamicin in cell pellets of chemically killed bacteria was quantified using LC-MS. (c): Mice were infected with mid-exponential-phase, WT *A. baumannii* exposed to media without antibiotics (LB) and co-inoculated with *A. baumannii Δhcp*::gm (Gm^R) exposed to LB ± gentamicin as indicated. Immediately after, mice received a second intranasal inoculum of either PBS with gentamicin (64 µg/mL) or PBS alone as indicated. At the indicated times post-infection, mice were euthanized, lungs were harvested, and bacterial burdens were enumerated. (d): concentration of gentamicin detected in lung homogenates of infected mice using a competitive ELISA. (a and b): N=3-4 biological replicates per group, per experiment. Columns depict the mean and error bars show standard deviation of the mean. (c): symbols represent individual animals, center bars depict the mean, and error bars show standard deviation of the mean. (d): Columns depict the mean and error bars show standard deviation of the mean. (c and d): For each time point, means were compared to all other means using a one-way ANOVA adjusted for multiple comparisons. *: $p<0.05$; **: $p<0.01$; ***: $p<0.001$; ****: $p<0.0001$; ns: not significant. Ab: *Acinetobacter baumannii*; Kp: *Klebsiella pneumoniae;* Pa: *Pseudomonas aeruginosa*; Ec: *Escherichia coli;* Sa: *Staphylococcus aureus*; Gm: gentamicin; h.p.i.: hours post-infection.

The Gram-negative outer membrane serves as a reservoir for AG antibiotics.

Gram-negative bacteria bind and retain AG antibiotics during *in vitro* exposure, which can be released inside the murine lung to affect killing of co-infecting bacteria with similar efficacy to mice treated with AG inhalation (**Fig. 2**). The Gram-negative outer membrane (OM) has a net negative charge due to anionic residues on the polar heads of phospholipids, lipopolysaccharide (LPS), and lipooligosaccharide (LOS). These anionic residues are the initial binding sites of polycationic AGs (27, 217-219), and binding can be reduced through the addition of Mg^{2+} (220, 221). AG internalization into the bacterial cytosol is facilitated by the proton motive force (PMF), which can be dissipated by the uncoupler CCCP, thereby reducing AG uptake into the cytosol (27, 74, 221-223). To determine the subcellular location of the Gram-negative AG reservoir, gentamicin-susceptible (Gm^S) *E. coli* or *A. baumannii* was incubated with gentamicin and CCCP or $MgSO_4$. The inhibition of gentamicin internalization or binding to the OM would be expected to reduce bacterial killing by gentamicin. Congruently, addition of either CCCP or $MgSO_4$ significantly reduced killing of *E. coli* and *A. baumannii* by gentamicin (**Fig. 3A** and **4A**). Relative to incubation with gentamicin alone, the addition of CCCP did not significantly alter the concentration of gentamicin detected in *E. coli* cell pellets, whereas addition of $MgSO_4$ decreased the detected concentration of gentamicin by approximately one third (**Fig. 3B**). This suggests that the OM, but not the cytosol, is the predominant bacterial AG reservoir during *in vitro* exposure.

As $MgSO_4$ decreases AG binding by Gram-negative bacteria, it was hypothesized that treatment with $MgSO_4$ would reduce the amount of AG introduced into the lung through the inoculation of AG-bound bacteria. To test this, Km^S *E. coli* was incubated with kanamycin ± CCCP or $MgSO_4$. Kanamycin-mediated killing *in vitro* was assessed, and bacteria were chemically killed and inoculated into the lungs of mice at the time of infection with live, AG-naïve *A. baumannii*. Consistent with data described above, treatment with either CCCP or $MgSO_4$ significantly reduced *in vitro* killing of *E. coli* by kanamycin (**Fig. 3C**). Further, mice co-inoculated with *E. coli* incubated with kanamycin and $MgSO_4$ had an approximate 3-$\log_{10}$ increase in bacteria recovered from the lung in comparison to mice co-inoculated with *E. coli*

incubated with kanamycin alone. Mice co-inoculated with *E. coli* incubated with kanamycin and CCCP had bacterial lung burdens similar to those of mice co-inoculated with *E. coli* incubated with kanamycin alone (**Fig. 3D**). These data indicate that AG binding to the OM, but not internalization to the cytosol, is required to induce AG-mediated killing of AG-naïve, co-infecting bacteria in the mouse lung.

The ability of $MgSO_4$ treatment to inhibit bacterial killing *in vivo* raised the hypothesis that the quantity of AG bound by Gram-negative bacteria is an important determinant of AG-naïve bacterial killing inside the murine lung. To test this, Km^R and Km^S *A. baumannii* were exposed to 0, 10, or 40 μg/mL of kanamycin, killed, and inoculated into the mouse lung at the time of challenge with live, AG-naive *A. baumannii*. Co-inoculation with kanamycin-bound *A. baumannii* enhanced bacterial killing of co-infecting *A. baumannii* in the lung in a dose-dependent manner. Further, Km^R and Km^S *A. baumannii* were equally effective at increasing AG-mediated killing of AG-naïve *A. baumannii* (**Fig. 3E**). These findings suggest that the quantity of AG bound by the OM *in vitro* determines the degree of AG-naïve bacterial killing in the mouse lung. Additionally, these data indicate that kanamycin modification in the cytosol by the AG 3'-phosphotransferase kanamycin resistance determinant does not impair bacterial killing mediated by the OM AG reservoir.

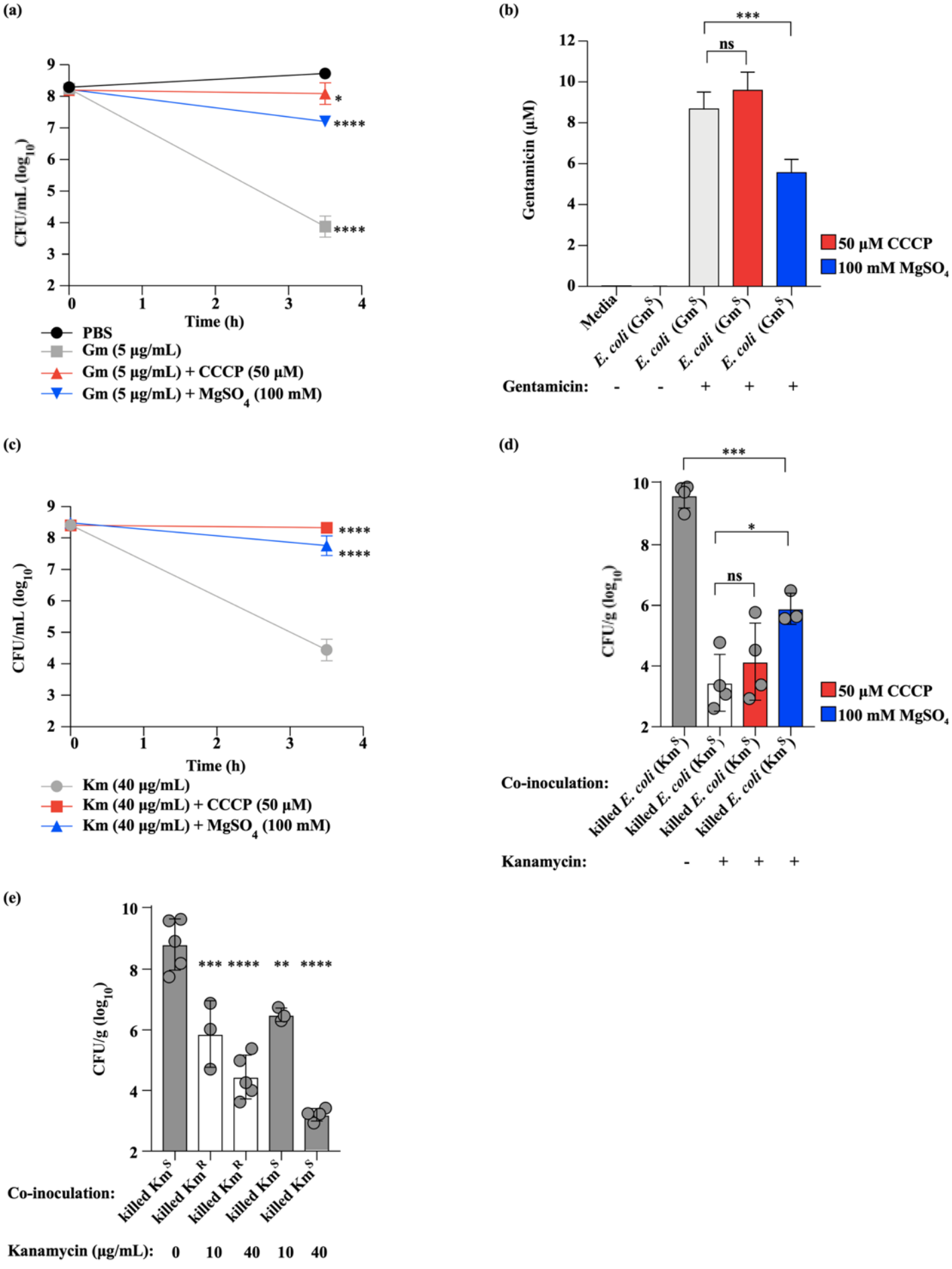
(a)
CFU/mL (log10)
Time (h)
PBS
Gm (5 μg/mL)
Gm (5 μg/mL) + CCCP (50 μM)
Gm (5 μg/mL) + MgSO4 (100 mM)
*
****
****
(b)
Gentamicin (μM)
***
ns
50 μM CCCP
100 mM MgSO4
Media
E. coli (Gm^S)
Gentamicin: - - + + +
(c)
CFU/mL (log10)
Time (h)
Km (40 μg/mL)
Km (40 μg/mL) + CCCP (50 μM)
Km (40 μg/mL) + MgSO4 (100 mM)
****
****
(d)
CFU/g (log10)
***
*
ns
50 μM CCCP
100 mM MgSO4
killed E. coli (Km^S)
Co-inoculation:
Kanamycin: - + + +
(e)
CFU/g (log10)
*** **** ** ****
killed Km^S
killed Km^R
Co-inoculation:
Kanamycin (μg/mL): 0 10 40 10 40

Figure 3. The Gram-negative outer membrane serves as a reservoir for AG antibiotics. (a and b): *E. coli* (Gm^S) was grown until mid-exponential phase in media alone (LB) and subsequently exposed to PBS or gentamicin ± CCCP or $MgSO_4$ for an additional 3.5 hours, after which all bacteria were chemically killed. Viable bacteria were enumerated immediately prior to and after exposure to gentamicin (a) and gentamicin in cell pellets of chemically killed bacteria was quantified using a competitive ELISA (b). (c and d): Mice were infected with mid-exponential phase *A. baumannii* grown in media alone (LB) and co-inoculated with chemically killed *E. coli* (Km^S) exposed to kanamycin ± CCCP or $MgSO_4$ as indicated. Viable *E. coli* were enumerated immediately prior to and after exposure to kanamycin (c). Mice were euthanized at 36 h.p.i. and *A. baumannii* burdens of the lungs were determined (d). (e): Mice were infected with mid-exponential phase, WT *A. baumannii* grown in media alone (LB) and co-inoculated with chemically killed *A. baumannii* Tn5A7 (Km^R) or WT *A. baumannii* (Km^S) exposed to kanamycin as indicated. Mice were euthanized at 36 h.p.i. and bacterial burdens of the lungs were determined. (a and c): N=4 (a) or N=5 replicates (c) per group, per experiment. Symbols depict the mean and error bars show standard deviation of the mean. Means were compared to the mean bacterial viability of the untreated group (PBS) (a) or to the group treated with kanamycin alone (Km) (c) using a one-way ANOVA adjusted for multiple comparisons. (b): N=3-4 biological replicates per group, per experiment. Columns depict the mean and error bars show standard deviation of the mean. Means were compared to all other means using a one-way ANOVA adjusted for multiple comparisons. (d and e): Circles represent individual animals, columns depict the mean, and error bars show standard deviation of the mean. Means were compared to all other means (d) or to the mean of the first column (e) using a one-way ANOVA adjusted for multiple comparisons. *: $p<0.05$; **: $p<0.01$; ***: $p<0.001$; ****: $p<0.0001$; ns: not significant. Km: kanamycin; Gm: gentamicin.

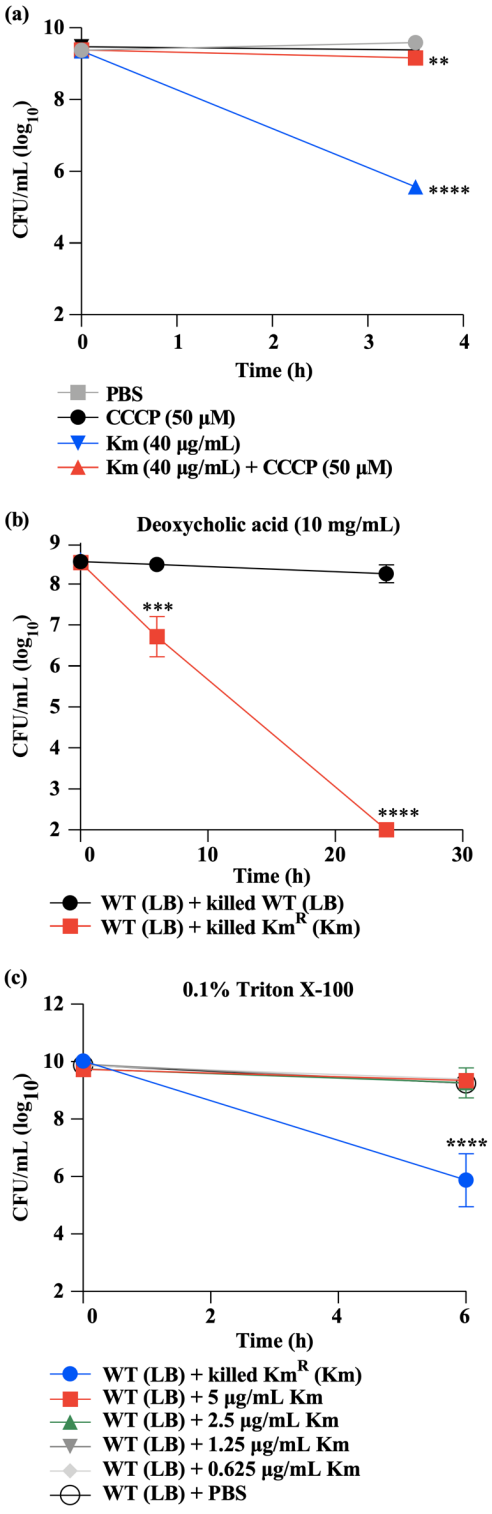
(a)
CFU/mL (log10)
Time (h)
**
****
PBS
CCCP (50 µM)
Km (40 µg/mL)
Km (40 µg/mL) + CCCP (50 µM)
(b)
Deoxycholic acid (10 mg/mL)
CFU/mL (log10)
Time (h)
***
****
WT (LB) + killed WT (LB)
WT (LB) + killed KmR (Km)
(c)
0.1% Triton X-100
CFU/mL (log10)
Time (h)
****
WT (LB) + killed KmR (Km)
WT (LB) + 5 µg/mL Km
WT (LB) + 2.5 µg/mL Km
WT (LB) + 1.25 µg/mL Km
WT (LB) + 0.625 µg/mL Km
WT (LB) + PBS

Figure 4. *In vitro* co-incubation with kanamycin-bound bacteria and biologic detergents potentiates AG-mediated killing of AG-naïve *A. baumannii*. (a): Mid-exponential phase *A. baumannii* was incubated with PBS, CCCP, and/or kanamycin as indicated for 3.5 hours and bacterial viability was monitored over time (b): Mid-exponential phase *A. baumannii* exposed to media alone (LB) was co-incubated with killed, WT *A. baumannii* exposed to media alone (LB) or killed, kanamycin-bound *A. baumannii* Tn5A7 (Km^R) as indicated and deoxycholic acid. Bacterial viability was measured over time. (c): Mid-exponential phase WT *A. baumannii*, grown in media alone (LB), was co-incubated with killed, kanamycin-bound *A. baumannii* Tn5A7 (Km^R) or varying concentrations of kanamycin as indicated. Bacterial mixtures were resuspended in PBS supplemented with Triton X-100, and bacterial viability was monitored over time. (a-c): N=3 biological replicates per group, per experiment. Graphs depict representative data from two independent experiments. Symbols depict the mean and error bars show standard deviation of the mean. For each time point, means were compared using a Welch's *t*-test (b) or one-way ANOVA adjusted for multiple comparisons (a and c). **: $p<0.01$; ***: $p<0.001$; ****: $p<0.0001$. Km: kanamycin.

AG-bound bacteria interact with pulmonary surfactant to affect AG-mediated killing of co-infecting bacteria.

AG molecules are released from AG-bound bacteria to increase killing of co-infecting bacteria inside the mouse lung with similar efficacy to inhalation treatment with AG solution (**Fig. 2**). However, AG-bound bacteria do not alter the viability of AG-naïve bacteria *in vitro* or in a mouse model of systemic infection (**Fig. 1D** and ref. 205). These findings suggest that AG-bound bacteria collaborate with host factors inside the mouse lung to affect bacterial killing. Pulmonary surfactant is abundant in the fluid lining the distal airways and alveolar spaces, and is encountered by bacteria upon pneumonic infection in mice (123, 124). To test the hypothesis that pulmonary surfactant combined with AG-bound bacteria affects bacterial killing, live, AG-naïve *A. baumannii* was incubated with killed, kanamycin-bound *A. baumannii* and porcine surfactant, and bacterial survival was assessed. Relative to incubation with *A. baumannii* exposed to media alone (LB), incubation with kanamycin-bound *A. baumannii* significantly decreased survival of AG-naïve *A. baumannii* in the presence of porcine surfactant (**Fig. 5A**). This suggests that AG-bound bacteria interact with pulmonary surfactant to increase killing of co-infecting bacteria inside the mouse lung.

To identify the component(s) of pulmonary surfactant that interact with AG-bound bacteria to affect bacterial killing, the antibacterial effects of individual components of pulmonary surfactant combined with AG-bound bacteria were determined. Pulmonary surfactant contains several proteins with antibacterial properties, such as SP-B and SP-D (72, 73). In the presence of 5 μg/mL SP-B and/or 25 μg/mL SP-D (72), co-incubation with killed, kanamycin-bound *A. baumannii* resulted in a small decrease in viable, AG-naïve *A. baumannii* after 24 hours (**Fig. 5B–D**). Pulmonary surfactant is composed of 90% lipids and acts as a molecular detergent (71). To test the hypothesis that detergent components of pulmonary surfactant combine with AG-bound bacteria to potentiate bacterial killing, live, AG-naïve *A. baumannii* was incubated with killed, kanamycin-bound *A. baumannii* and the nonionic detergent Triton X-100. Relative to co-incubation with killed, unexposed *A. baumannii*, co-incubation with kanamycin-bound *A. baumannii* significantly decreased the survival of AG-naïve *A. baumannii* over

time (**Fig. 5E**). Similar results were obtained with deoxycholic acid, an antimicrobial, detergent-like bile acid (**Fig. 4B**) (224). When combined with Triton X-100, AG-naïve *A. baumannii* killing increased with increasing concentrations of kanamycin, and co-incubation with kanamycin-bound *A. baumannii* was more potent than the highest concentration of kanamycin tested (**Fig. 5F** and **4C**). These findings demonstrate that the enhanced bacterial killing mediated by AG-bound bacteria is facilitated predominately by detergents – and to a lesser extent by proteins – of host-derived pulmonary surfactant. Collectively, these data suggest that collaboration between AG-bound bacteria and pulmonary surfactant enhances bacterial killing in the murine lung.

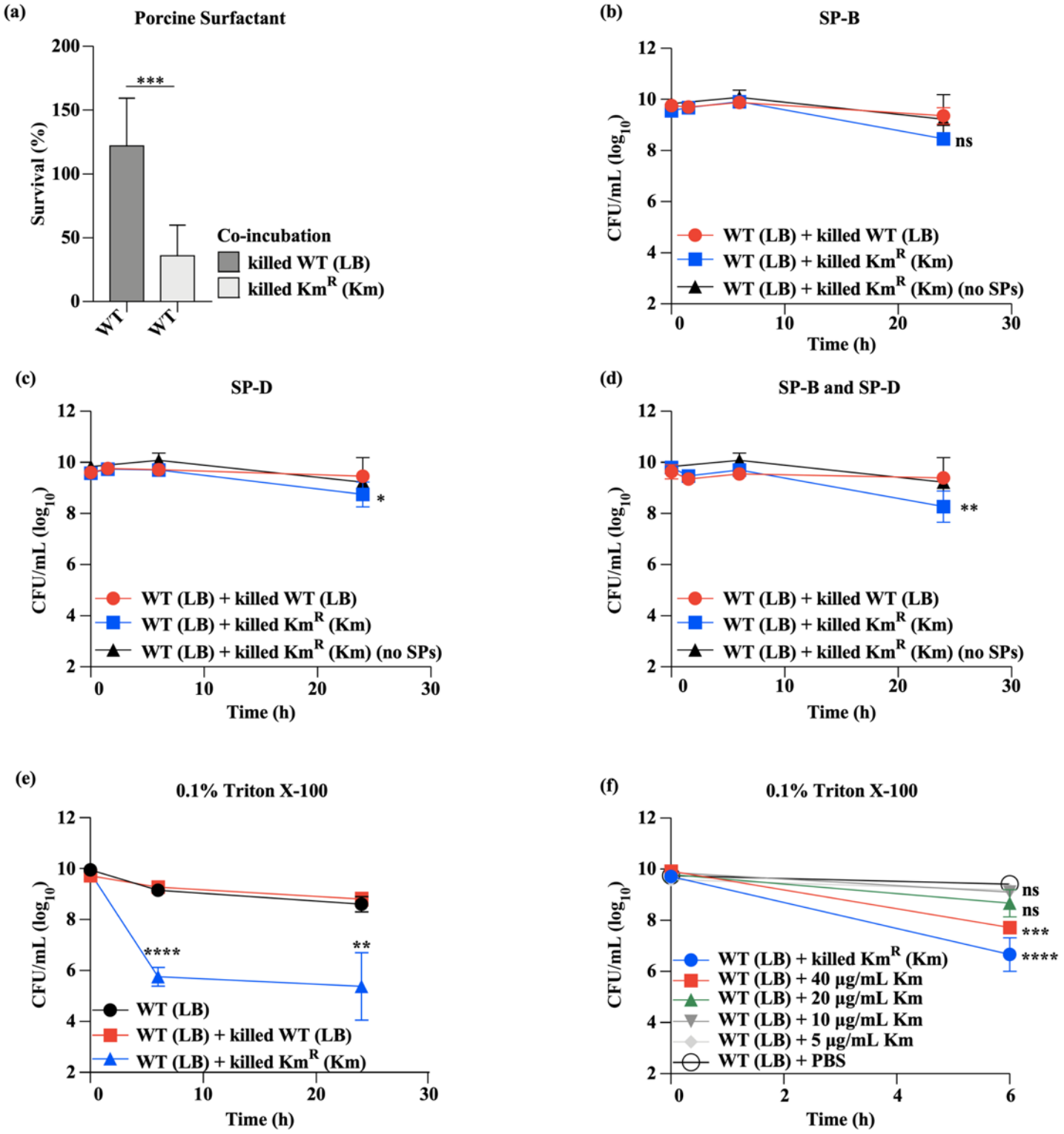
(a)
Porcine Surfactant
Survival (%)
200
150
100
50
0
***
WT
WT
Co-incubation
killed WT (LB)
killed Km^R (Km)
(b)
SP-B
CFU/mL (log10)
12
10
8
6
4
2
ns
WT (LB) + killed WT (LB)
WT (LB) + killed Km^R (Km)
WT (LB) + killed Km^R (Km) (no SPs)
0
10
20
30
Time (h)
(c)
SP-D
CFU/mL (log10)
*
WT (LB) + killed WT (LB)
WT (LB) + killed Km^R (Km)
WT (LB) + killed Km^R (Km) (no SPs)
Time (h)
(d)
SP-B and SP-D
CFU/mL (log10)
**
WT (LB) + killed WT (LB)
WT (LB) + killed Km^R (Km)
WT (LB) + killed Km^R (Km) (no SPs)
Time (h)
(e)
0.1% Triton X-100
CFU/mL (log10)
****
**
WT (LB)
WT (LB) + killed WT (LB)
WT (LB) + killed Km^R (Km)
Time (h)
(f)
0.1% Triton X-100
CFU/mL (log10)
ns
ns
***
****
WT (LB) + killed Km^R (Km)
WT (LB) + 40 µg/mL Km
WT (LB) + 20 µg/mL Km
WT (LB) + 10 µg/mL Km
WT (LB) + 5 µg/mL Km
WT (LB) + PBS
0
2
4
6
Time (h)

Figure 5. AG-bound bacteria interact with pulmonary surfactant to affect AG-mediated killing of co-infecting bacteria in the mouse lung. (a): Mid-exponential-phase WT *A. baumannii* exposed to media alone (LB) was co-incubated with killed, WT *A. baumannii* grown in media alone (LB) or killed, kanamycin-bound *A. baumannii* Tn5A7 (Km^R) as indicated. Bacterial mixtures were resuspended in PBS supplemented with 50% (v/v) porcine surfactant. Bacterial survival was measured 1.5 hours after incubation. (b-d): Mid-exponential-phase WT *A. baumannii* exposed to media alone (LB) was co-incubated with killed, WT *A.* baumannii grown in media alone (LB) or killed, kanamycin-bound *A. baumannii* Tn5A7 (Km^R) as indicated. Bacterial mixtures were resuspended in PBS supplemented with 5 µg/mL SP-B (b), 25 µg/mL SP-D (c), 5 µg/mL SP-B and 25 µg/mL SP-D (d), or PBS (no SPs). Bacterial survival was measured over time. (e and f): Mid-exponential-phase WT *A. baumannii*, grown in media alone (LB), was incubated with or without killed *A. baumannii* or varying concentrations of kanamycin as indicated. Where indicated, WT *A. baumannii* was co-incubated with killed, WT *A. baumannii* grown in media alone (LB) or killed, kanamycin-bound *A. baumannii* Tn5A7 (Km^R). Bacterial cultures were resuspended in PBS supplemented with 0.1% Triton X-100 and bacterial viability was monitored over time. (a-f): N=3-4 biological replicates per group, per experiment. Graphs depict average (a-d) or representative (e and f) data from at least two independent experiments. Columns (a) or symbols (b-f) depict the mean, and error bars show standard deviation of the mean. Means were compared using a Welch's *t*-test (a) or a one-way ANOVA adjusted for multiple comparisons, for the 24h time point (b-d) or for each time point (e and f). *: $p<0.05$; **: $p<0.01$; ***: $p<0.001$; ****: $p<0.0001$; ns: not significant. Km: kanamycin.

2.4 Discussion

The findings presented herein support a model by which the Gram-negative OM binds and retains AG molecules, that AGs are released from AG-bound bacteria in the lung, and that these AGs increase killing of AG-naïve bacteria (**Fig. 6**). The finding that AGs are bound and retained by exposed bacteria at high levels despite multiple washes was not expected. However, a labeled derivative of the AG neomycin binds OMs in a saturable fashion, and these interactions are strong enough to withstand multiple washes (225). Therefore, these findings suggest that the electrostatic interactions between cationic AGs and negatively charged bacterial OMs are strong enough to withstand multiple washes and that the OM may act as a reservoir for cationic small molecules such as AGs.

The studies described in this chapter expand on the observation that AGs continue to kill bacteria after the antibiotic itself is removed – the so-called post-antibiotic effect (226). AGs interact with bacteria by binding to anionic sites on Gram-negative cell envelopes such as the polar heads of phospholipids and LPS (or LOS) (27, 217-219). Here, several lines of evidence that implicate the OM as the predominant Gram-negative reservoir for AG molecules are presented. The divalent cation Mg^{2+} stabilizes Gram-negative OMs and prevents AG binding (219-221, 227). Addition of Mg^{2+} during AG exposure decreases the concentration of AG detected in bacterial cell pellets and inhibits the killing of co-infecting bacteria upon subsequent pneumonic infection of mice. However, addition of the uncoupler agent CCCP, which dissipates the PMF and prevents AG entry into the bacterial cytosol (221-223), does not. Further, both AG-resistant and AG-susceptible bacteria bind and retain AGs following exposure (**Fig. 1A** and **B; Fig. 2A**), and are equally capable of enhancing bacterial killing inside the mouse lung after AG-exposure (**Fig. 3D** and **E**). In the AG-resistant strains used in the present Chapter, resistance is imparted by AG modifying enzymes (**Table 1**). AGs modified by bacterial enzymes have decreased binding affinity for bacterial ribosomes (228), making the cytosol an unlikely AG reservoir. Although these findings are most consistent with the OM being the major reservoir for AG antibiotics, bacterial uptake of AGs can occur in the absence of the PMF (229). Therefore, some contribution of the bacterial cytosol to AG binding and retention cannot be completely excluded. Finally, in contrast to

Gram-negative bacteria, AG binding and retention by the Gram-positive pathogen *S. aureus* differed based on the specific AG antibiotic tested, as *S. aureus* bound gentamicin to a greater extent than kanamycin following *in vitro* exposure. The subcellular location of the Gram-positive AG reservoir remains to be identified.

This Chapter provides evidence that killing of co-infecting bacteria inside the mouse lung mediated by AG-bound bacteria may be facilitated by pulmonary surfactant. It is plausible that pulmonary surfactant permeabilizes the cell envelopes of AG-naïve bacteria, promoting entry of AGs introduced into the mouse lung by AG-bound bacteria. This notion is consistent with previous reports demonstrating that molecular detergents, SP-A, and SP-D increase bacterial membrane permeability, and that detergents increase bacterial susceptibility to AG antibiotics (72, 74). A more thorough understanding of the molecular interactions between these two factors may help explain why AG-mediated killing of co-infecting bacteria inside the mouse lung appears to be more effective when mice are co-inoculated with AG-bound bacteria as opposed to AGs in solution, even though pulmonary AG concentrations are higher in the latter group (**Fig. 2**). As this finding suggests that the greatest efficiency of bacterial killing inside the murine lung is achieved when AGs are bound to bacteria, a possible contribution of unidentified bacterial factors cannot be excluded. Similarly, a potential role for additional host-derived factors cannot be excluded.

This work may help explain why AGs are more often used to treat bacterial lung infections relative to bacterial infections of other organ systems. Inhaled AGs (with or without the addition of systemic antibiotics) are suggested for the treatment of VAP or HAP (6, 34). By contrast, in patients with urinary tract infections, AGs are equally as effective as beta-lactams or quinolones in achieving clinical improvement, but are associated with higher rates of bacteriological failure at the end of treatment (230). In patients with bacteremia, use of an AG instead of or in addition to a beta-lactam does not improve cure rates or reduce the risk of mortality, but does increase the risk of adverse events such as nephrotoxicity (204, 230-232). These data are consistent with previous work demonstrating that co-inoculation with AG-bound bacteria does not increase killing of co-infecting bacteria in a mouse

model of systemic infection (205). In patients with CF, treatment with inhaled AGs for bacterial lung infections has clinical benefits even if infecting isolates exhibit elevated MICs suggestive of *in vitro* resistance (≥ 8 mg/L) (37). Patients with CF are often colonized by a multitude of bacterial species with varying antibiotic resistance profiles, resulting in polymicrobial infections of the respiratory system (233-237). This Chapter raises the hypothesis that AG-resistant strains within the CF lung may bind and retain bioactive AG molecules during treatment with inhaled AGs, which could then kill susceptible, co-infecting organisms. This is consistent with the prior observation that co-inoculation with kanamycin-bound bacteria may increase bacterial killing even if the co-infecting strain has an elevated kanamycin MIC (> 40 mg/L) (205).

Limitations of the studies described in this Chapter include a lack of definitive evidence confirming the role for pulmonary surfactant interactions with AGs in facilitating bacterial killing in the lungs of mice. However, as mice deficient in pulmonary surfactant phospholipid synthesis exhibit respiratory distress and perinatal mortality, the impact of the loss of pulmonary surfactant during bacterial pneumonia cannot be ascertained using this model system (238). Similarly, AG binding and retention by bacterial OMs was not visualized directly. However, a recent study demonstrated that a fluorescent derivative of neomycin interacts with bacterial OMs (225).

Overall, this Chapter provides mechanistic insights into the antibacterial activity of AGs in the lung by demonstrating that: (i) Gram-negative pathogens act as a reservoir for AG antibiotics; (ii) AG-bound bacteria synergize with pulmonary surfactants in the lung to achieve AG-mediated enhanced bacterial killing; and (iii) AGs released from the Gram-negative bacterial reservoir may be more potent than AGs administered directly to the lung. These mechanisms may explain, in part, clinical observations of AG efficacy in the lung despite the organism's *in vitro* resistance to AG antibiotics.

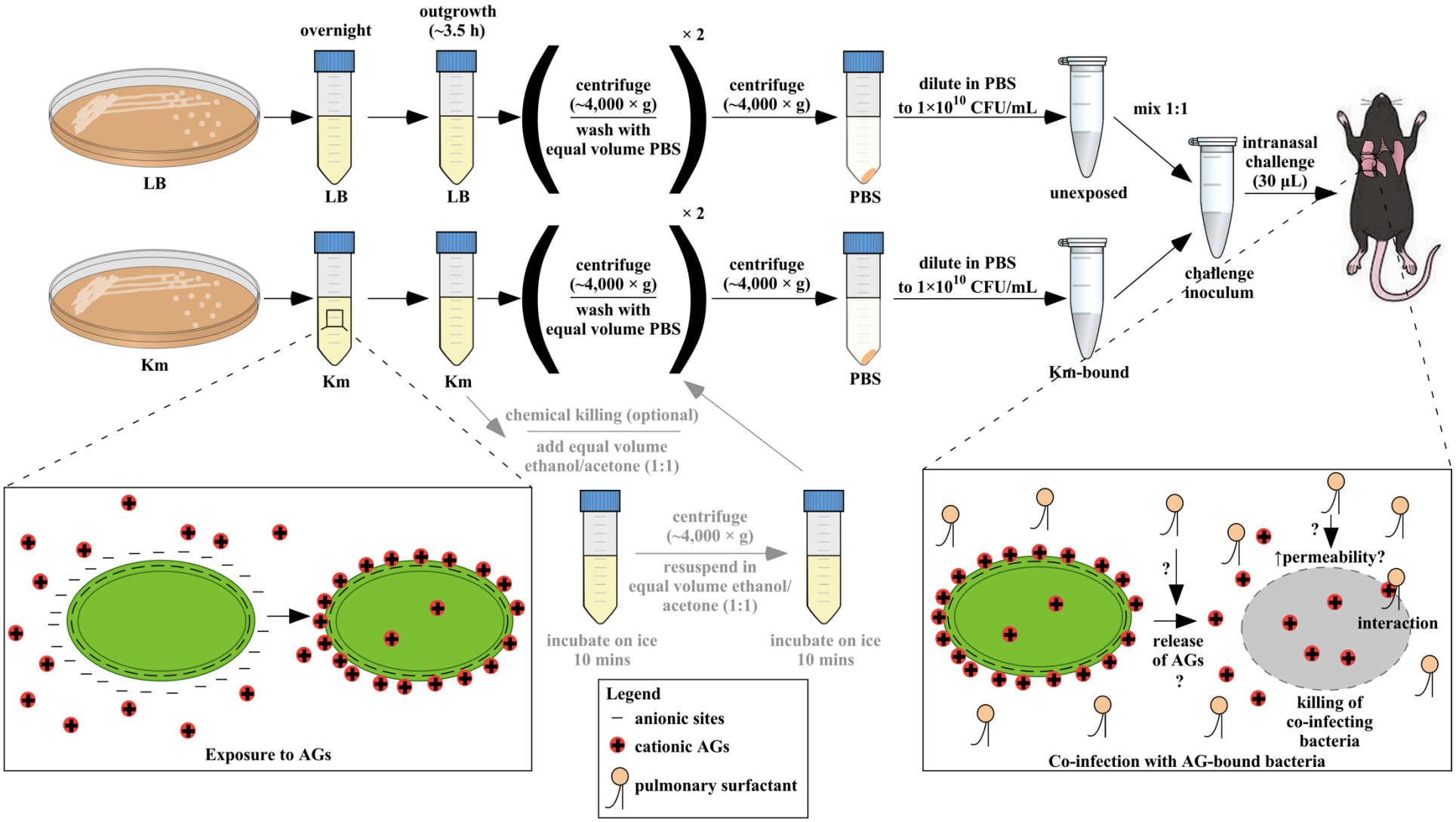

Figure 6. Working model of increased killing of co-infecting bacteria inside the murine lung mediated by AG-bound bacteria. Prior to intranasal challenge of mice, bacteria are grown in media alone (LB) or media supplemented with kanamycin (Km), washed, and diluted in PBS to 1×10^{10} cfu/mL. For co-infections and co-inoculations, bacterial suspensions (at 1×10^{10} cfu/mL) are mixed in a 1:1 ratio. During AG exposure, Gram-negative bacteria bind bioactive AG molecules to their OM which are retained despite multiple washes. Inside the mouse lung, AG-bound bacteria collaborate with pulmonary surfactant to enhance killing of susceptible, co-infecting bacteria.

CHAPTER III

IDENTIFICATION OF TWO VARIANTS OF *ACINETOBACTER BAUMANNII* STRAIN ATCC 17978 WITH DISTINCT GENOTYPES THAT DIFFERENTIALLY INTERACT WITH THE HOST IN EXPERIMENTAL PNEUMONIA

Portions of this Chapter have been adapted from:

(a): **Wijers CDM**, Pham L, Menon S, Boyd KL, Noel HR, Skaar EP, Gaddy JA, Palmer LD, and Noto MJ. 2021. Identification of Two Variants of *Acinetobacter baumannii* Strain ATCC 17978 with Distinct Genotypes and Phenotypes. Infect Immun 89(12): e0045421.

3.1 Introduction

Acinetobacter baumannii is a Gram-negative, opportunistic pathogen that is a common cause of infections such as pneumonia, wound infections, and sepsis (144-146). Infections with *A. baumannii* are often severe, and mortality rates associated with *A. baumannii* pneumonia are as high as 60% (151, 239). Further complicating infections with *A. baumannii* is the emergence of multi-drug resistant (MDR) isolates. Isolates resistant to aminoglycosides (174, 240, 241), carbapenems (175, 242-244), and the last resort antibiotic, colistin (176, 245-248), have emerged as the causative agents of human disease over the last few decades. Pan-resistant strains of *A. baumannii* that are resistant to all clinically available antimicrobials are also encountered at an increased frequency (177, 178). Because of this, the Centers for Disease Control and prevention have indicated carbapenem-resistant *A. baumannii* as an urgent threat (39). Studies of antibiotic resistant *A. baumannii* primarily rely on clinical isolates (249, 250), whereas studies of bacterial pathogenesis and infection biology often rely on type strains. Type strains are descendants of the original isolates that exhibit all of the relevant phenotypic and genotypic properties cited in the original published taxonomic circumscriptions (170). Strains 17978, 19606, and AB5075 are examples of type strains used to study *A. baumannii* pathogenesis. *A. baumannii* 17978 was isolated in 1951 from an infant with meningitis and is susceptible to most antibiotics (171), *A. baumannii* 19606 was isolated in 1948 from the urine of a patient with a urinary tract infection (172),

and *A. baumannii* AB5075 was isolated in 2008 from the tibia of a patient with osteomyelitis (173). These type strains have been used to identify *A. baumannii* genes required for persistence in the lung and to study *A. baumannii* virulence factors (173, 251-257).

Strains of *A. baumannii* exhibit genomic plasticity through the incorporation and loss of genetic material (144, 258), underscored by genomic analyses of *A. baumannii* that have revealed an unusually large number of "singleton" genes that are unique to a given strain of *A. baumannii* and do not occur in other strains (259). The majority of exogenous genetic material incorporated by *A. baumannii* constitutes antibiotic resistance genes (179-181), selected for in part by the use of antimicrobials in healthcare settings (182, 183). This suggests that gene acquisition contributes to the emergence of MDR isolates of *A. baumannii*. Gene loss also contributes to differential patterns of antimicrobial resistance among *A. baumannii* as a partial deletion of Tn1548 in *A. baumannii* ABUH315100 resulted in the deletion of *armA* amikacin resistance gene (249). *A. baumannii* genomic plasticity also facilitates changes that affect virulence and interactions with its environment, including competing bacteria and healthcare settings (179). For instance, disruption of the *gtr6* gene by spontaneous transposon insertion eliminates a branch point in the capsular carbohydrate structure of the clinical isolate HUMC1 and renders it hypervirulent in a mouse model of bacteremia (70). Further, several MDR strains of *A. baumannii* have acquired the plasmid pAB3 and related plasmids, which harbor multiple antibiotic resistance genes and encode repressors of the *A. baumannii* Type 6 Secretion System (T6SS), which can be used to directly kill competing bacteria (208, 260). Other clinical isolates of *A. baumannii* have lost genes encoding the T6SS (181, 261). This suggests that subpopulations of *A. baumannii* that have lost T6SS genes or harbor pAB3 have a competitive advantage in environments where antibiotics are present, such as healthcare facilities. By contrast, subpopulations of *A. baumannii* that harbor T6SS genes and lack pAB3 are able to actively attack competing bacteria.

Here, the identification of two variants of *A. baumannii* ATCC 17978 is described. These variants have been used interchangeably in pathogenesis studies but differ by the presence of an accessory locus and have unique attributes when interacting with host factors both *in vitro* and *in vivo*. The studies

described in this Chapter demonstrate how these interactions differentially affect the pathogenesis of *A. baumannii* pneumonia.

3.2 Results

Two common variants of A. baumannii ATCC 17978 differ by the presence of an accessory genetic locus and multiple single nucleotide polymorphisms.

During investigations into the genetic determinants of *A. baumannii* pathogenesis using a Tn5 transposon mutant library of *Ab* 17978, conserved phenotypes were observed among several Tn mutants containing insertions into unrelated genes. In a macrophage model of *A. baumannii* infection, murine bone marrow derived macrophages (BMDMs) produced differential quantities of the pro-inflammatory cytokine IL-1β upon infection with multiple Tn mutants than when infected with WT *A. baumannii* 17978 (**Fig. 7A**). In addition, phenotypic profiling of these mutants using scanning electron microscopy (SEM) revealed the presence of pili on the surface of multiple Tn mutants but not on the WT strain (**Fig. 7B** and **C**). As the Tn5 library had been constructed at a different institution, the finding of conserved phenotypes among multiple Tn insertion mutants raised concern that the parental *Ab* 17978 variant used for library construction differed from the *Ab* 17978 variant used as a comparator for the BMDM infection and SEM experiments. To test this hypothesis, the genome sequences of the parental variant used for library construction (*Ab* 17978 UN), and the variant used as the comparator in the BMDM infection and SEM assays (*Ab* 17978 VU) were determined by PacBio sequencing (262). Structural comparison of these genomes revealed several differences, including differences in the size of the genomes, as well as different locations of an IS701-like element within each genome (**Table 2**). Notably, the genome of *Ab* 17978 UN contained a 44 kb locus, encompassing multiple accessory genes, that was not present in the genome of *Ab* 17978 VU (**Table 2, Fig. 8A, Table 3**). This locus was named AbaAL44 (*Acinetobacter baumannii* accessory locus 44 kb). The accessory genes present within AbaAL44 include putative biosynthesis genes, transcriptional regulators, genes associated with replication, as well as several putative bacterial pathogenesis genes. AbaAL44 includes *smf-1, yadV,*

htrE, and *mrkD*, which together are predicted to encode a Type I pilus or fimbriae; a gene predicted to encode a catalase (*KZA74_09300*); and a gene predicted to encode a CL synthase (*clsC2*) (**Fig. 8A, Table 3**). Additional genetic differences between *Ab* 17978 UN and *Ab* 17978 VU, including single nucleotide polymorphisms (SNPs), are shown in **Table 4**.

The identification of two variants of *A. baumannii* ATCC 17978 within a laboratory raised the possibility that these two variants are present in other research laboratories. AbaAL44 is present in the *A. baumannii* 17978 genome published by the American Type Culture Collection (ATCC) in 2019 (https://genomes.atcc.org/genomes/e1d18ea4273549a0), but absent in two other *A. baumannii* 17978 reference genomes available in NCBI (NZ_CP018664; CP012004, **Table 2**), indicating that both *Ab* 17978 VU and *Ab* 17978 UN are represented among the published *A. baumannii* genomes. Frozen stocks of *A. baumannii* ATCC 17978 obtained from ATCC in 2009 and a different stock obtained in 2021 were streaked for individual colonies, which were screened for the presence of the accessory CL synthase gene (*clsC2*) included in AbaAL44 using PCR. The accessory *clsC2* was present in 4 out of 6 colonies screened from the 2009 laboratory stock and 35 out of 36 colonies screened from the 2021 laboratory stock, demonstrating that these culture collection stocks included a mixed population of *Ab* 17978 VU and UN (**Table 2, Fig. 8B**). To provide a high-quality reference genome, we performed Nanopore long-read sequencing on *A. baumannii* 17978 UN isolated from an ATCC stock in 2021 (NCBI Accession numbers CP079931, CP079932, CP079933, CP079934, **Table 2**). Illumina sequencing of *A. baumannii* 17978 UN isolates from 2009 and 2021 laboratory stocks found no predicted mutations compared to this new 17978 UN reference genome. These data indicate that the *Ab* 17978 UN and *Ab* 17978 VU variants differ from one another at a genetic level and that at least two ATCC-derived laboratory stocks of *A. baumannii* 17978 include these variants.

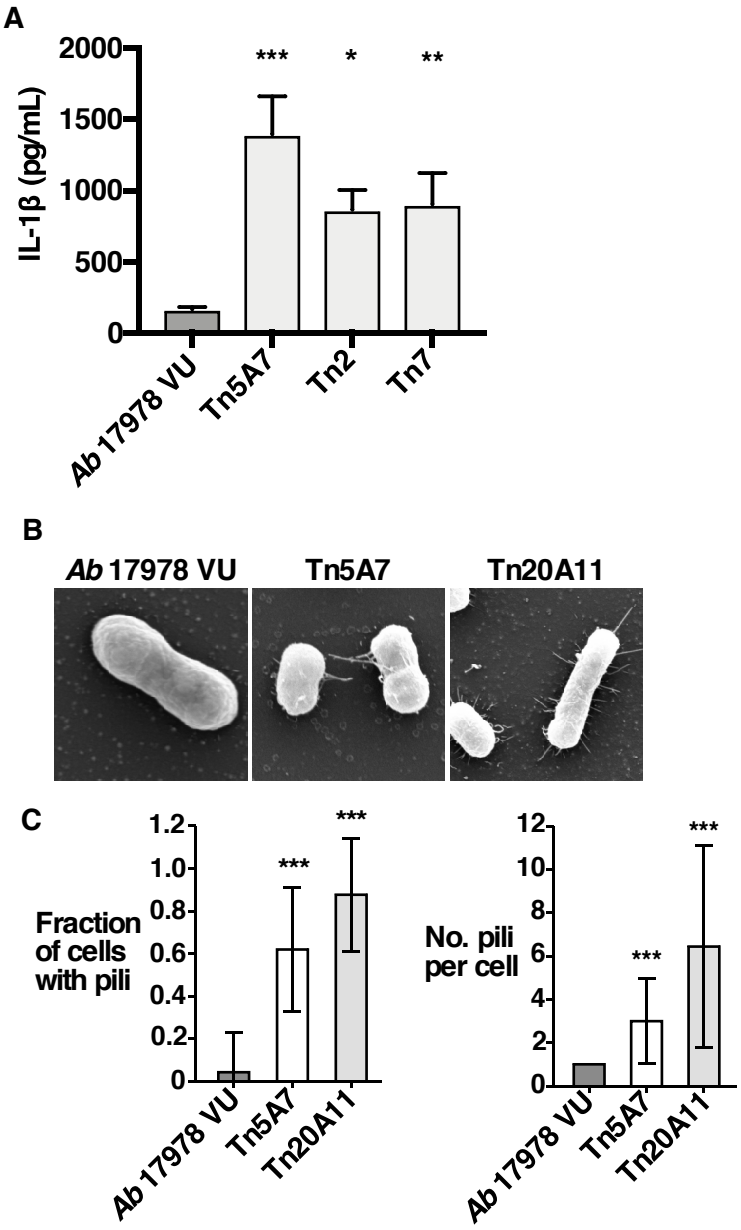

Figure 7. Conserved phenotypes exist among several Tn mutant strains of *A. baumannii*. A: Murine, bone marrow-derived macrophages were infected with chemically-killed, mid log-phase *Ab* 17978 VU or one of the Tn mutant strains made in the *Ab* 17978 UN background – Tn5A7, Tn2, or Tn7 – at an MOI of 10. At 18 h.p.i., supernatants were collected from each well, and the concentration of IL-1β was quantified via ELISA. **B**: Representative electron microscopy images of *Ab* 17978 VU and the Tn mutant strains Tn5A7 and Tn20A11. Numerous appendages (pili) are visible on the cell surface of both Tn mutant strains, but not on the cell surface of *Ab* 17978 VU. **C**: Quantification of the differences in cell surface appendages between strains in terms of the number of cells with pili and the average number of pili per cell. **A** and **C**: Columns depict the mean, and error bars show standard deviation of the mean. All means were compared with the mean of the first column using a one-way ANOVA adjusted for multiple comparisons. *: $p<0.05$; **: $p<0.01$; ***: $p<0.001$.

Table 2. Two variants of *A. baumannii* 17978; single nucleotide polymorphisms are shown in Table 4

	***Ab* 17978 VU**	***Ab* 17978 UN**
NCBI Reference Genomes (chromosome)	NZ_CP018664 (263); CP012004 (260)	CP079931 (this study)
UIC lab stock composition (ATCC 2021)	1/36 colonies	35/36 colonies
VUMC lab stock composition (ATCC 2009)	2/6 colonies	4/6 colonies
No. of bases	4066914	4100908
No. of genes	3910	3938
Average Nucleotide Identity (%)	99.99	99.99
AbaAL44	Absent	Present
IS701-like IS*Aba11* family transposase upstream of *pitA_2*	Absent	Present
IS*Aba18* downstream of *ACX60_00585*	Present	Absent

A Accessory Gene Locus

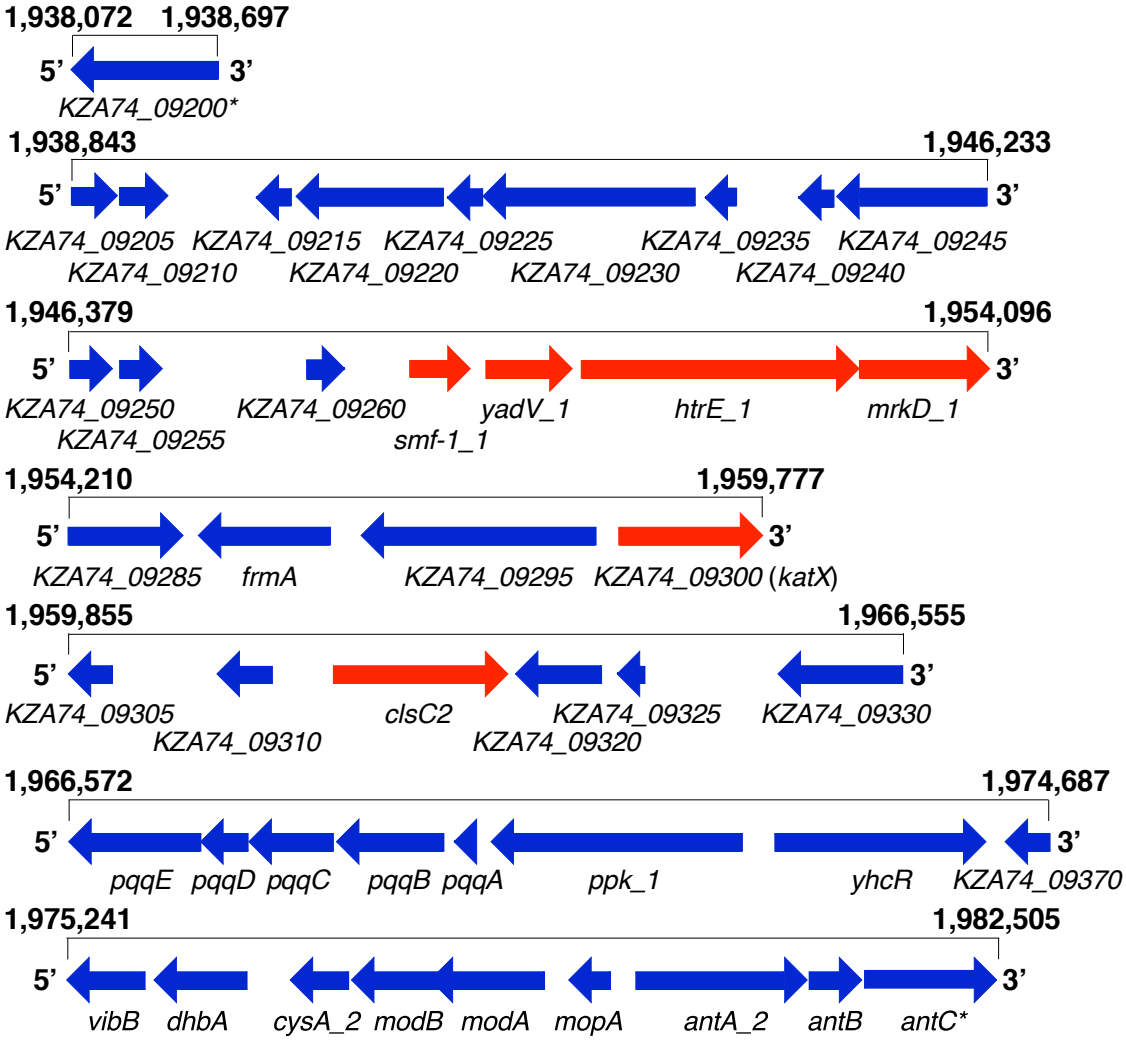

*: *KZA74_9200* and *antC* are only partially in AbaAL44

B

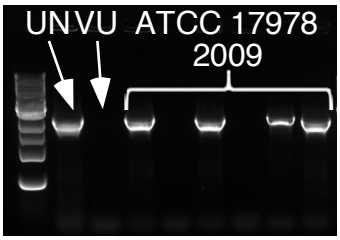

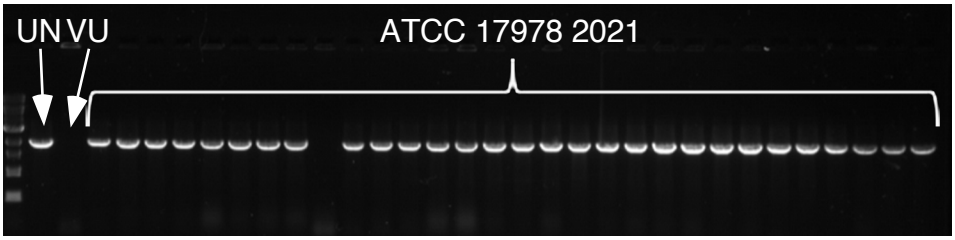

Figure 8. PacBio sequencing reveals structural differences between the genomes of *Ab* 17978 VU and *Ab* 17978 UN. The genome sequences of *Ab* 17978 VU and *Ab* 17978 UN were determined by PacBio and Nanopore sequencing and subsequently compared to the genome of the reference strain: *A. baumannii* ATCC17978-mff (RefSeq NZ_CP012004.1). **A**: Visual representation of AbaAL44 encompassing multiple accessory genes present in the genome of *Ab* 17978 UN based on analysis and inspection of new *Ab* 17978 UN reference genome (NCBI accession CP079931). The relative position (in terms of base pair number) within the assembled genome of *Ab* 17978 UN is indicated above each row, and gene names are indicated below each gene. Locus tags refer to CP079931. Arrows indicate the relative transcriptional direction of each gene. Genes indicated in red represent putative pathogenesis genes. **B**: Images of agarose gel electrophoresis indicating the differential presence of the accessory *clsC2* gene within individual colonies of *A. baumannii* 17978 laboratory stocks based on PCR detection of *clsC2*. The VUMC laboratory stock (left) was obtained from ATCC in 2009, and the UIC laboratory stock (right) was obtained from ATCC in 2021. Presence of accessory *clsC2* indicates that an isolate belongs to *Ab* 17978 UN variant.

Table 3. Annotated genes of the accessory cluster present in *Ab* 17978 UN

Gene	Locus Tag (CP079931)	Annotation	Notes
*3977**	KZA74_09200	phage/plasmid replication protein	Identical to *3978,* only partially in the island
*4059**	KZA74_09205	helix-turn-helix transcriptional regulator	Identical to *4060*
*3965**	KZA74_09210	putative replication initiation protein	Identical to *3966*
*390**	KZA74_09215	hypothetical protein	No putative conserved domains have been detected
*491**	KZA74_09220	putative Zonular occludens toxin (Zot)	
*191**	KZA74_09225	DUF2523 domain-containing protein	
*492**	KZA74_09230	hypothetical protein	No putative conserved domains have been detected. Truncated relative to Aba810CP_9780 in *A. baumannii* strain 810CP
*493**	KZA74_09235	uncharacterized protein	No putative conserved domains have been detected
*4011**	KZA74_09240	hypothetical protein	No putative conserved domains have been detected
*3978**	KZA74_09245	phage/plasmid replication protein	Identical to *3977*
*4060**	KZA74_09250	helix-turn-helix transcriptional regulator	Identical to *4059*
*3966**	KZA74_09255	putative replication initiation protein	Identical to *3965*
*495**	KZA74_09260	hypothetical protein	No putative conserved domains have been detected
smf-1_1	KZA74_09265	Major fimbrial subunit SMF-1	
yadV_1	KZA74_09270	putative fimbrial chaperone YadV	
htrE_1	KZA74_09275	Outer membrane usher protein HtrE	
mrkD_1	KZA74_09280	Fimbria adhesin protein	
*501**	KZA74_09285	DUF 4882 superfamily protein	This small family consists of several uncharacterized proteins around 325 residues in length and is mainly found in various Acinetobacter species. The function of this family is unknown.
frmA	KZA74_09290	S-(hydroxymethyl)glutathione dehydrogenase	
*193**	KZA74_09295	phage capsid protein	
*503**	KZA74_09300	catalase	
*504**	KZA74_09305	hypothetical protein	No putative conserved domains have been detected

*505**	KZA74_09310	hypothetical protein	No putative conserved domains have been detected
clsC2	KZA74_09315	Cardiolipin synthase C	
*506**	KZA74_09320	Uracil-DNA glycosylase	
*507**	KZA74_09325	hypothetical protein	No putative conserved domains have been detected
*509**	KZA74_09330	peptidase	
pqqE	KZA74_09335	Pyrroloquinoline quinone biosynthesis protein PqqE	
pqqD	KZA74_09340	Coenzyme PQQ synthesis protein D	
pqqC	KZA74_09345	Pyrroloquinoline-quinone synthase	
pqqB	KZA74_09350	Coenzyme PQQ synthesis protein B	
pqqA	KZA74_09355	pyrroloquinoline quinone precursor peptide PqqA	
ppk_1	KZA74_09360	Polyphosphate kinase	
yhcR	KZA74_09365	Endonuclease YhcR	
*516**	KZA74_09370	Fur family transcriptional regulator	
vibB	KZA74_09375	Vibriobactin-specific isochorismatase	
dhbA	KZA74_09380	2,3-dihydro-2,3-dihydroxybenzoate dehydrogenase	
cysA_2	KZA74_09385	Sulfate/thiosulfate import ATP-binding protein CysA	
modB	KZA74_09390	Molybdenum transport system permease protein ModB	
modA	KZA74_09395	Molybdate-binding protein ModA	
mopA	KZA74_09400	Molybdenum-pterin-binding protein MopA	
antA_2	KZA74_09405	Anthranilate 1,2-dioxygenase large subunit	
antB	KZA74_09410	Anthranilate 1,2-dioxygenase small subunit	
antC	KZA74_09415	anthranilate 1,2-dioxygenase electron transfer component	Partially in AbaLA44

*: Indicates name assigned by genome analysis software PROKKA

Table 4: Predicted mutations in *Ab* 17978 UN

Nucleotide Position (CP012004 [VU]/ CP079931 [UN])	Allele in VU (residue)	Allele in UN (residue)	Gene	Description
129,758	IS*Aba18*	Δ1,312 bp	*ACX60_00590–ACX60_00595*	transposase, transposase
207,638/206,237	G (A382)	A (T382)	*actP*	acetate permease
524,616/ 523,217	+A	Δ1 bp	*ACX60_02575/KZA74_02575*	Phosphohydrolase/pseudogene
807,273/805,874	G (P439)	A (P439)	*cysG*	sirohydrochlorin ferrochelatase
1,075,443/1,074,044	A (N258)	T (I258)	*ACX60_05080*/*cgtA*	GTPase *obgE*
1,226,257/1,224,858	G (G12)	A (D12)	*ACX60_05695*/*KZA74_05725*	membrane protein DUF817
1,685,154/1,683,755	T (M78)	C (T78)	*ACX60_07925*/*uppS*	UDP diphosphate synthase
2,068,076/2,111,105	T (stop codon)	A (L376)	Intergenic *ACX60_09755-ACX60_09765/KZA74_10025*	SurA N-terminal domain-containing protein
2,109,791/2,152,820	C (A55)	T (T55)	*ACX60_09960*/*KZA74_10230*	hypothetical protein/ putative transporter
2,135,294/2,178,324	+C	$(C)_{5\rightarrow4}$	*ACX60_10130*/*KZA74_10405*	DNA helicase AAA family ATPase
2,172,876/2,215,906	T (F799)	G (V799)	*ACX60_10365*/*KZA74_10630*	LPS biosynthesis protein LptD
2,189,235/2,232,265	A	G	*ACX60_10450 - ACX60_10455/KZA74_10715-putP*	Intergenic (NAD-dependent deacetylase/proline:sodium symporter PutP)
2,236,009/2,279,039	G	A	*ACX60_10685-ACX60_10690/KZA74_10950-KZA74_10955*	Intergenic (ABC transporter substrate-binding protein/glutathione S-transferase)
2,410,784/2,453,814	C (T2)	A (K2)	*ACX60_11495*/*KZA74_11775*	aspartate:proton symporter APC family permease
2,846,783/2,889,821	Δ1,106 bp	IS*Aba11*	*ACX60_17045/KZA74_13815*	transposase
3,384,892/3,429,018	Δ1 bp	+T	*ACX60_15995-ACX60_16000*/*KZA74_16315 - infA*	Intergenic (AraC family transcriptional regulator/translation initiation factor IF-1)

3,384,893/3,429,019	G	A	*ACX60_15995-ACX60_16000*/*KZA74_16315 - infA*	Intergenic (AraC family transcriptional regulator/translation initiation factor IF-1)
3,852,237	$(ATGGTG)_{9\rightarrow8}$	$(ATGGTG)_{9\rightarrow8}$	*ACX60_18165*/*dmeF*	cobalt transporter

Ab 17978 VU and Ab 17978 UN exhibit differential pathogenicity in a mouse model of pneumonia.

Ab 17978 has been used extensively in studies of *A. baumannii* pathogenesis (254-256). To determine whether *Ab* 17978 VU and *Ab* 17978 UN exhibit differential fitness *in vivo*, both variants were assessed in a murine model of pneumonia, and bacterial burdens in the lungs and spleens of infected mice were compared at 24 and 36 h.p.i.. Mice infected with *Ab* 17978 UN had a statistically significant decrease in lung bacterial burdens compared to mice infected with *Ab* 17978 VU both at 24 and 36 h.p.i. (**Fig. 9A** and **B**). At 24 hours, mice infected with *Ab* 17978 UN had lost significantly more weight (**Fig. 9C**), suggesting an increase in morbidity relative to mice infected with *Ab* 17978 VU. Histological examination of lungs from mice infected with *Ab* 17978 UN revealed fewer visible bacteria within the alveolar spaces and mice infected with *Ab* 17978 UN exhibit reduced extrapulmonary dissemination to the spleen relative to mice infected with *Ab* 17978 VU (**Fig. 9D** and **E**). Combined, these data suggest that *Ab* 17978 UN exhibits decreased fitness in a murine model of pneumonia compared to *Ab* 17978 VU.

Mice infected with *Ab* 17978 UN lost more weight than mice infected with *Ab* 17978 VU (**Fig. 9C**), which could indicate inappetence or increased metabolic demand due to increased inflammation. Neutrophilic inflammation is a characteristic response to *A. baumannii* infection and is essential for host resistance to infection (264-266). To determine if *Ab* 17978 VU or *Ab* 17978 UN induce differential neutrophil recruitment, mice were challenged with either variant, and the relative abundance of immune cell populations in both the lungs and blood was determined. Relative to mice infected with *Ab* 17978 VU, mice infected with *Ab* 17978 UN exhibited a decrease in the abundance of both T cells, B cells, and overall lymphocytes, and a statistically significant increase in the relative abundance of neutrophils in the lungs (**Fig. 10A-D**). However, no significant differences in the number or percentage of neutrophils or lymphocytes were detected in the blood of mice infected with *Ab* 17978 VU relative to mice infected with *Ab* 17978 UN (**Fig. 11**). These data demonstrate that *Ab* 17978 UN promotes a shift toward neutrophilic inflammation upon pneumonic infection of mice relative to *Ab* 17978 VU.

Neutrophil recruitment to the site of infection is dependent upon the production of cytokines and chemokines. Interleukin 1β (IL-1β) is a potent, pro-inflammatory cytokine that promotes neutrophil recruitment and stimulates neutrophil survival (267-270), whereas IL-10 is an anti-inflammatory cytokine that impedes neutrophil recruitment to the site of infection (271, 272). To test the hypothesis that infection with *Ab* 17978 UN potentiates neutrophilic lung inflammation by inducing differential cytokine or chemokine production by host cells, murine bone marrow derived macrophages (BMDMs) were infected with *Ab* 17978 VU or *Ab* 17978 UN, and cytokines and chemokines were quantified from cell culture supernatants. BMDMs infected with *Ab* 17978 UN produced significantly more IL-1β and less IL-10 when compared to BMDMs infected with *Ab* 17978 VU (**Fig. 10E** and **F**). By contrast, the production of the murine neutrophil chemokines KC and MIP-2 did not differ between BMDMs infected with *Ab* 17978 UN and *Ab* 17978 VU (**Fig. 10G** and **H**). No differences in serum or lung IL-1β levels were detected between mice infected with *Ab* 17978 VU and *Ab* 17978 UN at 24 h.p.i. (**Fig. 12**). These data demonstrate that host responses to two common variants of *A. baumannii* 17978 differ in terms of induced cytokine production by macrophages, as well as the degree of induced neutrophilic lung inflammation, bacterial persistence in the lung, and dissemination to the spleen in a mouse model of pneumonia.

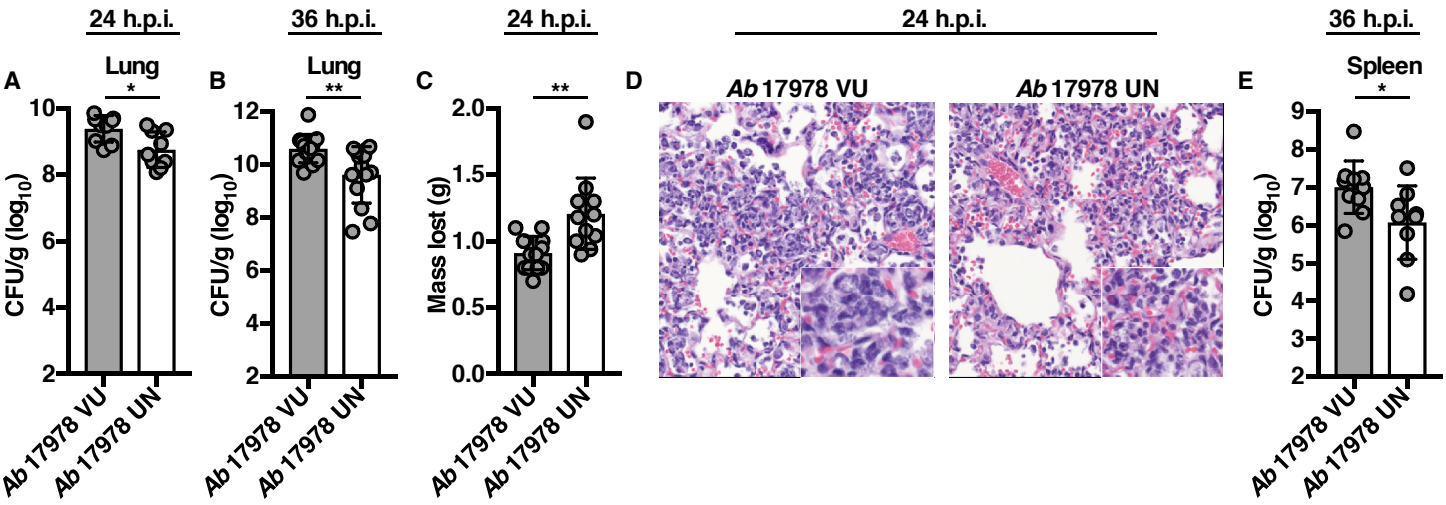

Figure 9. *Ab* 17978 VU and *Ab* 17978 UN exhibit differential virulence in a mouse model of pneumonia. Mice were challenged intranasally with 3×10^8 CFU of mid log-phase *Ab* 17978 VU or *Ab* 17978 UN. At 24 (**A** and **C**) or 36 (**B** and **E**) h.p.i., mice were euthanized, and organs were harvested. **A** and **B**: bacterial burdens in the lungs of mice at 24 and 36 h.p.i., respectively. **C**: Mean number of grams of total body weight lost by infected mice at 24 h.p.i. **D**: Representative hematoxylin and eosin (H&E)-stained lung sections of mice infected with *Ab* 17978 VU (left) or *Ab* 17978 UN (right) at 24 h.p.i. **E**: Bacterial burdens in the spleens of mice at 36 h.p.i. **A**, **B**, **C**, and **E**: Circles represent individual animals, columns depict the mean, and error bars show standard deviation of the mean. Means were compared using an unpaired Welch's *t*-test. CFU/g: colony forming units per gram of organ homogenate. *: $p<0.05$; **: $p< 0.01$. H&E: hematoxylin and eosin.

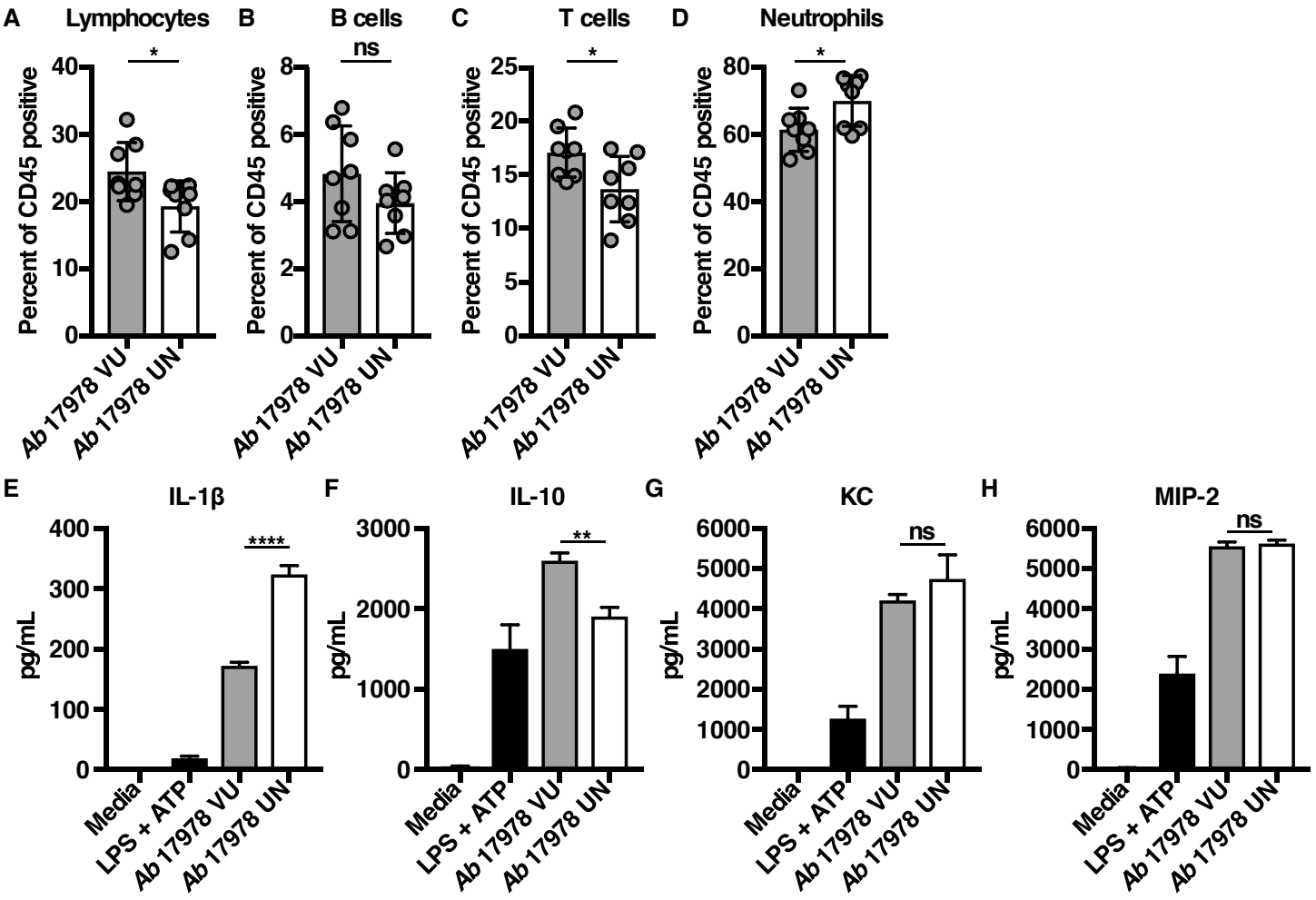

Figure 10. Mice infected with *Ab* 17978 UN exhibit increased neutrophilic inflammation in comparison to mice infected with *Ab* 17978 VU. A-D: Mice were challenged intranasally with 3×10^8 CFU of mid log-phase *Ab* 17978 VU or *Ab* 17978 UN. At 24 h.p.i., mice were euthanized, lungs were harvested, and immune cell recruitment to the lungs was quantified using flow cytometry analysis. **E-H**: Murine, bone marrow-derived macrophages were infected with mid log-phase cultures of *Ab* 17978 VU or *Ab* 17978 UN at an MOI of 10 and incubated at 37°C. At 18 h.p.i., supernatants of infected BMDMs were collected and the concentrations of IL-10 (**E**), IL-1β (**F**), KC (**G**), or MIP-2 (**H**) in the supernatants of infected BMDMs were determined by ELISA. **A-D**: Circles represent individual animals, columns depict the mean, and error bars show standard deviation of the mean. Means were compared using an unpaired Welch's *t*-test. **E-H**: N=3-4 biological replicates per group, per experiment. Experiments were repeated for a total of at least two times, with graphs depicting representative data. Columns depict the mean, and error bars show standard deviation of the mean. Means were compared to the mean of the *Ab* 17978 VU column using a one-way ANOVA adjusted for multiple comparisons. *: $p<0.05$; **: $p<0.01$; ****: $p<0.0001$; ns: not significant.

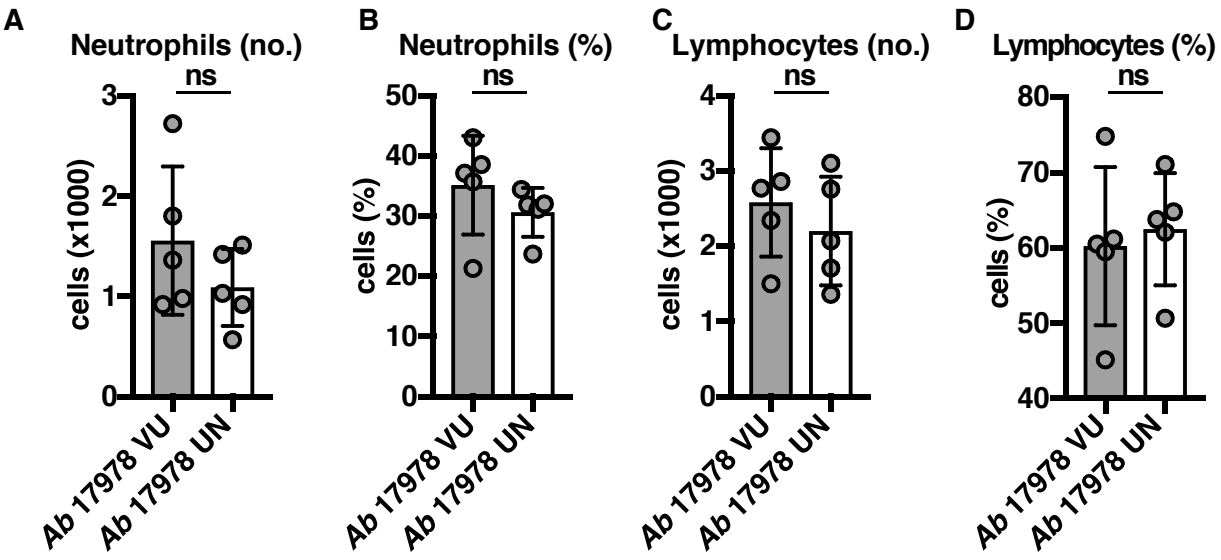

Figure 11. No differences in blood neutrophil or lymphocyte abundance exist between mice infected with *Ab* 17978 VU and mice infected with *Ab* 17978 UN. A-D: Mice were challenged intranasally with 3×10^8 CFU of mid log-phase *Ab* 17978 VU or *Ab* 17978 UN. At 24 h.p.i., mice were euthanized, blood was collected via cardiac puncture, and blood cell counts were determined using an automated hematology analyzer. Circles represent individual animals, columns depict the mean, and error bars show standard deviation of the mean. Means were compared using an unpaired Welch's *t*-test. ns: not significant.

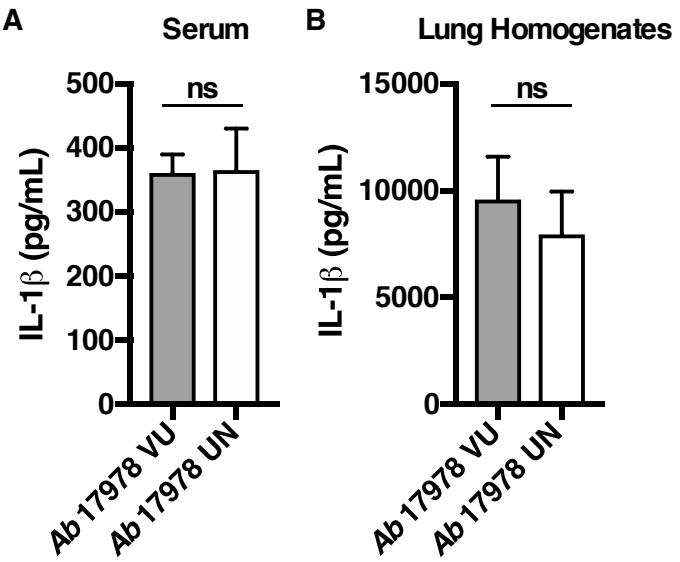

Figure 12. Lung and serum levels of IL-1β do not differ between mice infected with *Ab* 17978 VU and mice infected with *Ab* 17978 UN at 24 h.p.i. Mice were challenged intranasally with 3×10^8 CFU of mid log-phase *Ab* 17978 VU or *Ab* 17978 UN. At 24 h.p.i., mice were euthanized, blood was collected via cardiac puncture, and lungs were harvested. IL-1β in the serum (**A**) or lung homogenates (**B**) was quantified using ELISA. **A**: N=3-5 biological replicates per group, per experiment. Experiments were repeated for a total of at least two times, with graphs depicting representative data. **B**: N=3-5 biological replicates per group, per experiment. Graphs depict average results from at least two independent experiments. **A** and **B**: Columns depict the mean, and error bars show standard deviation of the mean. Means were compared using an unpaired Welch's *t*-test. ns: not significant.

The AbaAL44 katX gene promotes bacterial resistance to hydrogen peroxide stress and neutrophil-mediated killing.

To interrogate the role of putative pathogenesis genes contained within AbaAL44 in the differential pathogenicity of *Ab* 17978 UN, the candidate accessory pilus assembly locus comprised of *smf-1, yadV, htrE,* and *mrkD*, the accessory catalase gene (*KZA74_09300*; *katX*), or the accessory CL synthase gene (*clsC2*) was replaced with a kanamycin resistance cassette to create *Ab* 17978 UN *Δsmf-1_1-mrkD_1*::kan (*Ab* 17978 UN *Δpilus*), *Ab* 17978 UN *ΔKZA74_09300*::kan (*Ab* 17978 UN *ΔkatX*), and *Ab* 17978 UN *ΔclsC2*::kan (*Ab* 17978 UN *ΔclsC2*), respectively (273). Type I pili are bacterial surface appendages involved in bacterial uptake by macrophages, biofilm formation, attachment to host cells, motility, and agglutination of red blood cells (274-277). However, *Ab* 17978 UN *Δpilus* did not differ from *Ab* 17978 UN in terms of bacterial uptake by macrophage-like RAW 264.7 cells (**Fig. 13A**), biofilm formation (**Fig. 13B**), bacterial attachment to A549 epithelial cells (**Fig. 13C**), bacterial surface associated motility (**Fig. 13D**), hemagglutination of human erythrocytes (**Fig. 13E**), or differential production of cytokines by infected BMDMs (**Fig. 13F** and **G**). These data suggest that the type I pilus locus does not contribute to the interactions with host cells under these *in vitro* conditions.

Catalases are enzymes that catalyze the decomposition of hydrogen peroxide (H_2O_2) to water and oxygen and thereby protect bacteria from reactive oxygen species (ROS)-mediated oxidative stress and killing by innate immune cells (278-280). To test the hypothesis that the AbaAL44 accessory catalase present in *Ab* 17978 UN contributes to bacterial resistance to oxidative stress, the relative susceptibilities of *Ab* 17978 VU, *Ab* 17978 UN, *Ab* 17978 UN *ΔkatX*/Empty Vector (EV), and *Ab* 17978 UN *ΔkatX* in which the AbaAL44 *katX* gene was expressed *in trans* (*Ab* 17978 UN *ΔkatX*/p*katX*) to hydrogen peroxide stress *in vitro* was determined. Thirty minutes after incubation of 1×10^7 CFU/mL of bacteria in the presence of 1 mM of hydrogen peroxide, the density of viable *Ab* 17978 UN remained virtually unchanged at approximately 7-$\log_{10}$ CFU/mL. By contrast, the densities of viable *Ab* 17978 VU and *Ab* 17978 UN *ΔkatX*/EV were significantly reduced to approximately 5.5-$\log_{10}$ CFU/mL.

Expression of the AbaAL44 *katX in trans* restored hydrogen peroxide stress resistance in *Ab* 17978 UN *ΔkatX*/p*katX* to levels approximating that of the parental strain (**Fig. 14A**). These data indicate that the *katX* present in AbaAL44 enhances bacterial resistance to oxidative stress *in vitro*. Neutrophils are innate immune effector cells that phagocytose and subsequently kill engulfed pathogens using an array of antimicrobial molecules, including ROS produced by the enzyme nicotinamide adenine dinucleotide phosphate (NADPH) oxidase (281, 282). Based on this, we hypothesized that the *katX* present in *Ab* 17978 UN promotes bacterial resistance to neutrophil-mediated killing. To test this, differentiated neutrophil-like HL-60 cells were incubated with *Ab* 17978 UN, *Ab* 17978 VU, *Ab* 17978 UN *ΔkatX*/EV, or *Ab* 17978 UN *ΔkatX*/p*katX* and bacterial resistance to neutrophil-mediated extra- and intracellular killing was determined by measuring relative bacterial survival post-incubation. After incubation in the presence of differentiated neutrophil-like HL-60 cells, relative survival of *Ab* 17978 UN was significantly greater than that of both *Ab* 17978 VU and *Ab* 17978 UN *ΔkatX*/EV (**Fig. 14B**). Similar results were obtained with murine, bone marrow-derived neutrophils (**Fig. 15**). *In trans* expression of the AbaAL44 *katX* restored *Ab* 17978 UN *ΔkatX*/EV survival to levels of the parental strain (**Fig. 14B**). Deletion of the AbaAL44 *katX* gene negatively affected the growth of *Ab* 17978 UN *in vitro* in both rich (LB) and minimal (TMS) media, which was restored by expressing AbaAL44 *katX in trans* (**Fig. 16**). Taken together, these data suggest that the *katX* present in AbaAL44 contributes to *Ab* 17978 UN growth *in vitro* as well as bacterial resistance to oxidative stress and neutrophil-mediated killing.

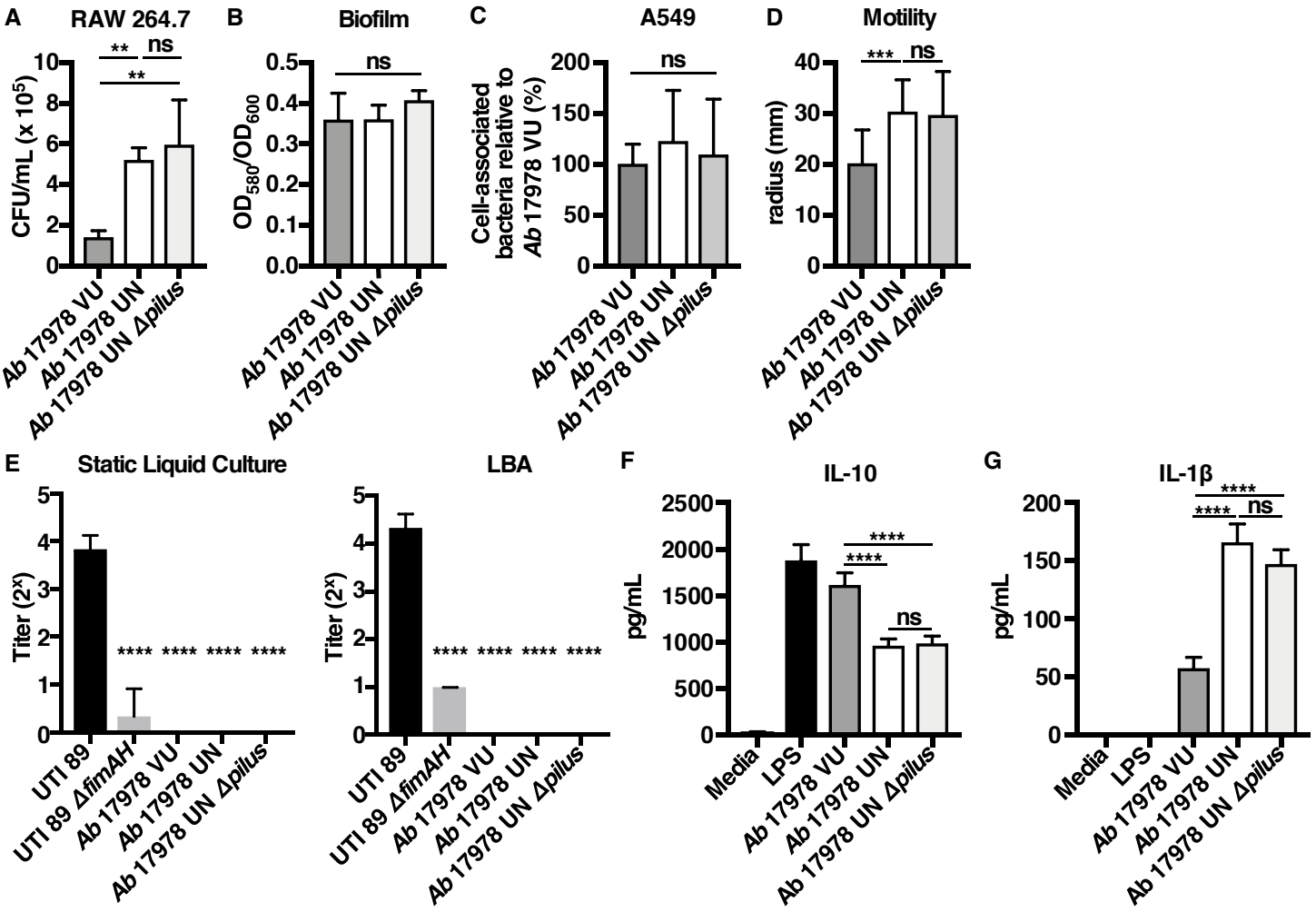
A
RAW 264.7
CFU/mL (x 10^5)
**
ns
**
Ab 17978 VU
Ab 17978 UN
Ab 17978 UN Δpilus
B
Biofilm
OD580/OD600
ns
C
A549
Cell-associated bacteria relative to Ab 17978 VU (%)
ns
D
Motility
radius (mm)
***
ns
E
Static Liquid Culture
Titer (2^x)
****
UTI 89
UTI 89 ΔfimAH
LBA
F
IL-10
pg/mL
Media
LPS
G
IL-1β

Figure 13. The accessory pilus assembly genes present in *Ab* 17978 UN do not contribute to increased phagocytosis by macrophages, biofilm formation, bacterial surface associated motility, bacterial association with epithelial cells and erythrocytes, or differential production of cytokines by infected macrophages. A: Macrophage-like RAW 264.7 cells were infected with mid log-phase *Ab* 17978 VU, *Ab* 17978 UN, or *Ab* 17978 UN *Δpilus* at an MOI of 15. At 1 h.p.i., and extracellular bacteria were killed with gentamicin at 1 h.p.i. Thirty minutes after the addition of gentamicin, RAW cells were lysed, and intracellular bacterial burdens were determined. **B**: Stationary-phase cultures of *Ab* 17978 VU, *Ab* 17978 UN, and *Ab* 17978 UN *Δpilus* were diluted 1:10 in PBS, coated onto the wells of a 96-well plate, and incubated at 37 °C without agitation for 24-48 hours. After incubation, biofilm formation was quantified using crystal violet staining, and the ratio of biofilm to biomass was determined by measuring the optical densities at 580 nm and 600 nm, respectively. **C**: A549 cells were infected with mid log-phase *Ab* 17978 VU, *Ab* 17978 UN, or *Ab* 17978 UN *Δpilus* at an MOI of 100, and incubated at 37 °C for two hours. At 2 h.p.i., non-adherent bacteria were removed by washing with PBS, A549 cells were lysed, and the number of cell-associated bacteria was determined. **D**: Stationary-phase *Ab* 17978 VU, *Ab* 17978 UN, and *Ab* 17978 UN *Δpilus* were spotted on the surface of motility agar plates at the center and incubated overnight at 37 °C without agitation. After incubation, the maximum motility radius was measured. **E**: *Ab* 17978 VU, *Ab* 17978 UN, and *Ab* 17978 UN *Δpilus* were grown in static liquid culture (left) or on LBA plates (right), and incubated overnight at 4 °C with an equal volume of 1% human erythrocytes in PBS. Static liquid cultures of *E. coli* UTI89 and *E. coli* UTI89 *ΔfimAH* served as positive and negative controls, respectively. After incubation, hemagglutination titers (i.e. the maximum dilution at which bacteria are able to agglutinate erythrocytes) were determined. **F** and **G**: Murine, bone marrow-derived macrophages were infected with mid log-phase cultures of *Ab* 17978 VU, *Ab* 17978 UN, or *Ab* 17978 UN *Δpilus* at an MOI of 10 and incubated at 37°C. At 18 h.p.i., supernatants of infected BMDMs were collected. The concentrations of IL-10 (**F**) and IL-1β (**G**) in the supernatants of infected BMDMs were determined by ELISA. **A**-**G**: N=3-4 biological replicates per group, per experiment. Experiments were repeated for a total of at least two times, with graphs depicting representative (**A**, **B**, **E**-**G**) or average (**C** and **D**) data. Columns depict the mean, and error bars show standard deviation of the mean. **A**-**D**, **F** and **G**: Means were compared to all other means using a one-way ANOVA adjusted for multiple comparisons. **E**: Means were compared to the mean of the first column using a one-way ANOVA adjusted for multiple comparisons. CFU/mL: colony forming units per milliliter. **: $p<0.01$; ***: $p<0.001$; ****: $p<0.0001$; ns: not significant.

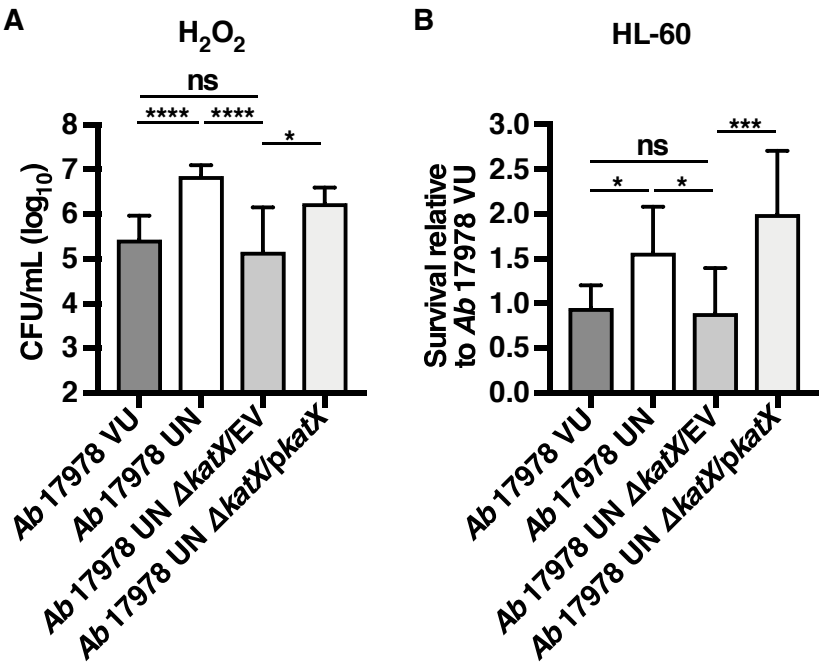

Figure 14. The AbaAL44 *katX* gene promotes bacterial resistance to hydrogen peroxide stress and neutrophil-mediated killing. A: Mid log-phase *Ab* 17978 VU, *Ab* 17978 UN, *Ab* 17978 UN *ΔkatX*/EV*,* or *Ab* 17978 UN *ΔkatX*/p*katX* was incubated in LB medium supplemented with 1 mM of hydrogen peroxide at a starting inoculum of 1×10^7 CFU/mL. Following a 30-minute incubation, remaining viable bacteria were enumerated. **B**: Differentiated neutrophil-like HL-60 cells were incubated with mid log-phase *Ab* 17978 VU, *Ab* 17978 UN, *Ab* 17978 UN *ΔkatX*/EV*,* or *Ab* 17978 UN *ΔkatX*/p*katX* at an MOI of 2. At 90 minutes post-incubation, HL-60 cells were lysed, and neutrophil-mediated killing of bacteria was assessed by determining the number of viable bacteria in each well. Data are represented as bacterial survival relative to *Ab* 17978 VU. **A** and **B**: N=3-4 biological replicates per group, per experiment. Experiments were repeated for a total of at least two times, with graphs depicting average data. **A** and **B**: Columns depict the mean, and error bars show standard deviation of the mean. All means were compared to all other means using a one-way ANOVA adjusted for multiple comparisons. *: $p<0.05$; ***: $p<0.001$; ****: $p<0.0001$; ns: not significant.

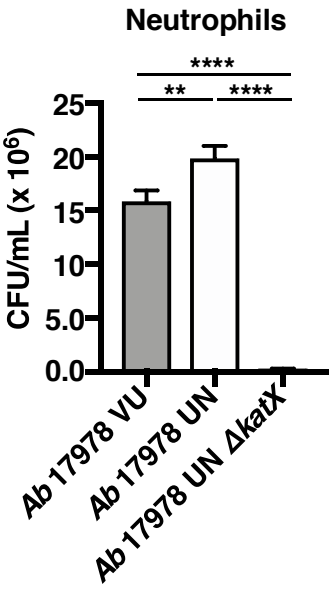

Figure 15. The AbaAL44 *katX* gene promotes *Ab* 17978 UN resistance to neutrophil-mediated killing. Murine, bone marrow-derived neutrophils were incubated with mid log-phase *Ab* 17978 VU, *Ab* 17978 UN, or *Ab* 17978 UN *ΔkatX* at an MOI of 1. Two hours post-incubation, neutrophils were lysed, and neutrophil-mediated killing of bacteria was assessed by determining the number of viable bacteria in each well. N=3 per group, per experiment. Experiments were repeated for a total of at least two times, with graphs depicting representative data. Columns depict the mean, and error bars show standard deviation of the mean. Means were compared to all other means using a one-way ANOVA adjusted for multiple comparisons. **: $p<0.01$; ****: $p<0.0001$.

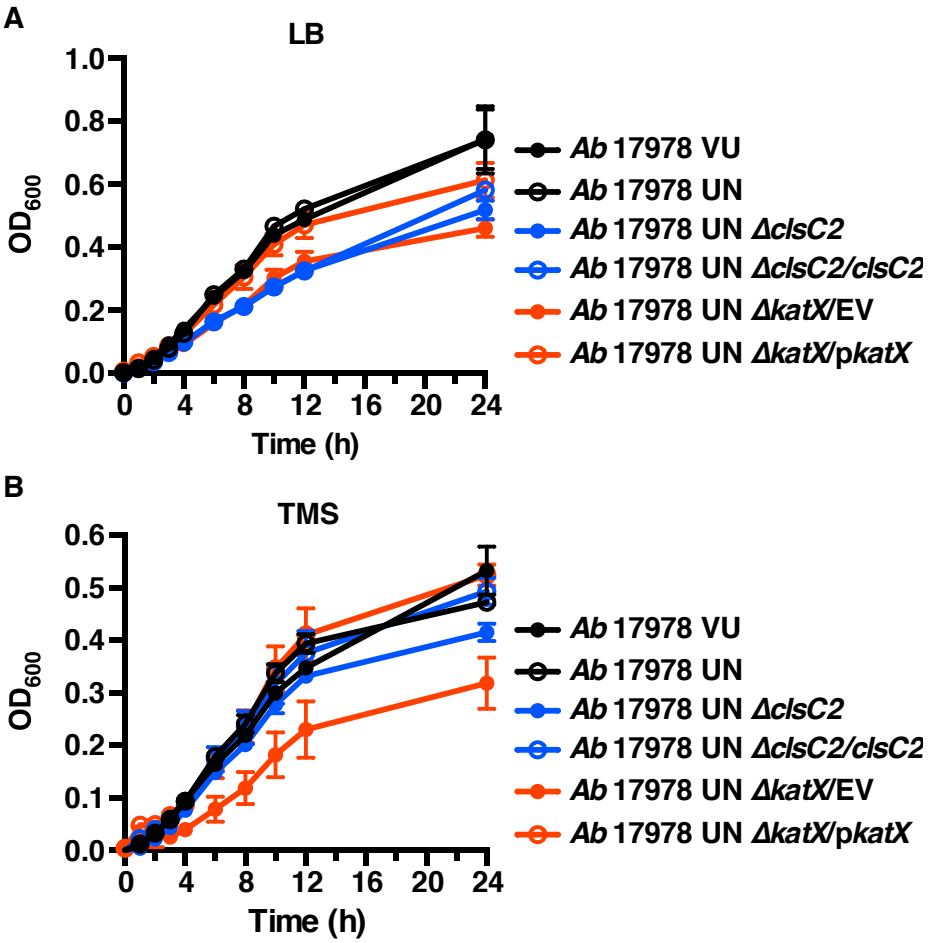

Figure 16. AbaAL44 *clsC2* and *katX* mutants generated in the *Ab* 17978 UN background exhibit growth defects *in vitro*. **A** and **B**: Stationary-phase cultures of the indicated strains of *A. baumannii* were normalized to a similar OD_{600} and inoculated into fresh rich media (LB) or minimal media (TMS). Growth was assayed by measuring OD_{600} over time. Symbols depict the mean, and error bars show standard deviation of the mean. N=3-4 biological replicates per group, per experiment. Graphs depict representative data from two independent experiments. For 8, 10, and 12 hour time points, the means of *Ab* 17978 UN Δ*clsC2*, *Ab* 17978 UN Δ*clsC2*/*clsC2*, *Ab* 17978 UN Δ*katX*/EV, *Ab* 17978 UN Δ*katX*/p*katX*, and *Ab* 17978 UN were compared using a one-way ANOVA adjusted for multiple comparisons. **A**: Differences between *Ab* 17978 UN and *Ab* 17978 UN Δ*clsC2*, *Ab* 17978 UN Δ*clsC2*/*clsC2*, or *Ab* 17978 UN Δ*katX*/EV: $p<0.0001$ for each comparison, for each time point; Difference between *Ab* 17978 UN and *Ab* 17978 UN Δ*katX*/p*katX*: $p<0.05$ for the10 hour time point and $p>0.05$ for 8 and 12 hour time points. **B**: Differences between *Ab* 17978 UN and *Ab* 17978 UN Δ*clsC2*, *Ab* 17978 UN Δ*clsC2*/*clsC2*, or *Ab* 17978 UN Δ*katX*/p*katX*: $p>0.05$ for each comparison, for each time point; Difference between *Ab* 17978 UN and *Ab* 17978 UN Δ*katX*/EV: $p<0.0001$, $p<0.0001$, or $p<0.001$ for 8, 10, and 12 hour time points, respectively.

The AbaAL44 clsC2 contributes to bacterial resistance to cell envelope stress and affects bacterial interactions with host immune cells.

Bacterial CL synthases are enzymes that utilize PG and/or PE as substrates to catalyze the formation of CL (136, 283). CL is one of several anionic phospholipids that comprise the Gram-negative cell envelope, and, in *Escherichia coli*, has been demonstrated to localize to the cellular poles (119). Because CL promotes bacterial resistance to envelope stressors such as high salinity (284, 285), it was hypothesized that *Ab* 17978 UN is more resistant to conditions of high salinity than *Ab* 17978 UN *ΔclsC2*. To test this, the susceptibility of *Ab* 17978 VU, *Ab* 17978 UN, *Ab* 17978 UN *ΔclsC2*, and *Ab* 17978 UN *ΔclsC2* in which *clsC2* has been reintroduced chromosomally under its native promoter by mini-Tn7 integration (*Ab* 17978 UN *ΔclsC2/clsC2*) to conditions of high salinity was determined by comparing bacterial survival after incubation in LB supplemented with 2.5M NaCl. After two hours of incubation in high salinity, bacterial survival of *Ab* 17978 UN *ΔclsC2* was significantly reduced by approximately 30% compared to the survival of *Ab* 17978 UN. After incubation in high salinity, survival of *Ab* 17978 UN *ΔclsC2/clsC2* did not differ significantly from *Ab* 17978 UN (**Fig. 17A**). Perturbations in bacterial membrane phospholipid homeostasis involving CL have been demonstrated to increase bacterial susceptibility to molecular detergents such as surfactants, which are found in high concentrations in the lungs and may be relevant to bacterial pneumonia pathogenesis (122). To determine if the AbaAL44 *clsC2* present in *Ab* 17978 UN promotes bacterial resistance to detergents, the susceptibility of *Ab* 17978 VU, *Ab* 17978 UN, *Ab* 17978 UN *ΔclsC2*, and *Ab* 17978 UN *ΔclsC2/clsC2* to the detergent Triton X-100 was assessed. After six hours of incubation in 0.1% Triton X-100, bacterial survival of *Ab* 17978 UN *ΔclsC2* was significantly less than that of *Ab* 17978 UN. Survival of *Ab* 17978 UN *ΔclsC2/clsC2* was significantly greater than that of *Ab* 17978 UN *ΔclsC2*, and similar to that of *Ab* 17978 UN (**Fig. 17B**). Taken together, these data indicate that the accessory CL synthase gene present in *Ab* 17978 UN contributes to this strain's resistance to conditions of high salinity and detergent stress.

Previous work has demonstrated that CL promotes uptake of bacteria by professional phagocytes such as macrophages through the scavenger receptor CD36 (137). Therefore, it was hypothesized that the previously observed increase in intracellular bacterial burden in macrophage-like RAW cells infected with *Ab* 17978 UN is mediated by the AbaAL44 *clsC2* (**Fig. 13A**). To test this, the relative intracellular bacterial burdens of RAW cells infected with *Ab* 17978 VU, *Ab* 17978 UN, *Ab* 17978 UN *ΔclsC2*, or *Ab* 17978 UN *ΔclsC2*/*clsC2* were determined. The relative intracellular bacterial burden of RAW cells infected with *Ab* 17978 UN *ΔclsC2* was significantly reduced by approximately 75% relative to the intracellular bacterial burden of RAW cells infected with *Ab* 17978 UN, and was similar to the intracellular bacterial burden of RAW cells infected with *Ab* 17978 VU. There was a small but statistically significant increase in the intracellular bacterial burden of RAW cells infected with *Ab* 17978 UN *ΔclsC2*/*clsC2* relative to that of RAW cells infected with *Ab* 17978 UN *ΔclsC2* (**Fig. 17C**). Expression of *clsC2 in trans* in *Ab* 17978 VU (*Ab* 17978 VU/p*clsC2*) also significantly increased the intracellular bacterial burden of infected RAW cells compared to RAW cells infected with *Ab* 17978 VU/EV (**Fig. 17D**). These data suggest that the AbaAL44 *clsC2* gene contributes to *Ab* 17978 UN phagocytosis by macrophages.

Chromosomal reintroduction of *clsC2* in *Ab* 17978 UN *ΔclsC2* did not fully restore phagocytosis by infected RAW cells to the levels observed with *Ab* 17978 UN (**Fig. 17C**). The deletion of *clsC2* negatively affected the growth of *Ab* 17978 UN *in vitro* in rich media (LB) but not in minimal media (TMS) (**16**). The growth defect of *Ab* 17978 UN *ΔclsC2* in rich media was also not restored by chromosomal reintegration of *clsC2* under its native promoter (**Fig. 16A**). Further, the supernatants of RAW cells infected with *Ab* 17978 UN *ΔclsC2* or *Ab* 17978 UN *ΔclsC2*/*clsC2* contained small, punctate colonies (**Fig. 18B**). These colonies were also present in lysates of RAW cells infected with *Ab* 17978 UN *ΔclsC2* or *Ab* 17978 UN *ΔclsC2*/*clsC2* collected prior to treatment with gentamicin, but absent from the starting inoculums (**Fig. 18A** and **C**). Small, punctate colonies were not observed in any samples collected from RAW cells infected with the *Ab* 17978 UN parental strain (**Fig. 18**). These findings

suggest a reduction *Ab* 17978 UN *ΔclsC2* fitness that is not restored by integration of *clsC2* elsewhere on the chromosome and are indicative of another genetic difference between the parental *Ab* 17978 UN and the *ΔclsC2* derivative or polar effects of the inserted kanamycin cassette. As expression of *clsC2* in *Ab* 17978 VU resulted in an increase in macrophage phagocytosis, the differential growth phenotype between Ab 17978 UN and *Ab* 17978 UN *ΔclsC2* was not pursued further.

Mitochondrial CL activates the NLRP3 inflammasome resulting in the production of IL-1β, and saturated CLs increase IL-1β production through Toll like receptor (TLR) 4 signaling (102, 125). This raised the hypothesis that the increase in IL-1β production observed in macrophages infected with *Ab* 17978 UN is due to the presence of AbaAL44 *clsC2*. Given the reduced fitness of the *ΔclsC2* mutant in the *Ab* 17978 UN background, this hypothesis was tested by expressing the AbaAL44 *clsC2* gene *in trans* in *Ab* 17978 VU, which naturally lacks AbaAL44 and thus *clsC2*. BMDMs were infected with *Ab* 17978 VU/EV or *Ab* 17978/p*clsC2* and the concentrations of pro-inflammatory IL-1β and anti-inflammatory IL-10 in the supernatants of infected BMDMs were determined at 18 h.p.i. Relative to infection with *Ab* 17978 VU/EV, infection with *Ab* 17978 VU/p*clsC2* significantly increased the production of IL-1β by infected BMDMs (**Fig. 17E**). These findings indicate that the presence of AbaAL44 *clsC2* increases pro-inflammatory IL-1β production by macrophages infected with *Ab* 17978 UN. Infection with *Ab* 17978 UN decreases the production of IL-10 by infected macrophages relative to infection with *Ab* 17978 VU (**Fig. 17F**). In contrast, expression of *clsC2* in *Ab* 17978 VU significantly increased IL-10 production by infected macrophages (**Fig. 17F**). This finding suggests that the decrease in IL-10 production observed in macrophages infected with *Ab* 17978 UN cannot be explained by the presence of *clsC2* alone. Together, these data indicate that AbaAL44 influences *A. baumannii's* interactions with the host.

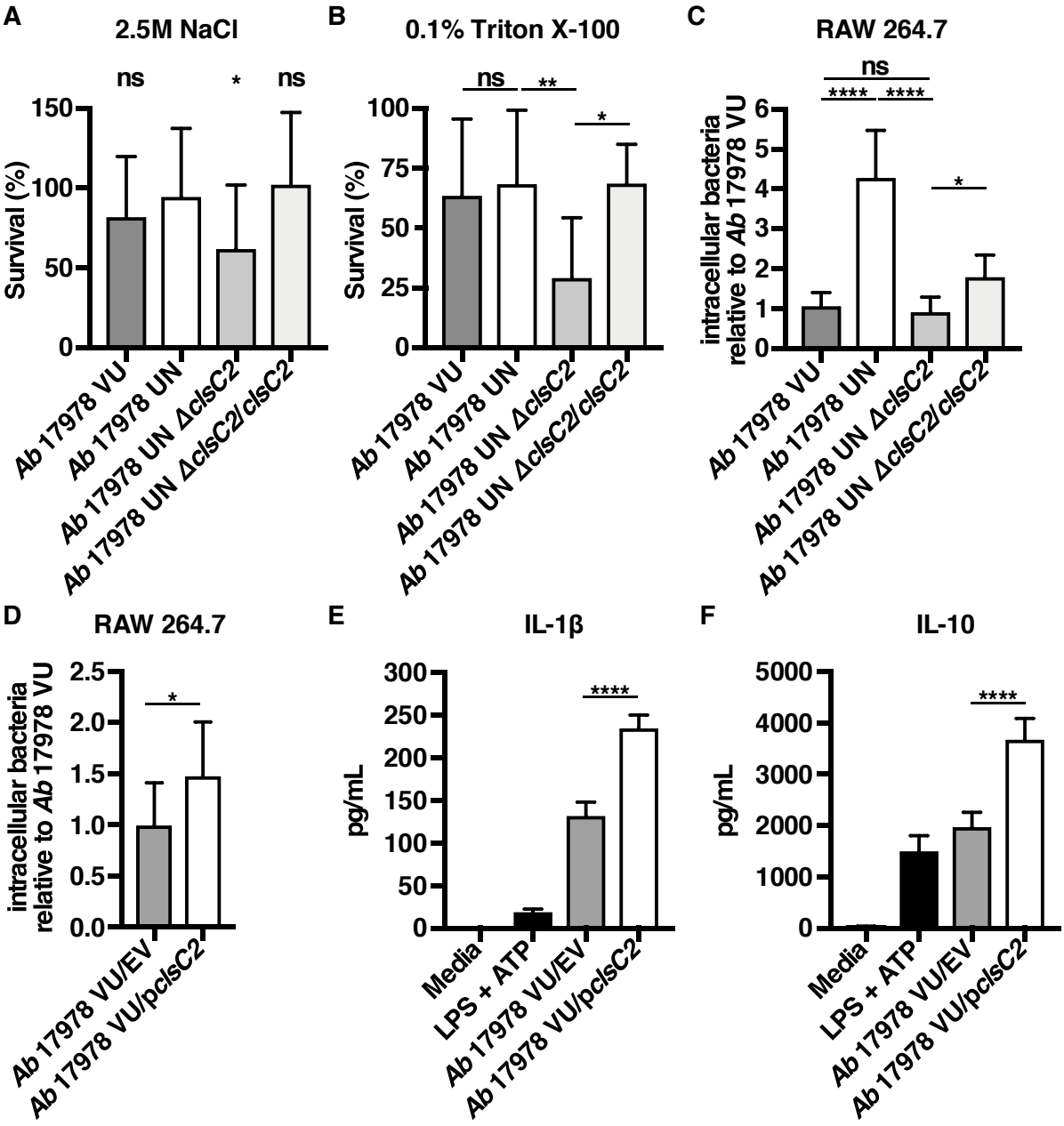
A
2.5M NaCl
ns
*
ns
Survival (%)
150
100
50
0
Ab 17978 VU
Ab 17978 UN
Ab 17978 UN ΔclsC2
Ab 17978 UN ΔclsC2/clsC2
B
0.1% Triton X-100
ns
**
*
Survival (%)
100
75
50
25
0
Ab 17978 VU
Ab 17978 UN
Ab 17978 UN ΔclsC2
Ab 17978 UN ΔclsC2/clsC2
C
RAW 264.7
ns
****
****
*
intracellular bacteria relative to Ab 17978 VU
6
5
4
3
2
1
0
Ab 17978 VU
Ab 17978 UN
Ab 17978 UN ΔclsC2
Ab 17978 UN ΔclsC2/clsC2
D
RAW 264.7
*
intracellular bacteria relative to Ab 17978 VU
2.5
2.0
1.5
1.0
0.5
0.0
Ab 17978 VU/EV
Ab 17978 VU/pclsC2
E
IL-1β
****
pg/mL
300
250
200
150
100
50
0
Media
LPS + ATP
Ab 17978 VU/EV
Ab 17978 VU/pclsC2
F
IL-10
****
pg/mL
5000
4000
3000
2000
1000
0
Media
LPS + ATP
Ab 17978 VU/EV
Ab 17978 VU/pclsC2

Figure 17. The AbaAL44 *clsC2* gene contributes to bacterial resistance to cell envelope stress and affects bacterial interactions with host immune cells. A: Mid log-phase *Ab* 17978 VU, *Ab* 17978 UN, *Ab* 17978 UN *ΔclsC2*, or *Ab* 17978 UN *ΔclsC2*/*clsC2* was inoculated into LB medium supplemented with 2.5M NaCl at a starting inoculum of 1×10^7 CFU/mL, and incubated at 37°C for 2 hours. After 2 hours of incubation, bacterial viability was determined for each strain, and bacterial survival was calculated as the percentage of viable bacteria post-incubation relative to the number of viable bacteria pre-incubation. **B**: Mid log-phase *Ab* 17978 VU, *Ab* 17978 UN, *Ab* 17978 UN *ΔclsC2*, or *Ab* 17978 UN *ΔclsC2*/*clsC2* was inoculated into PBS supplemented with 0.1% Triton X-100 at a starting inoculum of 1×10^{10} CFU/mL, and incubated at 37°C for 6 hours. After incubation, bacterial viability was determined for each strain, and survival was calculated as above. **C** and **D**: Macrophage-like RAW 264.7 cells were infected with mid log-phase *Ab* 17978 VU, *Ab* 17978 UN, *Ab* 17978 UN *ΔclsC2*, *Ab* 17978 UN *ΔclsC2*/*clsC2*, *Ab* 17978 VU/EV, or *Ab* 17978 VU/p*clsC2* at an MOI of 15, and extracellular bacteria were killed with gentamicin at 30 minutes post-infection. Thirty minutes after the addition of gentamicin, RAW cells were washed, lysed, and intracellular bacterial burdens were determined. **E** and **F**: Murine, bone marrow-derived macrophages were infected with mid log-phase cultures of *Ab* 17978 VU/EV or *Ab* 17978 VU/p*clsC2* at an MOI of 10 and incubated at 37°C. At 18 h.p.i., supernatants of infected BMDMs were collected and the concentrations of IL-1β (**E**) or IL-10 (**F**) in the supernatants of infected BMDMs were determined by ELISA **A**-**D**: N=3-4 biological replicates per group, per experiment. Graphs depict average results from at least three independent experiments. **E** and **F**: N=4 biological replicates per group, per experiment. Graphs depict representative data. **A**-**F**: Columns depict the mean, and error bars show standard deviation of the mean. Means were compared to the mean of *Ab* 17978 UN (**A**) or all other means (**B**-**F**) using a Welch's *t*-test (**D**) or one-way ANOVA adjusted for multiple comparisons (**A**-**C**, **E** and **F**). *: $p<0.05$; **: $p<0.01$; ****: $p<0.0001$; ns: not significant.

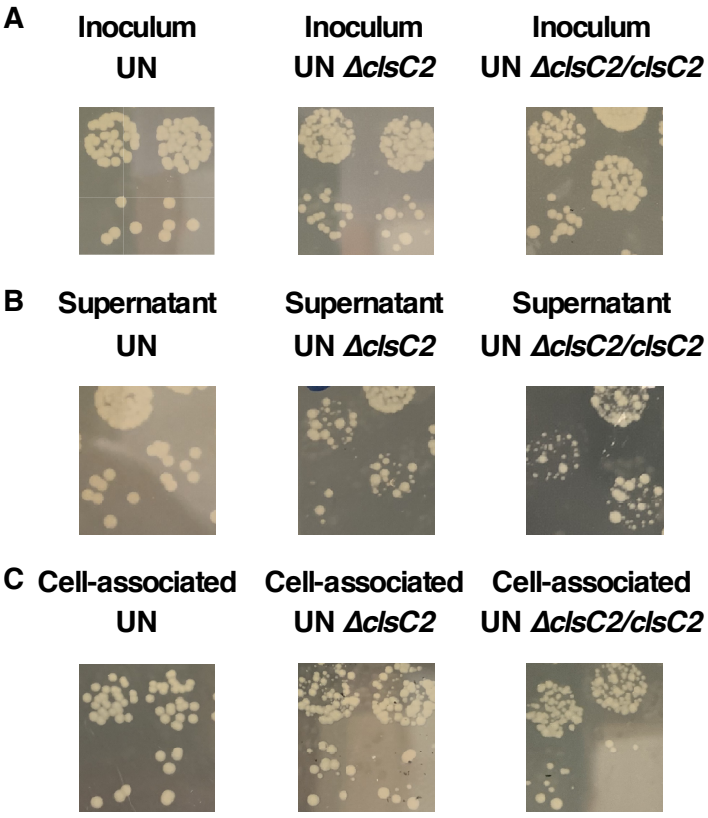

Figure 18. Small, punctate colonies are present in supernatants and lysates of macrophage-like RAW 264.7 cells infected with *Ab* 17978 UN *ΔclsC2* or *Ab* 17978 UN *ΔclsC2*/*clsC2*. A-C: Macrophage-like RAW 264.7 cells were infected with *Ab* 17978 UN, *Ab* 17978 *ΔclsC2*, or *Ab* 17978 *ΔclsC2*/*clsC2* at a target MOI of 15 and starting inoculums were serially diluted in PBS and plated on LBA (**A**). **B**: At 30 minutes post-infection, supernatants were serially diluted in PBS and plated on LBA. **C**: The remaining supernatant was aspirated, cells were washed twice with PBS, lysed with 0.01% Triton X-100, and lysates were serially diluted in PBS and plated on LBA.

3.3 Discussion

The process by which *A. baumannii* acquires or loses resistance to antimicrobials from gain or loss of genetic material is well characterized (249, 259). By contrast, less is known about how such genomic plasticity affects *A. baumannii* pathogenicity. Here, the discovery that two variants of *A. baumannii* ATCC 17978 differ based on the presence of the AbaAL44 accessory locus encompassing several pathogenesis genes is described. Review of the 5301 publicly available *A. baumannii* genome assemblies in the NCBI database reveals that genetic elements similar to AbaAL44 are present in at least 100 strains of *A. baumannii*. Of the 8 *A. baumannii* ATCC 17978 genome sequences published in NCBI, AbaAL44 is not present in any of them, but AbaAL44 is present in the *A. baumannii* 17978 genome published by the ATCC in 2019 (https://genomes.atcc.org/genomes/e1d18ea4273549a0). However, if laboratories assemble sequenced genomes of their *A. baumannii* 17978 laboratory stocks to a reference genome that does not include AbaAL44 (e.g. NZ_CP018664), the presence of AbaAL44 in these sequenced genomes would not be detected. When combined with data presented here, these findings suggest that the differential presence of AbaAL44 is a common structural genetic variant among *A. baumannii* strains, that laboratories studying *A. baumannii* ATCC 17978 may be working with either variant without awareness, or may be working with cultures containing a mix of the two variants. The differential presence of AbaAL44 among two variants of a type strain is most likely due to loss of AbaAL44 by *Ab* 17978 VU during the course of laboratory propagation. Adaptive loss of genetic material has been previously described for *Acinetobacter* spp. (286). Further, genetic differences among lineages of a given laboratory strain have previously been demonstrated for other species. Continuous maintenance and propagation of *Pseudomonas aeruginosa* strain PAO1 in laboratories throughout the world has led to substantial genotypic differences among sublines of this strain (195), and two lineages of *Clostridioides difficile* R20291 differ based on a small number of single nucleotide genomic changes leading to distinct phenotypic differences (196).

Ab 17978 VU and *Ab* 17978 UN exhibit differential fitness in a mouse model of pneumonia, which is likely due, in part, to the differential presence of AbaAL44. Putative pathogenesis genes present in AbaAL44, including the *katX* and *clsC2* genes, increase *Ab* 17978 UN resistance to oxidative stress, neutrophil-mediated killing, and surfactant stress. *A. baumannii* encounters hydrogen peroxide, the substrate of catalase enzymes, and surfactant inside the mouse lung (124, 287), and neutrophils are an essential component of the host immune response to infection with this pathogen (264-266). As such, the presence of an accessory *katX* and *clsC2* gene may confer some *in vivo* advantage to *Ab* 17978 UN in the setting of experimental bacterial pneumonia. *Ab* 17978 UN also potentiates neutrophilic lung inflammation *in vivo*, and increases the production of pro-inflammatory IL-1β by infected macrophages. This increase in inflammation and neutrophil recruitment to the site of infection may overwhelm any increased bacterial resistance to neutrophil-mediated killing in *Ab* 17978 UN, resulting in net decreased bacterial survival inside the mouse lung. The effects of other genes contained in AbaAL44 or polymorphisms elsewhere on the chromosome on *A. baumannii* fitness have not been interrogated but may contribute to the net differences in pathogenesis between these variants.

As IL-1β promotes the recruitment of neutrophils to the site of infection (267), the increased production of pro-inflammatory IL-1β by macrophages infected with *Ab* 17978 UN is likely to play a role in the shift toward neutrophilic inflammation observed in infected mice. Although differences in IL-1β concentration at 24 h.p.i. between mice infected with *Ab* 17978 VU and mice infected with *Ab* 17978 UN were not observed, such differences may occur earlier in the course of infection, culminating in the differential abundance of neutrophils observed at 24 h.p.i. Mitochondrial CL is a known activator of the NLRP3 inflammasome resulting in the production of IL-1β, and saturated CLs increase IL-1β production in a TLR4-dependent manner (102, 125). *In trans* expression of *clsC2* in *Ab* 17978 VU increased IL-1β production by infected macrophages, suggesting that the presence of the AbaAL44 *clsC2* gene in Ab 17978 UN may increase cell envelope CL content, resulting in NLRP3 inflammasome activation and enhanced IL-1β production by macrophages. Therefore, the differential presence of *clsC2* described

herein may lead to the modification of the *A. baumannii* cell envelope resulting in differences in pneumonia pathogenesis.

Infection with *Ab* 17978 UN resulted in decreased IL-10 production by infected macrophages relative to infection with *Ab* 17978 VU. Mitochondrial CL inhibits IL-10 production by recruiting a repressor complex to the *IL10* promoter. The reduction in anti-inflammatory IL-10 promotes persistent inflammation in experimental bacterial pneumonia (288, 289). It is conceivable that bacterial CL similarly inhibits IL-10 production and that modulation of bacterial CL content through the AbaAL44 *clsC2* gene is responsible for modulating macrophage IL-10 production. However, macrophage infection with a strain of *Ab* 17978 VU in which *clsC2* was expressed *in trans* did not recapitulate this finding. Paradoxically, macrophage infection with *Ab* 17978 VU/p*clsC2* increased IL-10 production. This suggests that the presence of *clsC2* alone cannot explain the relative decrease in IL-10 production observed in macrophages infected with *Ab* 17978 UN. Regulation of IL-10 production by immune cells is complex, and multiple factors affect its expression (290). Bacterial products such as cell wall components and lipopolysaccharide (LPS) increase macrophage IL-10 production through TLR2- and TLR4-mediated signaling, respectively (290, 291). By contrast, interferon gamma (IFNγ) inhibits IL-10 production (290). IFNγ production by macrophages is induced by IL-18, which, like IL-1β, is a product of NLRP3 inflammasome activation, and IL-1β production is increased in macrophages infected with *Ab* 17978 UN (292-294). Therefore, any combination of these factors may account for the differences in IL-10 production between macrophages infected with *Ab* 17978 UN and macrophages infected with *Ab* 17978 VU/p*clsC2*. Other genes contained in AbaAL44 or other genetic differences between the two *A. baumannii* 17978 variants may also account for the differential cytokine production by macrophages infected with *Ab* 17978 UN.

This Chapter demonstrates that the AbaAL44 *katX* and *clsC2* genes are advantageous to *Ab* 17978 UN survival *in vitro*. Specifically, the AbaAL44 *katX* gene present in *Ab* 17978 UN increases bacterial resistance to oxidative stress. In addition to the AbaAL44 *katX* gene described in this Chapter, two catalase genes – *katE* and *katG* – have previously been identified in *A. baumannii* (295). Increased

transcription of *katG* as a consequence of upstream insertion of IS*Aba1* has been demonstrated to increase *A. baumannii* resistance to oxidative stress (296). Taken together, these findings highlight the importance of catalases in *A. baumannii* pathogenesis, and provide an example of how increasing bacterial catalase gene abundance can contribute to *A. baumannii* pathogenicity, particularly in the setting of experimental pneumonia.

The findings presented herein implicate a dichotomous role for the AbaAL44 *clsC2* gene in *Ab* 17978 UN. While this gene promotes uptake of *Ab* 17978 UN by phagocytes, its presence also increases *Ab* 17978 UN resistance to envelope stressors such as surfactants. These findings are consistent with previous reports demonstrating that membranes with bacterial CL on their surface promote macrophage phagocytosis through the scavenger receptor CD36 (137), and that bacterial CL promotes resistance to osmotic and surfactant stress (122, 285). CL has also been demonstrated to increase *A. baumannii* resistance to cationic antimicrobial peptides, another envelope stressor, suggesting that increasing cell envelope CL content is a relevant survival strategy for this pathogen (297). In addition to the accessory *clsC2* described in this Chapter, both *Ab* 17978 VU and *Ab* 17978 UN contain two additional CL synthase genes. To our knowledge, however, the role of these genes in *A. baumannii* biology and pathogenesis remains to be fully elucidated. It has previously been reported that *A. baumannii* cell membranes contain a variety of unique, coexisting CL species (197). In *E. coli*, different CL synthase genes are active during distinct stages of bacterial growth (136). It is possible that the three CL synthase genes present in *A. baumannii* may be expressed during different growth phases, and/or may be responsible for synthesizing distinct species of CL. This notion is supported by recent findings demonstrating that individual enzymes of the same family are implicated in the production of either CL or monolysocardiolipin, an intermediate species in the CL remodeling pathway, in *A. baumannii* (297, 298). The *in vitro* growth defect and reduced uptake by RAW cells observed in *Ab* 17978 UN ∆*clsC2* could not be restored to levels of the parental strain by chromosomally reintroducing *clsC2* under its native promoter. This may be due to unidentified genetic differences between the ∆*clsC2* mutant and the parental *Ab* 17978 UN strain, or due to polar effects of the

Δ*clsC2*::kan deletion-insertion on nearby genes. However, expression of AbaAL44 *clsC2* in the Ab 17978 VU strain increased phagocytosis and IL-1β production by macrophages indicating that *clsC2* impacts *A. baumannii* interactions with the host. Given the fact that both the Gram-negative cell envelope and neutrophilic inflammation are molecular drivers of lung injury (**Chapter I**), these findings implicate a role for *A. baumannii* cell envelope lipid content modification in pneumonia pathogenesis.

Together, these findings indicate that two genotypically and phenotypically distinct variants of the common type strain, *A. baumannii* ATCC 17978, exist and are indiscriminately used in published studies of *A. baumannii* (299). As such, careful genotyping and phenotyping of *A. baumannii* type strains by individual laboratories may be warranted. Further, this Chapter demonstrates how *A. baumannii* genomic plasticity can affect pathogenicity and interactions with the host in the setting of *A. baumannii* pneumonia.

3.4 Materials and methods

Bacterial strains and culture conditions

Bacterial strains and plasmids used in this Chapter are listed in **Table 5**. *Ab* 17978 UN and *Ab* 17978 VU were received from ATCC in 2009 and in March, 2021. Strains were maintained as frozen stocks in lysogeny broth (LB) supplemented with 30% (vol/vol) glycerol at -80 °C. Unless noted otherwise, bacteria were grown on LB agar (LBA) at 37 °C, and single, isolated colonies were resuspended in LB and incubated overnight at 37 °C with constant agitation. Overnight cultures were diluted 1:100 in fresh LB and incubated for 3.5 hours at 37 °C with constant agitation until exponential phase. Exponential-phase cultures were washed twice with cold phosphate-buffered saline (PBS) and diluted to 1×10^{10} colony-forming units (CFUs) per mL in PBS. Bacterial cultures were diluted further as appropriate for each experiment.

Genome sequencing and analyses

The genomes of *A. baumannii* strains *Ab* 17978 VU and *Ab* 17978 UN were sequenced using PacBio sequencing by GENEWIZ (South Plainfield, NJ) (262). Pangenomes were assembled and annotated as follows: the raw sequence reads of the strains of *A. baumannii* were assembled using Flye version 2.4.2 with the genome size set to 3.86Mb, choosing the option for plasmid assembly and three polishing iterations. An Amazon AWS EC2 m5.2xlarge instance was used for all the assembly runs. Assembly statistics were compared and analyzed using Quast version 5.0.2 against the reference *A. baumannii* ATCC17978-mff genome from RefSeq NZ_CP012004.1. The assembled genomes were annotated using Prokka version 1.13.5. Pangenomes were created from these annotated genomes using Roary version 3.12.0 with the options -e -n -v. Average Nucleotide Identity (ANI) of the genomes of *Ab* 17978 VU and *Ab* 17978 UN was determined using an online ANI calculator (http://enve-omics.ce.gatech.edu/ani/). The assembled genomes of *Ab* 17978 VU and *Ab* 17978 are available in NCBI (accession numbers CP079213 for *Ab* 17978 VU and CP079212 for *Ab* 17978 UN). Additionally, *Ab* 17978 UN received from ATCC in 2021 was sequenced using Nanopore long read sequencing technology by the Microbial Genome Sequencing Center (MiGS, Pittsburgh, PA). This reference genome was deposited in NCBI and annotated using the Prokaryotic Genome Annotation Pipeline (PGAP) (accession numbers as follows: chromosome, CP079931; pAB3, CP079932; pAB1, CP079933; pAB2, CP079934).

To screen for other differences between the genomes of *Ab* 17978 VU and *Ab* 17978 UN such as SNPs, the genomes of both variants were sequenced as follows. DNA was isolated from *Ab* 17978 UN and *Ab* 17978 VU using Wizard Genomic DNA Purification Kit (Promega) or DNeasy Blood and Tissue Kit (Qiagen). DNA concentration was estimated with NanoDrop (Thermo). Library preparation by Nextera FLEX and sequencing by Illumina Novaseq 2X150 bp reads were performed at University of Illinois at Chicago Sequencing Core (UICSQC) or 2X100 bp reads at MiGS. The resulting reads were mapped to the ATCC *A. baumannii* 17978 VU genome (accession NZ_CP012004, NZ_CP012005,

CP000522.1, and CP000523.1) or Ab 17978 UN genome (CP079931, CP079932, CP079933, CP079934) using breseq version 0.35.5 with default settings (300, 301).

To screen for the presence of AbaAL44 in Vanderbilt University Medical Center (VUMC) and University of Illinois Chicago (UIC) laboratory *A. baumannii* 17978 stocks, individual colonies were screened for the presence of the accessory *clsC2* gene by standard PCR using primers specific to this gene (forward primer: TCTTTCTGGCTGGTTGCTTACTCAGC; reverse primer: CCGCAGCTTTCTGATTGAGACAGGC). PCR products were visualized on an agarose gel. Presence of PCR product indicated presence of *clsC2*, signifying that that particular colony belonged to the *Ab* 17978 UN variant. Absence of PCR product indicated absence of *clsC2*, signifying that that particular colony belonged to the *Ab* 17978 VU variant.

Construction of Ab 17978 UN ΔpilUs, Ab 17978 UN ΔkatX, Ab 17978 UN ΔclsC2, and complemented strains

Ab 17978 UN *ΔpilUs*, *Ab* 17978 UN *ΔkatX*, and *Ab* 17978 UN *ΔclsC2* were constructed by recombineering using the protocol by Tucker *et al.* (273). Briefly, primers were designed that include approximately 125 bp of sequence upstream of the gene/locus to be deleted fused to the kanamycin resistance (kan^R) cassette forward primer, CCGGAATTGCCAGCTGGG, and 125 bp of sequence downstream of the gene/locus to be deleted fused to the kan^R cassette reverse primer, TTCAGAAGAACTCGTCAAG (Integrated DNA Technologies). These primer pairs were used to amplify the kan^R cassette from pCR2.1 plasmid DNA (Invitrogen). After purification, approximately 10 μg of each amplification product was electroporated into electrocompetent *Ab* 17978 UN containing the recombinase plasmid, pAT02. Transformants were recovered at 37°C with shaking in LB containing 2 mM IPTG for 4 hours to induce recombinase expression prior to plating onto LB agar containing kanamycin. Kanamycin-resistant colonies were purified by serial passage and confirmed to have the appropriate deletion in two ways: first, by the difference in size of PCR amplification products using

primers that amplify the recombineered locus by binding the chromosome outside the flanking sequences included in the recombineering primers, and second, by PCR amplification using a primer that binds within the *kan*^{R} cassette and a primer that binds the chromosome outside of the flanking sequence included in the recombineering primer.

For *Ab 17978 UN ΔkatX*, the genetic defect was restored by expressing the accessory *katX* gene *in trans* as follows. *katX* was PCR-amplified using a forward primer annealing to the region upstream of *katX* (GTAATTGGATGAGGTGATGTATTAG) and a reverse primer annealing to the region downstream of *katX* (GGCCATCCTCATCAAATACTG). Forward and reverse primers contained a 20-nucleotide sequence overlapping with the BamHI- or SalI-digested plasmid, respectively. Subsequently, the amplicon was ligated into the BamHI and SalI restriction sites of the *E. coli – A. baumannii* shuttle vector pWH1266 under its native promoter using NEBuilder HiFi DNA Assembly (New England Biolabs, Ipswich, MA) to create pWH1266(*katX*) (287). Appropriate plasmid constructs were electroporated into *Ab 17978 UN ΔkatX* as described above.

For *Ab* 17978 UN *ΔclsC2*, the genetic defect was restored by reintegrating the accessory *clsC2* gene under its native promoter into a different part of the bacterial chromosome using methods described elsewhere (302). Briefly, *clsC2* was cloned into the pKNOCK-mTn7 plasmid to make pKNOCK(*clsC2*) as described above using a forward primer annealing to the region upstream of *clsC2* (CGCATCTTATAACGACAAAGAGAAC) and a reverse primer annealing to the region downstream of *clsC2* (GGGCGATAAAGCCACAGATAC). Next, *E. coli λpir116* was transformed with pKNOCK(*clsC2*), and *clsC2* was integrated into *Ab* 17978 UN *ΔclsC2* by setting up a four-way mate between *E. coli λpir116*/pKNOCK(*clsC2*), *E. coli* HB101/pRK2013, *E. coli* 100D/pTNS2*,* and *Ab* 17978 UN *ΔclsC2* to make Ab 17978 UN *ΔclsC2*/*clsC2*. Successful integration of *clsC2* into the correct spot on the *Ab* 17978 UN *ΔclsC2* chromosome was verified in two ways: first, by PCR amplification using a forward primer that binds the *A. baumannii* chromosome near the target insertion site (GTCGTTTTCGCTGATGAAAATAG) and a reverse primer that binds within the Tn7 element

(CACAGCATAACTGGACTGATTTC), and second, by PCR amplification of the *clsC2* gene inserted into the Tn7 element.

To express *clsC2* in trans in *Ab* 17978 VU, *clsC2* was cloned into pWH1266 as described above using a forward primer annealing to the region upstream of *clsC2* (AACCTTCTTAGATTATAACAAAATCATACAGTTATTG) fused to a 20-nucleotide sequence overlapping with the BamHI-digested plasmid and a reverse primer annealing to the region downstream of *clsC2* (GCTCTCGAGAAAAAAGCAGAAG) fused to a 20-nucleotide sequence overlapping with the SalI-digested plasmid to generate pWH1266(*clsC2*). This plasmid construct (or the empty vector) was electroporated into *Ab* 17978 VU as described above.

Murine infection models

All animal experiments were approved by the Vanderbilt University Medical Center (VUMC) Institutional Care and Use Committee and conform to policies and guidelines established by VUMC, the Animal Welfare Act, the National Institutes of Health, and the American Veterinary Medical Association. Wildtype, female, eight-week-old C57BL/6 mice were purchased from Jackson Laboratories. The murine model of *A. baumannii* pneumonia was performed as previously described (216). Briefly, *A. baumannii* was back-diluted 1:100 from overnight culture and grown in (LB) for 3.5 hours at 37°C with constant agitation, washed twice with cold PBS, and resuspended in PBS at an appropriate cell density for infection. Mice were infected intranasally with 3×10^8 CFUs of *A. baumannii* in 30 µL PBS. At 24 or 36 h.p.i., mice were euthanized and organs were harvested. Lungs and spleens were homogenized, serially diluted in PBS, and plated onto LBA for bacterial enumeration. For histological analyses, lungs were inflated with 1 mL of 10% formalin, fixed, embedded and stained as described previously (303). Mice were randomized to treatment groups using the GraphPad QuickCalcs online randomization software available at (https://www.graphpad.com/quickcalcs/randomize1.cfm).

Histology

Paraffin-embedded mouse tissue sections were stained with hematoxylin and eosin by the Vanderbilt University Medical Center Translational Pathology Shared Resource. Specimens were examined and imaged by K. L. B. who was blinded to the treatment. Images are representative of at least 2 independent experiments.

Bacterial growth assays

Overnight cultures of single, isolated colonies were generated as described above. To prepare for growth assays, overnight cultures were standardized to a similar optical density at 600 nm (OD_{600}) and subsequently diluted 1:100 in 200 µL of rich media (LB) or minimal media (Tris Minimal Succinate – TMS) in 96-well flat bottom tissue culture plates (Corning™ Costar™). Plates were incubated for 24 hours at 37°C with shaking and growth was assayed by measuring OD_{600} at the indicated times using a BioTek Synergy 2 Multi-Mode Reader (BioTek).

Scanning electron microscopy analyses

Bacterial cells were analyzed by scanning electron microscopy as previously described with some modifications (304). Briefly, bacteria were cultured in LB at 37 ºC overnight. The following day, samples were fixed with 2.0% paraformaldehyde (Electron Microscopy Sciences), 2.5% glutaraldehyde (Electron Microscopy Sciences) in 0.05 M sodium cacodylate (Electron Microscopy Sciences) buffer for 24 hours. After primary fixation, samples were secondarily fixed in fresh 2.0% paraformaldehyde, 2.5% glutaraldehyde in 0.05 M sodium cacodylate buffer on poly-L-lysine coated glass coverslips (ThermoFisher) for 4 hours. Samples were washed three times with 0.05 M sodium cacodylate buffer before sequential dehydration with increasing concentrations of absolute ethanol. After ethanol dehydration, samples were dried at the critical point using a critical point dryer machine (Tousimis), mounted onto aluminum SEM sample stubs (Electron Microscopy Sciences), and sputter-coated with 5 nm of gold-palladium. Afterward, samples were painted with a thin strip of colloidal silver (Electron

Microscopy Sciences) at the edge to facilitate charge dissipation. Bacteria were imaged with an FEI Quanta 250 field-emission gun scanning electron microscope. Micrographs shown are representative of at least four biological replicates. Pili were quantified as the fraction of cells expressing pili (no. cells with pili/ total no. cells in each image) and the number of pili per piliated cell. At least 12 representative images of each strain were scored in a blinded manner for each of four independent experiments.

Hemagglutination assay

Hemagglutination experiments were performed based on a protocol by Greene et al. (305) with modifications. *Ab* 17978 VU, *Ab* 17978 UN, and *Ab* 17978 UN *Δpilus* were grown overnight on LBA or in LB for 48 hours at 37 °C without agitation as indicated. *E. coli* UTI 89 (positive control) and *E. coli* UTI89 *ΔfimAH* (negative control) were grown in LB for 24 hours at 37 °C without agitation, diluted 1:1000 in LB and incubated for another 24 hours at 37 °C without agitation. Bacteria were normalized to an OD_{600} of 1.0, after which 1 mL of each culture was pelleted and resuspended in 100 μL of PBS. 25 μL of bacteria were diluted serially in wells of a 96-well, U-bottom plate containing 25 μL of PBS, after which an equal volume of a 1% suspension of washed, human erythrocytes (Innovative Research, Novi, MI, USA) was added to each well. Wells were incubated overnight at 4 °C without agitation, after which the hemagglutination titer (i.e. the maximum dilution at which bacteria are able to agglutinate erythrocytes) was recorded for each strain.

Biofilm formation

Stationary-phase cultures of *Ab* 17978 VU, *Ab* 17978 UN, and *Ab* 17978 UN *Δpilus* were diluted 1:10 in LB in wells of a 96-well plate and incubated statically at 37 °C for 24-48 hours. After incubation, half of the wells were used for the determination of biomass by measuring OD_{600}, and the other half was used for the measurement of biofilm formation. Biofilm formation was determined as follows: supernatants were aspirated from each well, cells were permeabilized with 100% EtOH, and biofilms

were stained with crystal violet solution (0.41% in 12% EtOH) for 20 minutes. After staining, wells were washed vigorously with PBS, and biofilms were solubilized with 33% acetic acid, after which OD_{580} was measured for each well. Biofilm formation was recorded as the ratio of biofilm to biomass (i.e. OD_{580}/OD_{600}) (306).

A549 epithelial cell adhesion assay

Immortalized, human A549 epithelial cells were maintained as frozen stocks in liquid nitrogen. Prior to infection experiments, A549 cells were maintained in Gibco Dulbecco's Modified Eagle Medium (DMEM, ThermoFisher Scientific) supplemented with 10% heat-inactivated fetal bovine serum (FBS) and 1% penicillin/streptomycin (P/S). A549 cells were grown until ~75% confluency after which they were split 1:3 in fresh medium. To prepare for infection experiments, A549 cells were seeded onto wells of 12-well plates and grown until confluency. Next, media was aspirated from each well, and A549 cells were washed twice with pre-warmed PBS. A549 cells were then infected with mid log-phase bacteria suspended in DMEM without antibiotics at a multiplicity of infection (MOI) of 100, after which wells were incubated at 37 °C for 2 hours. At 2 h.p.i., media was aspirated from each well, and non-adherent bacteria were removed by washing wells three times with PBS. A549 cells were then lysed by adding 1% Triton X-100 to each well, and incubating plates at RT for 10 minutes. After lysis, 800 µL of ice-cold PBS was added to each well, and the contents of each well were pipetted up and down several times to suspend bacteria. The number of cell-associated bacteria was then determined via serial dilution in PBS and plating onto LBA. Data are represented as the percentage of cell-associated bacteria relative to *Ab* 17978 VU.

Bacterial surface associated motility assay

Stationary-phase cultures of *Ab* 17978 VU, *Ab* 17978 UN, and *Ab* 17978 UN *Δpilus* were washed once in LB, resuspended in LB, and standardized to a similar OD_{600} using LB as a diluent. Next, 1 µL

of standardized bacterial cultures was inoculated on the surface of motility agar plates at the center. Bacterial inoculums were allowed to dry, after which plates were wrapped in parafilm and incubated overnight, upside down, single file at 37 °C. After incubation, the maximum motility radius was measured.

Hydrogen peroxide susceptibility assay

Ab 17978 VU, *Ab* 17978 UN, *Ab* 17978 UN *ΔkatX*/EV, and *Ab* 17978 UN *ΔkatX*/p*katX* were grown to mid-exponential phase as previously described, and inoculated into LB supplemented with 1 mM H_2O_2 at a starting inoculum of 1×10^7 CFU/mL. Bacteria were then incubated at 37 °C for 30 minutes with constant agitation, after which the remaining number of viable bacteria was determined via serial dilution in PBS and plating onto LBA.

Total neutrophil-mediated killing (extra- and intracellular)

Neutrophil-like HL-60 cells were maintained in RPMI medium (25 mM HEPES buffer) supplemented with 10% heat-inactivated FBS and 1% P/S. Prior to infection experiments, HL-60 cells were differentiated in media supplemented with 1.3% DMSO for 6 days. On the day of infection, differentiated HL-60 cells were seeded at a density of $1.4\text{-}1.8\times10^5$ cells/well in wells of a 96-well suspended in RPMI supplemented with 0.5% heat-inactivated FBS and incubated at 37 °C for 30 minutes. Bacteria for the infection were prepared as follows: *Ab* 17978 VU, *Ab* 17978 UN, *Ab* 17978 UN *ΔkatX*/EV, and *Ab* 17978 UN *ΔkatX*/p*katX* were grown to mid log-phase and washed and diluted in PBS as previously described. Prior to infection of neutrophils, bacteria were opsonized by resuspension in 20% normal human serum in RPMI and subsequent incubation at 37 °C for 30 minutes with constant shaking at 50 RPM. Immediately following opsonization, bacteria were resuspended in RPMI supplemented with 0.5% heat-inactivated FBS and diluted further to the appropriate cell density for infection. Next, bacteria were added to each well at an MOI of 2, and the infection was synchronized

by centrifuging the 96-well plate at 200×g for 9 minutes at 4 °C. Inoculums were verified by serially diluting in PBS and plating on LBA. The plate was then incubated for 90 minutes at 37 °C, after which infected HL-60 cells were lysed by adding saponin to a final concentration of 0.1% to each well and incubating on ice for 15 minutes. Next, lysates were serially diluted in PBS and plated onto LBA for bacterial enumeration.

Murine neutrophils were isolated as follows. Murine hind limbs were dissected and bone marrow was isolated as previously described (307). Briefly, bone marrow was isolated from the long bones of C57BL/6 mouse hind limbs via centrifugation, washed, red blood cells were lysed, and the bone marrow suspension was passed through a cell strainer prior to counting. Neutrophils were isolated using a mouse neutrophil isolation kit (Miltenyi Biotec) according to the manufacturer's protocol. Infection of murine neutrophils was performed as described above with modifications: Purified neutrophils were seeded at a density of 1.6-3.2×10^5 cells/well in wells of a 96-well plate pre-treated with 100 μL of 20% normal human serum, after which they were allowed to attach to well bottoms by incubating plates at room temperature for 30 minutes. *Ab* 17978 VU, *Ab* 17978 UN, and *Ab* 17978 UN *ΔkatX* were opsonized by resuspension in 50% C57BL/6 mouse complement serum (Innovative Research, Novi, MI, USA) in RPMI medium supplemented with 10 mM HEPES buffer (RPMI/H). Immediately following opsonization, bacteria were washed twice with RPMI/H and diluted in RPMI/H to the appropriate cell density for infection. Bacteria were added to each well at an MOI of 1, and the plate was incubated for two hours at 37 °C following synchronization of the infection as described above. Neutrophils were lysed and viable bacteria were enumerated as described above.

Bacterial uptake by macrophages

Immortalized, macrophage-like RAW 264.7 cells were maintained as frozen stocks in liquid nitrogen. Prior to infection experiments, RAW cells were maintained in DMEM supplemented with 10% heat-inactivated FBS and 1% P/S. RAW cells were grown until ~75% confluency after which they were

split 1:10-1:20 in fresh medium. To prepare for infection experiments, RAW cells were seeded onto wells of 12-well plates at a seeding density of 5×10^5 cells/well and activated with 100 ng/mL of LPS, after which they were incubated overnight at 37 °C. On the day of infection, mid log-phase cultures of *A. baumannii* were prepared as previously described, after which bacteria were resuspended in DMEM + 10% FBS devoid of antibiotics at the appropriate bacterial density to reach a target MOI of 15. Media was then aspirated from all wells, RAW cells were washed once with pre-warmed PBS, and 1 mL of appropriate bacteria suspended in media was added to each well. Inoculums were verified by serially diluting in PBS and plating on LBA. Infected RAW cells were then incubated at 37 °C for 30 minutes, after which media was aspirated and wells were washed twice with pre-warmed PBS. Next, extracellular bacteria were killed by adding 1 mL of media supplemented with 200 µg/mL gentamicin to each well and incubating at 37 °C. Thirty minutes after the addition of gentamicin, media was aspirated, cells were washed once with PBS, and cells were lysed by adding 200 µL of 0.01% triton to each well. Each well was scraped with a sterile cell scraper, after which the lysate was serially diluted in PBS and plated onto LBA for the enumeration of intracellular bacterial burden.

Bacterial cell envelope stress assays

Bacterial susceptibility to osmotic stress was assayed as follows: *Ab* 17978 VU, *Ab* 17978 UN, *Ab* 17978 UN *ΔclsC2*, and *Ab* 17978 UN *ΔclsC2*/*clsC2* were grown to mid-exponential phase as previously described, and inoculated into LB supplemented with 2.5M of NaCl at a starting inoculum of 1×10^7 CFU/mL. Bacteria were then incubated at 37 °C for two hours with constant agitation, after which bacterial viability was determined via serial dilution in PBS and plating onto LBA. Bacterial survival was calculated as the percentage of viable bacteria post-incubation relative to the number of viable bacteria pre-incubation. Bacterial susceptibility to detergent stress was assayed as follows: *Ab* 17978 VU, *Ab* 17978 UN, *Ab* 17978 UN *ΔclsC2*, and *Ab* 17978 UN *ΔclsC2*/*clsC2* were prepared as above, and resuspended in PBS supplemented with 0.1% Triton X-100 at a starting inoculum of 1×10^{10} CFU/mL.

Bacteria were then incubated at 37 °C for six hours with constant agitation, after which bacterial viability and survival were determined and calculated as above.

Detection of cytokines produced by infected macrophages

BMDMs were isolated and maintained as previously described (308). Briefly, bone marrow was isolated from the long bones of C57BL/6 mouse hind limbs via centrifugation, washed, red blood cells were lysed, and the bone marrow suspension was passed through a cell strainer prior to counting. The bone marrow cell suspension was plated at a density of 3 x 10^6 cells/ml in BMDM medium (RPMI medium supplemented with 10% FBS and 20% LC medium) and incubated at 37°C with 5% CO_2. Every 48 hours, media was aspirated and fresh BMDM medium was added to each plate. On day six, BMDMs were collected and seeded onto 12-well plates at a density of 1-2.5×10^6 cells/well in BMDM media, and incubated overnight at 37 °C. On day 7, mid log-phase cultures of *A. baumannii* were prepared as previously described, and diluted to the appropriate bacterial density in RPMI medium supplemented with 10% FBS for a target MOI of 10. Media was then aspirated from all wells, and BMDMs were washed once with pre-warmed PBS, after which bacteria suspended in 1 mL of media were added. As a negative control, BMDMs were infected with media alone, and as a positive control, BMDMs were treated with media supplemented with 100 ng/mL of LPS or 100 ng/mL of LPS + 2 mM ATP. Plates were then incubated at 37 °C and the supernatant was collected at 18 h.p.i. Cytokines and chemokines (IL-1β, IL-10, KC, MIP-2) in BMDM supernatants were quantified using an ELISA kit (R&D systems, Minneapolis, MN) according to the manufacturer's protocol for each.

Complete blood count

Complete blood counts with five-part differential were performed on EDTA-treated whole mouse blood by the Vanderbilt University Medical Center Translational Pathology Shared Resource.

Immune cell recruitment

Flow cytometric analyses were performed with total erythrocyte-free lung cells isolated at 24 h.p.i. from individual mice infected with *Ab* 17978 VU or *Ab* 17978 UN as indicated. Lungs were minced, digested with collagenase and DNase for 30 minutes, and passed through a 70 μm cell strainer prior to erythrocyte lysis. Cells were stained with a myeloid panel that included antibodies against CD45 (clone 104, FITC, eBioscience), CD103 (clone 2E7, PerCP-Cy5.5, BioLegend), CD64 (clone X54-5/7.1, PE, BioLegend), CD11c (clone HL-3, PE-Cy7, BD Pharmingen), Siglec F (clone E50-2440, Horizon PE-CF594, BD Pharmingen), CD11b (clone M1/70, eFluor-450, eBioscience), MHCII (clone M5/114.15.2, BV605, BD Pharmingen), CD24 (clone M1/69, APC, eBioscience), Ly6C (clone AL-21, APC-Cy7, BD Pharmingen), and Ly6G (clone 1A8, Alexa Fluor 700, BD Pharmingen). Analyses were carried out on the 5-laser BD LSR Fortessa (BD Biosciences) at the Vanderbilt Flow Cytometry Shared Resource, and analyses were performed using FlowJo software (Treestar Inc). Myeloid populations were gated according to the strategy of Misharin and colleagues (205, 309).

Quantification and statistical analysis

Statistical analyses were performed using GraphPad Prism version 6. Mean comparisons were performed using unpaired Welch's *t*-test or one-way ANOVA adjusted for multiple comparisons as indicated. P values less than 0.05 were considered statistically significant. Statistical details of experiments can be found in the figure legends.

Table 5. Bacterial strains and plasmids used in this Chapter

Strain/plasmid	Description	Source	Reference
Ab 17978 VU	Variant of *A. baumannii* ATCC 17978 that lacks AbaAL44, stored at Vanderbilt University	Vanderbilt University	ATCC
Ab 17978 UN	Variant of *A. baumannii* ATCC 17978 that harbors AbaAL44, stored at the University of Nebraska	University of Nebraska	ATCC, (303)
Ab 17978 UN *Δpilus*/pAT02	*Ab* 17978 UN with accessory pilus locus (*smf1, yadV, htrE, and mrkD*) replaced by kan^R cassette		This Chapter
Ab 17978 UN *ΔkatX*	*Ab* 17978 UN with accessory *katX* gene (KZA74_09300) replaced by kan^R cassette		This Chapter
Ab 17978 UN *ΔkatX*/EV	*Ab* 17978 UN *ΔkatX* transformed with pWH1266		This Chapter
Ab 17978 UN *ΔkatX*/p*katX*	*Ab* 17978 UN *ΔkatX* transformed with pWH1266(*katX*)		This Chapter
Ab 17978 UN *ΔclsC2*	*Ab* 17978 UN with accessory cardiolipin synthase gene (*clsC2*) replaced by kan^R cassette		This Chapter
Ab 17978 UN *ΔclsC2*/*clsC2*	*Ab* 17978 UN *ΔclsC2* with *clsC2* reintegrated chromosomally under its native promoter		This Chapter
Ab 17978 VU/EV	*Ab* 17978 VU transformed with pWH1266		This Chapter
Ab 17978 VU/p*clsC2*	*Ab* 17978 VU transformed with pWH1266(*clsC2*)		This Chapter
E. coli UTI89	Prototypical UPEC strain	Dr. Maria Hadjifrangiskou (Nashville, TN)	(310)

E. coli UTI89 *ΔfimAH*	Prototypical UPEC strain with *fimA* and *fimH* genes deleted	Dr. Maria Hadjifrangiskou (Nashville, TN)	(311)
E. coli 100D/pTNS2	*E. coli* 100D transformed with helper plasmid encoding the site-specific TnsABCD Tn7 transposition pathway		(302)
E. coli HB101/pRK2013	*E. coli* HB101 transformed with oriT helper-containing plasmid		(302)
E coli DH5α *λpir116*	Strain that permits maintenance of plasmids at high copy numbers	Dr. Eric Skaar (Nashville, TN)	
pCR2.1	Vector to amplify kan^R cassette for insertion		(213)
pAT02	precET-carb confers carb/amp resistance and *A. baumannii* recombinase		(273)
pWH1266	*E. coli – A. baumannii* shuttle vector conferring ampicillin and tetracycline resistance		(312)
pKNOCK-mTn7-amp	Plasmid with R6K origin of replication and mini-Tn7 element		(302, 313)

CHAPTER IV

DELINEATING THE ROLE OF CARDIOLIPIN OVEREXPRESSION BY *ACINETOBACTER BAUMANNII* IN PNEUMONIA PATHOGENESIS

4.1 Introduction

The lipid composition of the Gram-negative cell envelope is dominated by LPS (or LOS) and PE. A small minority is comprised of the anionic lipids PG and CL (**Chapter I**). Despite this, the model Gram-negative organism *E. coli* harbors three genes encoding CL synthase enzymes: *clsA*, *clsB*, and *clsC* (136). Similarly, the nosocomial pathogen *A. baumannii* encodes up to three such genes as well: *clsA*, *clsC1*, and *clsC2* (**Chapter III)**. This implies an important role for CL in bacterial physiology and pathogenesis. Although there may be some functional redundancy, the activity of different *cls* genes is temporally regulated. In *E. coli*, ClsA synthesizes the majority of CL during logarithmic growth phase. During stationary phase, ClsA activity increases and ClsB and ClsC are activated as well, resulting in an overall increase in CL abundance during this growth phase (136, 314). The temporal regulation of *cls* gene expression in *A. baumannii* remains to be experimentally verified. Further, *A. baumannii* synthesizes multiple species of CL and monolysocardiolipin (197), and different enzymes are implicated in the synthesis of either CL or monolysocardiolipin (297). In *S. aureus*, increased CL biosynthesis due to enhanced *cls2* activity promotes persistent infection and leads to resistance to the antibiotic daptomycin (315). These findings suggest that bacterial pathogens may be capable of modulating CL abundance and/or composition by differentially expressing Cls enzymes. However, to what extent pathogenic bacteria such as *A. baumannii* vary in cell envelope CL content within species, between species, and/or over the course of infection remains to be fully elucidated.

It is well-established that pathogenic bacteria can modify LPS composition over the course of infection (114, 115). Furthermore, bacterial LPS/LOS is a recognized driver of pneumonia pathogenesis through TLR4-mediated immune signaling and inflammasome activation (89, 93, 97, 316). Similarly, CL affects the host response to infection. Bacterial CL differentially activates TLR4-mediated pro-

inflammatory cytokine production depending on acyl chain saturation (125), and promotes phagocytic uptake by macrophages (137). In addition, mitochondrial CL is a direct agonist of the NLRP3 inflammasome, leading to the production of the pro-inflammatory cytokines IL-1β and IL-18 (102). In the setting of pneumonia, release of mitochondrial CL into the extracellular environment promotes lung injury (104). By contrast, the role of bacterial CL as a molecular driver of inflammation and lung injury during bacterial pneumonia is underexplored. The contribution of bacterial variability in cell envelope CL content to these processes remains to be investigated as well.

In the present chapter, preliminary inquiries into intra- and inter-species variability in cell envelope CL content are described, and the differential expression of *cls* genes during logarithmic growth phase in *A. baumannii* is interrogated. Further, some of the effects of *A. baumannii* CL overexpression on the interactions between this pathogen and host innate immune cells are assessed.

4.2 Results

Pathogenic bacteria vary in genomic cls gene content, and increased cls gene content correlates with increased CL content in A. baumannii.

Two variants of *A. baumannii* strain 17978 differ based on the presence of a 44-kb accessory locus (AbaAL44), which encompasses a *cls* gene: *clsC2*. As such, *Ab* 17978 UN harbors three *cls* genes (*clsA*, *clsC1*, and *clsC2*), whereas *Ab* 17978 VU only harbors *clsA* and *clsC* (**Chapter III**). This finding is suggestive of intra-species variability in genomic *cls* gene content in *A. baumannii*. To test the hypothesis that other pathogenic bacteria vary in genomic *cls* gene content, a preliminary literature review was conducted. The pathogenic bacteria included in this preliminary review or in the studies described in **Chapter III** harbor at least one, and up to three, *cls* genes (**Fig. 19A**). Specifically, *Moraxella catarrhalis* harbors 1 *cls* gene; *S. aureus*, *K. pneumoniae* HS11286, and *A. baumannii* 17978 VU all harbor two *cls* genes; and *P. aeruginosa*, *K. pneumoniae* ST67, *Salmonella enterica*, and *A. baumannii* 17978 UN all harbor three *cls* genes (198, 199, 317) (**Fig. 19A**). These findings demonstrate

that there is both inter- and intra-species variation in genomic *cls* gene content among pathogenic bacteria.

To test the hypothesis that increased genomic *cls* gene content correlates with increased CL abundance in *A. baumannii*, total lipids were extracted from mid-logarithmic-phase cultures of *Ab* 17978 VU and *Ab* 17978 UN, and CL was quantified using liquid chromatography coupled with tandem mass spectrometry (LC-MS/MS). Poly-unsaturated CL was by far the most prevalent type of CL in both variants, followed by mono-unsaturated CL and saturated CL, respectively (**Fig. 19C-E**). Relative to *Ab* 179878 VU, there was a statistically significant, 2 – 2.5-fold increase in the abundance of saturated, mono-unsaturated, poly-unsaturated CL, and total CL in lipids extracted from *Ab* 17978 UN (**Fig. 19C-E**). These data demonstrate that, in *A. baumannii*, increased genomic *cls* gene content correlates with increased CL abundance, and that *Ab* 17978 UN overexpresses CL in comparison to *Ab* 17978 VU.

To determine the relative activity of each *cls* gene – *clsA*, *clsC1*, and *clsC2* – during logarithmic growth phase in *A. baumannii*, expression of each gene was quantified using reverse transcription quantitative PCR (RT-qPCR). With the exception of *clsC2* in *Ab* 17978 VU (which lacks this gene), expression of each gene was detected in both *Ab* 17978 VU and *Ab* 17978 UN during logarithmic growth phase (**Fig. 20**). There was no significant difference in *clsA* expression between the two variants (**Fig. 20A**), but there was an approximate 2.5-fold increase in *clsC1* expression in *Ab* 17978 VU compared to *Ab* 17978 UN, although this did not reach statistical significance (**Fig. 20B**). These data suggest that all three *cls* genes are expressed during logarithmic growth phase in *A. baumannii*. In addition, *clsC1* may potentially be more highly expressed in *Ab* 17978 VU, which does not express *clsC2* (**Fig. 20B and C**). These data suggest that expression of *clsC2* may downregulate expression of *clsC1*, and imply some functional redundancy between *clsC1* and *clsC2*.

Given the fact that AbaAL44, which harbors *clsC2*, is present in at least 100 isolates of *A. baumannii* (**Chapter III**), these data suggest that increased cell envelope CL content is not uncommon among strains of *A. baumannii* and may therefore be relevant to its (infection) biology. Furthermore, these two variants of *A. baumannii* may provide an opportunity to study the effects of increased CL

content on *A. baumannii* infection biology, and of bacterial cell envelope CL content variability on pneumonia pathogenesis in general.

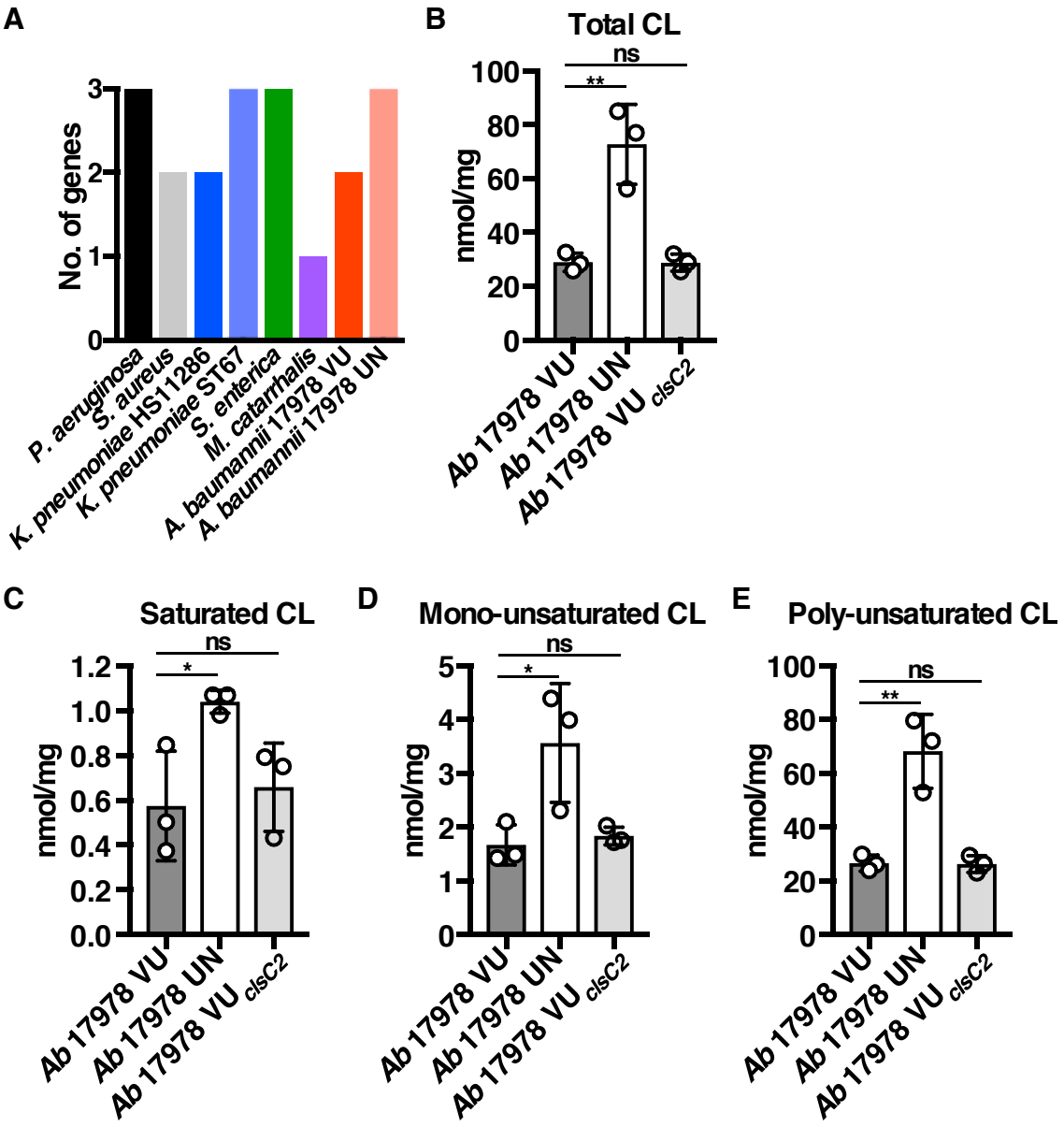

Figure 19. Pathogenic bacteria vary in genomic *cls* gene content, and increased *cls* gene content correlates with increased CL abundance in *A. baumannii*. A: Literature and publicly accessible databases (NCBI, UniProt) were reviewed to assess the number of different *cls* genes present in the genomes of pathogenic bacteria. **B-E**: Total lipids were extracted from mid-logarithmic-phase cultures of *Ab* 17978 VU, *Ab* 17978 UN, and *Ab* 17978 VU_{clsC2}. The relative abundance of __ distinct species of CL were quantified using LC-MS/MS, and the average abundance of total (**B**), saturated (**C**), mono-unsaturated (**D**), and poly-unsaturated (**E**) CLs were compiled for each variant/strain and depicted in each graph as indicated. **B-E**: N=3 biological replicates per variant/strain, and data are from one experiment. Circles represent individual samples, columns depict the mean and error bars show standard deviation of the mean. Means were compared using a one-way ANOVA adjusted for multiple comparisons. *: $p<0.05$; **: $p<0.01$; ns: not significant.

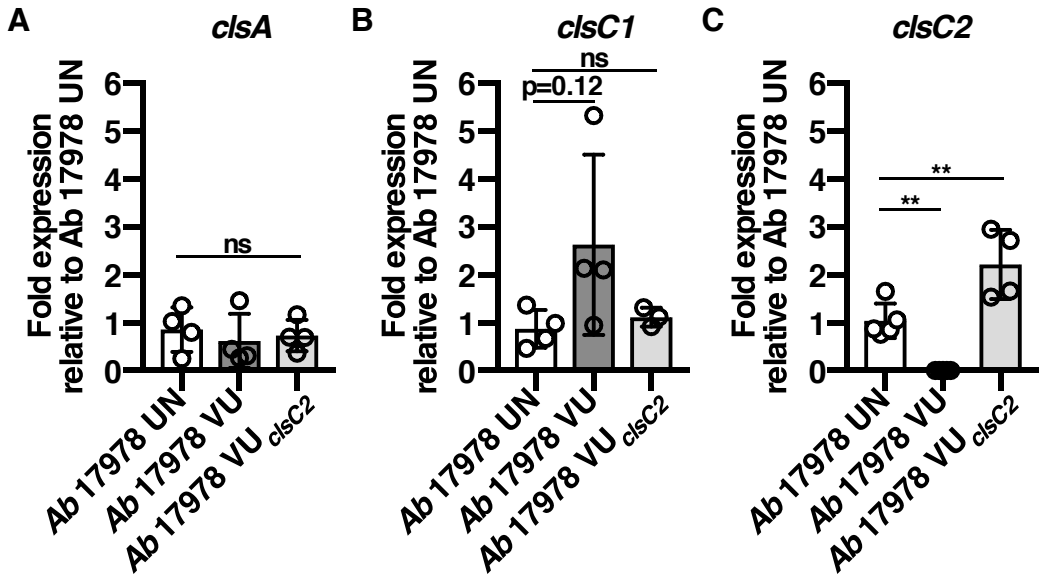

Figure 20. Relative expression of three *cls* genes in *A. baumannii* variants during logarithmic growth phase. A-C: Total RNA was extracted from mid-logarithmic-phase cultures of *Ab* 17978 VU, *Ab* 17978 UN, and *Ab* 17978 VU$_{clsC2}$, and the relative expression of *clsA*, *clsC1*, and *clsC2* was quantified using RT-qPCR. Expression of each gene is depicted as fold-expression relative to expression of that gene in *Ab* 17978 UN. **A-C**: N=3-5 biological replicates per variant/strain, and data are from one experiment. Circles represent individual samples, columns depict the mean and error bars show standard deviation of the mean. Means were compared using a one-way ANOVA adjusted for multiple comparisons. **: $p<0.01$; ns: not significant.

Expression of clsC2 under the control of an inducible promoter in Ab 17978 VU may promote bacterial resistance to osmotic stress.

Besides the differential presence of *clsC2*, there are additional genetic differences between *Ab* 17978 VU and *Ab* 17978 UN (**Chapter III**). As such, these two variants cannot be used in a head to head comparison to determine the effects of CL overexpression on *A. baumannii* pathogenesis. Instead, *clsC2* was introduced into the genetic background of *Ab* 17978 VU in three different ways: *in trans*, chromosomally under its native promoter, or chromosomally under an inducible promoter (*lac*). In *Ab* 17978 UN, *clsC2* promotes resistance to osmotic and detergent stress (**Chapter III**), and *clsC2* expression is correlated with increased abundance of CL (**Fig. 19 and 20**). Therefore, the hypothesis that *clsC2* expression promotes bacterial resistance to osmotic and detergent stress in *Ab* 17978 VU was tested. Specifically, *Ab* 17978 VU (WT), *Ab* 17978 VU_{clsC2}, *Ab* 17978 VU_{lac}, and *Ab* 17978 VU_{lac_clsC2} were grown in or exposed to varying concentrations of NaCl or the detergent Triton X-100. Both NaCl and Triton X-100 impeded growth of *Ab* 17978 VU and *Ab* 17978 VU_{clsC2} in a dose-dependent manner (**Fig. 21A** and **B**). However, there were no biologically meaningful or statistically significant differences between these two strains (**Fig. 21A** and **B**). Similarly, there were no differences in bacterial survival between these two strains after exposure to 2.5 M NaCl or 0.1% Triton X-100 (**Fig. 21C** and **D**). Intriguingly, *Ab* 17978 VU_{clsC2} showed similar gene expression patterns for both *clsA* and *clsC1* compared to *Ab* 17978 UN, and exhibited two-fold greater expression of *clsC2* during logarithmic phase (**Fig. 20**). Despite high expression of *clsC2*, there were no significant increases in the abundance of saturated, mono-unsaturated, poly-unsaturated, or total CLs between *Ab* 17978 VU_{clsC2} and the *Ab* 17978 VU parental strain (**Fig. 19B-E**). These data suggest that expression of *clsC2* alone is not sufficient to increase cell envelope CL content in *A. baumannii*.

By contrast, induction of *clsC2* expression in *Ab* 17978 VU_{lac_clsC2} with 8 mM of IPTG increased bacterial survival after exposure to 2.5 M NaCl or 0.1% Triton X-100 compared to *Ab* 17978 VU_{lac}. For NaCl, this difference was statistically significant (**Fig. 21E and F**). Thus, these data imply that expression of *clsC2* under the control of an inducible promoter may promote *A. baumannii* resistance

to osmotic and possibly detergent stress. However, expression levels of *clsC2* were not empirically determined in these strains.

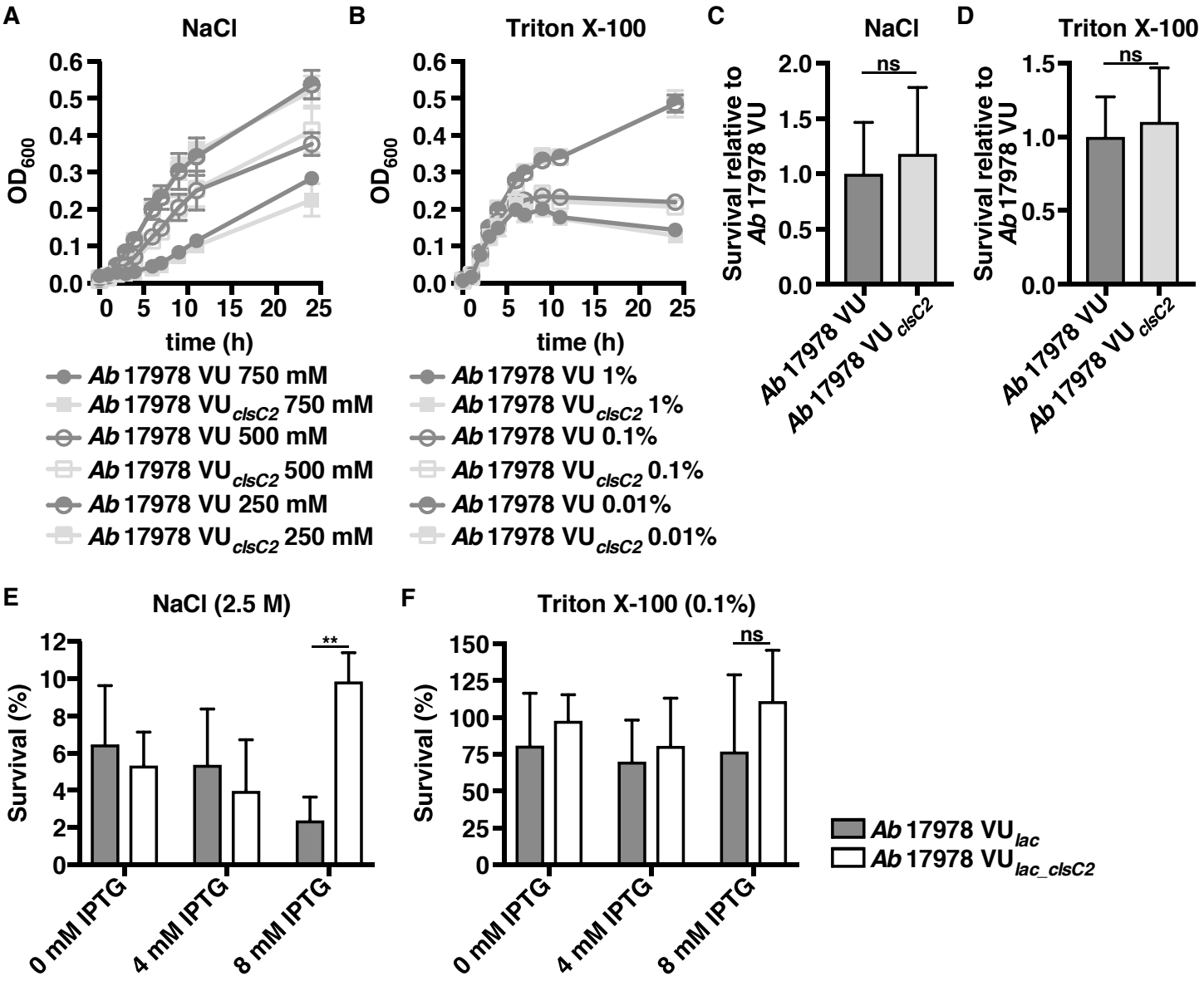

Figure 21. Expression of *clsC2* under the control of an inducible promoter in *Ab* 17978 VU may promote bacterial resistance to osmotic stress. A and B: *Ab* 17978 VU (WT) and *Ab* 17978 VU_{clsC2} were grown in the presence of varying concentrations of NaCl or Triton X-100 as indicated, and bacterial growth was monitored by measuring OD_{600} over time. **C and D**: Mid-logarithmic-phase cultures of *Ab* 17978 VU (WT) and *Ab* 17978 VU_{clsC2} were incubated in the presence of 2.5 M NaCl or 0.1% Triton X-100, and bacterial survival was determined after 2 (NaCl) or 6 (Triton X-100) hours. **E and F**: *Ab* 17978 VU_{lac} and *Ab* 17978 VU_{lac_clsC2} were grown in the presence of varying concentrations of IPTG as indicated until mid-logarithmic-phase, after which cultures were incubated in the presence of 2.5 M NaCl or 0.1% Triton X-100 as indicated. Bacterial survival was determined as above. **A and B**: symbols depict the mean, and error bars show standard deviation of the mean. N=4 biological replicates per strain, and data are from one experiment. **C-F**: N=3-4 biological replicates per strain, and data are from one (**E and F**) or two (**C and D**) independent experiments. Columns depict the mean, and error bars show standard deviation of the mean. Where indicated, means were compared using an unpaired Welch's *t*-test. **: $p<0.01$; ns: not significant.

Expression of clsC2 by Ab 17978 VU alters pathogen-macrophage interactions.

In *Ab* 17978 UN, *clsC2* promotes bacterial uptake by macrophage-like RAW 264.7 cells, and increases the production of pro-inflammatory IL-1β and decreases the production of anti-inflammatory IL-10 by murine BMDMs (**Chapter III**). Similarly, *in trans* expression of *clsC2* in *Ab* 17978 VU promotes bacterial uptake by RAW 264.7 cells, and increases the production of IL-1β by BMDMs. In contrast to *Ab* 17978 UN, *in trans* expression of *clsC2* in *Ab* 17978 VU increases the production of IL-10 by infected BMDMs (**Chapter III**). To test the hypothesis that chromosomal expression of *clsC2* under the control of either its native promoter or an inducible promoter (*lac*) in *Ab* 17978 VU increases bacterial uptake by phagocytes, RAW 264.7 cells were infected with *Ab* 17978 VU (WT), *Ab* 17978 VU_{clsC2}, *Ab* 17978 VU_{lac}, or *Ab* 17978 VU_{lac_clsC2}. Congruent with previous results (**Chapter III**), relative intracellular bacterial burdens were significantly greater in RAW cells infected with *Ab* 17978 VU_{clsC2} compared to RAW cells infected with the parental strain (*Ab* 17978 VU) (**Fig. 22A**). Similarly, the relative intracellular bacterial burdens of RAW cells infected with *Ab* 17978 VU_{lac_clsC2} in which *clsC2* expression was induced with 8 mM IPTG were significantly greater than those of RAW cells infected with *Ab* 17978 VU_{lac} (**Fig. 22B**). These data provide further evidence that expression of *clsC2* by *A. baumannii* promotes bacterial uptake by macrophages.

To determine the effects of *in trans* expression of *clsC2* by *A. baumannii* on the production of KC by infected macrophages, BMDMs were infected with *Ab* 17978VU/EV or *Ab* 17978VU/p*clsC2*. BMDMs infected with *Ab* 17978VU/p*clsC2* produced significantly more KC than BMDMs infected with *Ab* 17978VU/EV (**Fig. 22C**), suggesting that introducing *clsC2* into *A. baumannii* on a plasmid promotes the production of this neutrophil chemokine by infected host innate immune cells. To determine how chromosomal expression of *clsC2* under the control of either its native promoter or an inducible promoter (*lac*) by *Ab* 17978 VU affects IL-10 production by infected macrophages, macrophage-like RAW 264.7 cells were infected with *Ab* 17978 VU (WT), *Ab* 17978 VU_{clsC2}, *Ab* 17978 VU_{lac}, or *Ab* 17978 VU_{lac_clsC2}. RAW cells infected with *Ab* 17978 VU_{lac_clsC2}, in which *clsC2* expression was induced with 8 mM, produced significantly more IL-10. Similar results were found in RAW cells infected with *Ab* 17978

VU/p*clsC2* or *Ab* 17978 VU_{clsC2}, although the increase in IL-10 production was not statistically significant for the latter (**Fig. 22D-F**). Infection with *clsC2*-expressing *Ab* 17978 UN decreases IL-10 production by infected macrophages (**Chapter III**), whereas *in trans* or chromosomal expression of *clsC2* by *Ab* 17978 VU increased IL-10 production by infected macrophages (**Fig. 22**). Therefore, the effects of *A. baumannii clsC2* expression on host phagocyte IL-10 production remain ambiguous.

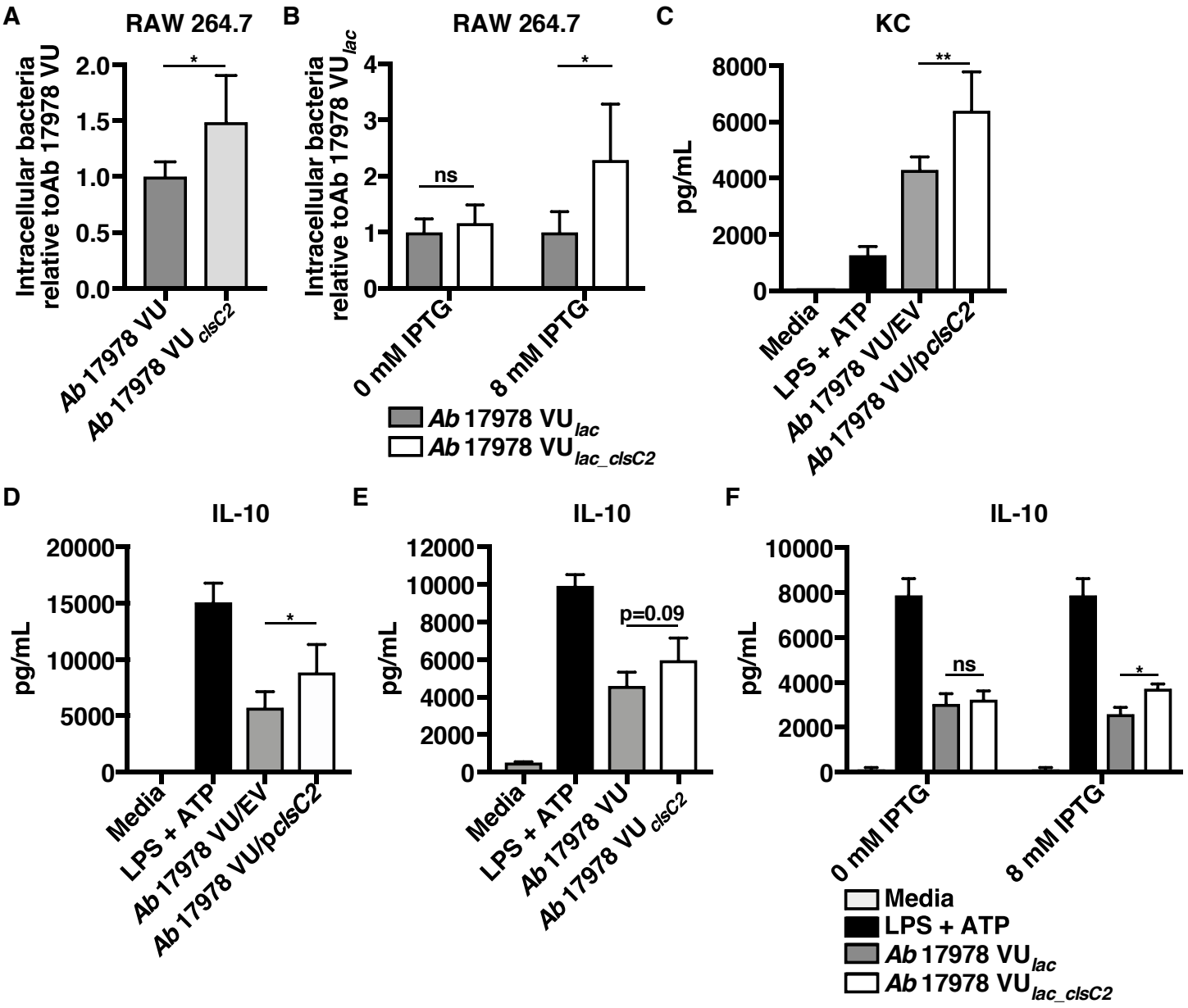

Figure 22. Expression of *clsC2* by *Ab* 17978 VU alters pathogen-macrophage interactions. A and B: Different strains of *A. baumannii* were grown until mid-logarithmic phase in the presence or absence of varying concentrations of IPTG to induce *clsC2* expression as indicated. Subsequently, macrophage-like RAW 264.7 cells were infected with *A. baumannii*, and intracellular bacterial burdens of infected RAW cells were determined at 90 minutes post-infection. **C**: Murine BMDMs were infected with mid-logarithmic-phase cultures of *Ab* 17978 VU/EV or *Ab* 17978 VU/p*clsC2* as indicated, or mock-infected with media alone or media supplemented with LPS and ATP. At 18 h.p.i., the concentration of KC in the supernatants of infected BMDMs was determined using an ELISA. **D-F**: RAW cells were infected with mid-logarithmic-phase cultures of *A. baumannii*, which were prepared as described above (**A and B**). At 18 h.p.i., the concentration of IL-10 in the supernatants of infected RAW cells was determined using an ELISA. **A and B**: N=3-4 biological replicates per experiment. Graphs depict average data from at least two independent experiments. **C-F**: N=3-4 biological replicates, and data are from one experiment. **A-F**: Columns depict the mean, and error bars show standard deviation of the mean. Means were compared using a one-way ANOVA adjusted for multiple comparisons. *: $p<0.05$; **: $p<0.01$; ns: not significant.

4.3 Discussion

clsC2 is differentially present in two variants of *A. baumannii* 17978: *Ab* 17978 VU (*clsC2* absent) and *Ab* 17978 UN (*clsC2* present) (**Chapter III**). Here, it is demonstrated that expression of *clsC2* by *Ab* 17978 UN correlates with increased CL abundance. In addition to *clsC2*, both *clsA* and *clsC1* are expressed during logarithmic growth phase by *A. baumannii*. Further, *A. baumannii* strains expressing *clsC2* may potentially exhibit decreased *clsC1* expression during logarithmic growth phase compared to a strain that lacks *clsC2*. This finding implies that *clsC2* and *clsC1* are at least somewhat functionally redundant, and suggests that expression of one may downregulate expression of the other. In *E. coli*, *clsA* is responsible for the majority of CL synthesis during logarithmic growth phase, and *clsB* and *clsC* are activated during stationary phase (136, 314). To what extent each of the three Cls enzymes contribute to CL synthesis in *A. baumannii* during logarithmic growth phase remains to be investigated. Further, it remains to be fully elucidated if and how expression of the three *cls* genes changes during stationary phase in *A. baumannii*. *A. baumannii* is capable of synthesizing several different types of CL (**Fig. 19 B-D** and ref. 197). If and to what extent each of the three Cls enzymes differentially contributes to the synthesis of each type of CL is currently unknown. As saturated and unsaturated CLs differentially stimulate pro-inflammatory cytokine production (125), determining how different Cls enzymes contribute to the synthesis of different CL species may further our understanding of the molecular pathogenesis of bacterial pneumonia.

Chromosomal introduction of *clsC2* under the control of its native promoter into *Ab* 17978 VU resulted in expression of this gene during logarithmic phase. In fact, *clsC2* expression in *Ab* 17978 VU_{clsC2} was significantly higher than in *Ab* 17978 UN (**Fig. 20C**). Nevertheless, there were no statistically significant differences in CL abundance between *Ab* 17978 VU_{clsC2} and the parental strain (*Ab* 17978 VU). This finding suggests that expression of *clsC2* alone is not sufficient to increase cell envelope CL content by *A. baumannii*. In addition to *clsC2*, other genetic elements that are present in *Ab* 17978 UN but absent in *Ab* 17978 VU may be required for CL overexpression. Chromosomal expression of *clsC2* by *Ab* 17978 VU resulted in several phenotypes associated with increased CL

abundance, including increased bacterial uptake by macrophages (**Fig. 22A and B**). This was independent of whether *clsC2* was under the control of its native promoter or an inducible promoter. However, the magnitudes of each of these phenotypes were smaller than in the *Ab* 17978 UN parental strains (**Chapter III**). It was recently demonstrated that CL promotes LPS transport to the bacterial OM (135). Therefore, expression of *clsC2* may alter the relative abundance of LOS or other lipids in the cell envelope of *Ab* 17978 VU_{clsC2}, resulting in the phenotypes observed in this strain. This may explain why IL-10 expression is decreased in macrophages infected with the *clsC2*-expressing *Ab* 17978 UN parental strain but increased in macrophages infected with any *clsC2*-expressing *Ab* 17978 VU strain as well.

As demonstrated in this chapter, *A. baumannii* and several other pathogenic bacteria vary in genomic *cls* gene content (**Fig. 19A**). If increased *cls* gene abundance correlates with increased CL abundance in other pathogenic bacteria such as *P. aeruginosa*, bacterial variability in cell envelope CL content may be an unrecognized determinant of pathogenesis in bacterial pneumonia. However, to test this hypothesis, tools beyond the strains described in this chapter must first be developed (see **Chapter V**).

4.4 Materials and methods

Bacterial strains and culture conditions

Bacterial strains and plasmids used in this Chapter are listed in **Table 6**. Strains were maintained as frozen stocks in lysogeny broth (LB) supplemented with 30% (vol/vol) glycerol at -80 °C. Unless noted otherwise, bacteria were grown on LB agar (LBA) at 37 °C, and single, isolated colonies were resuspended in LB and incubated overnight at 37 °C with constant agitation. Overnight cultures were diluted 1:100-1:1,000 in fresh LB and incubated for 3.5 hours at 37 °C with constant agitation until exponential phase. Exponential-phase cultures were washed twice with cold phosphate-buffered saline (PBS) and diluted to 1×10^{10} colony-forming units (CFUs) per mL in PBS. Bacterial cultures were diluted

further as appropriate for each experiment. *clsC2* was integrated under its native promoter into the chromosome of *Ab* 17978 VU as described in **Chapter III**. The *clsC2* open reading frame (ORF) under an inducible promoter (*lac*), or the inducible promoter alone, was integrated into the chromosome of *Ab* 17978 VU in a similar manner. Specifically, the *lac* promoter ± the *clsC2* ORF were cloned into the pKNOCK-mTn7 plasmid to make pKNOCK(*lac*) or pKNOCK(*lac_clsC2*) using a forward primer annealing to the region upstream of the *lac* promoter (GCGTTGCGCTCACTGCCC) and a reverse primer annealing to the region downstream of the *lac* promoter (GCTCGAATTCTGTTTCCTGTGTG). In the case of pKNOCK(*lac_clsC2*), this reverse primer overlapped with part of a second forward primer annealing to the start of the *clsC2* ORF (ATGATCAATCAGCTATATGAGCAGTATAG). A second reverse primer annealed to the end of this ORF (TTACATCATCCACTCAATTGGC). Transformation of these constructs into *E. coli λpir116*, as well as the four-way mate, were done as described in **Chapter III**.

Identification of cls genes in genomes of pathogenic bacteria

Literature, publicly accessible genomes in NCBI, and the publicly accessible UniProt database were searched for the presence of (putative) *cls* genes in the genomes of pathogenic bacteria. Search terms included, but were not limited to: “[genus and species] (e.g. *Staphylococcus aureus*)”; “cardiolipin synthase”; “cls”, and “phospholipase D superfamily”. It is recognized that this review is not exhaustive.

Measurement of CL in A. baumannii

Ab 17978 UN, *Ab* 17978 VU, and *Ab* 17978 VU_{clsC2} were grown until mid-logarithmic phase and total lipids were extracted using the Folch method (318). Briefly, bacterial cell pellets were diluted 1:20 in an ice-cold mixture of chloroform/methanol (2:1), after which 0.2 volume equivalents of ice-cold water were added. Samples were centrifuged for 10 minutes at 1000 × g, and the bottom, organic phase was collected and transferred to 2-mL glass vials. Next, samples were dried under liquid nitrogen.

Comprehensive CL quantification of dried lipid samples was done via LC-MS/MS (Creative Proteomics, Shirley, NY).

Expression of cls genes in A. baumannii

Ab 17978 UN, *Ab* 17978 VU, and *Ab* 17978 VU_{clsC2} were grown until mid-logarithmic phase and bacteria were lysed in RNase-free TE buffer (ThermoFisher Scientific, Waltham, MA) using 100 µm silica beads and an HT6 benchtop homogenizer (OPS Diagnostics, Lebanon, NJ). Total RNA was extracted using a RNeasy kit (Qiagen, Hilden, Germany), and genomic DNA was removed using a Turbo DNA-free kit (Waltham, MA). Purified RNA was converted to cDNA using an iScript cDNA synthesis kit (Bio-Rad laboratories, Hercules, CA) per manufacturers' protocols. Transcripts of *clsA*, *clsC1*, and *clsC2* were quantified using transcript-specific primers (*clsA*: AAAAAGTGCCCAAGAACGTG and GCCAGCAGCATGTAACTCTG; *clsC1*: AATCAGGTTGCGCTTATTGG and CCAACCAACATGACATCGAC; *clsC2*: CCATCACGAAGACCATAGCC and GGAGAGTCAGCAACAAAATGG) and SYBR Green master mix.

NaCl and Triton X-100 growth and survival assays

Stationary-phase cultures of *Ab* 17978 VU and *Ab* 17978 VU_{clsC2} were standardized to a similar OD_{600} and diluted 1:100 in fresh LB supplemented with varying concentrations of NaCl or Triton X-100 as indicated. Bacterial growth was monitored over time by taking serial OD_{600} measurements. Bacterial survival after exposure to 2.5 M NaCl or 0.1% Triton X-100 was assessed as described previously (**Chapter III**).

Bacterial uptake and cytokine production by macrophages

Ab 17978 VU, *Ab* 17978 VU_{clsC2}, *Ab* 17978 VU_{lac}, and *Ab* 17978 VU_{lac_clsC2} were grown to mid-logarithmic phase in the presence or absence of varying concentrations of IPTG to induce *clsC2* expression as indicated. To determine uptake of bacteria by macrophage-like RAW 264.7 cells or

cytokine production by RAW 264.7 cells or murine BMDMs, macrophages were infected as previously described (**Chapter III**). Concentrations of KC or IL-10 in the supernatants of infected macrophages were determined using an ELISA (R&D systems, Minneapolis, MN) per the manufacturer's protocol.

Table 6. Bacterial strains and plasmids used in this Chapter

Strain/plasmid	Description	Source	Reference
Ab 17978 VU	Variant of *A. baumannii* ATCC 17978 that lacks AbaAL44, stored at Vanderbilt University	Vanderbilt University	ATCC
Ab 17978 UN	Variant of *A. baumannii* ATCC 17978 that harbors AbaAL44, stored at the University of Nebraska	University of Nebraska	ATCC, (303)
Ab 17978 VU_{clsC2}	*Ab* 17978 VU in which *clsC2* has been chromosomally integrated under its native promoter		This chapter
Ab 17978 VU_{lac}	*Ab* 17978 VU in which the inducible promoter *lac* has been chromosomally integrated		This chapter
Ab 17978 VU_{lac_clsC2}	*Ab* 17978 VU in which the *clsC2* ORF has been chromosomally integrated under an inducible promoter (*lac*)		This chapter
Ab 17978 VU/EV	*Ab* 17978 VU transformed with pWH1266		**Chapter III**
Ab 17978 VU/p*clsC2*	*Ab* 17978 VU transformed with pWH1266(*clsC2*)		**Chapter III**
pWH1266	*E. coli – A. baumannii* shuttle vector conferring ampicillin and tetracycline resistance		(312)

CHAPTER V

CONCLUSIONS AND FUTURE DIRECTIONS

The studies described in this thesis highlight the complexity of the molecular interactions at the host-microbe interface in the setting of bacterial pneumonia. Bacterial pneumonia poses a major burden on global public health, and increased mechanistic insights into the molecular interactions between causative agents of pneumonia and the host response to infection may enhance our understanding of pneumonia pathogenesis. Additionally, inquiries into these interactions may uncover novel molecular targets of potential therapeutic interest. **Chapter II** demonstrates how Gram-negative bacteria may act as a reservoir for AG antibiotics, and how these antibiotics can synergize with host-derived pulmonary surfactant to increase bacterial killing inside the lung. The studies described in this chapter, therefore, provide mechanistic insights into why AG antibiotics appear to be uniquely effective in the lungs as compared to other organ systems, and may thereby expand their clinical utility.

In addition to serving as a reservoir for polycationic antibiotics such as AGs, the Gram-negative cell envelope is a major molecular determinant of pneumonia pathogenesis. **Chapters III** and **IV** illustrate how variants of the nosocomial pathogen *A. baumannii* modulate cell envelope composition through differential expression of the anionic lipid CL. Overexpression of CL promotes bacterial resistance to host-imposed stressors such as osmotic and detergent stress, and alters the molecular interactions between bacteria and macrophages by promoting bacterial uptake and altering cytokine production. As described in these chapters, differential expression of CL may be relevant to multiple species of bacterial pathogens, and may therefore be an unrecognized determinant of inflammation and injury in bacterial pneumonia. Several questions regarding the molecular interactions between the Gram-negative cell envelope and the host environment in the setting of bacterial pneumonia remain. In this Chapter, ongoing as well as future studies aimed at answering these questions are described.

Definitively determine the subcellular location of the Gram-negative and Gram-positive AG reservoir.

Studies described in **Chapter II** demonstrate that Gram-negative bacteria serve as a reservoir for AG antibiotics. Experiments with pharmacological inhibitors of AG binding to the Gram-negative OM or AG uptake into the bacterial cytosol implicate the OM as the predominant AG reservoir. However, definitive evidence to support this conclusion is presently lacking. A recent study demonstrated that a labeled derivative of the AG antibiotic neomycin binds the Gram-negative OM in a saturable fashion over the course of several minutes of exposure. These binding interactions were strong enough to withstand multiple washes (225). For the experiments described in **Chapter II**, bacteria were exposed to AG antibiotics for several hours, as opposed to several minutes. Even though pharmacological inhibition of PMF-mediated AG uptake did not reduce AG binding to Gram-negative bacteria, AG uptake into the bacterial cytosol can occur in the absence of the PMF (229). As such, experiments with (fluorescently) labeled AG antibiotics can definitively determine whether the bacterial cytosol, or any other subcellular locations in addition to the OM, contributes to the Gram-negative AG reservoir over the course of several hours of exposure.

In addition, as demonstrated in **Chapter II**, the Gram-positive pathogen *S. aureus* may serve as a reservoir for gentamicin, but not for kanamycin. This finding suggests that, in contrast to Gram-negative bacteria, AG antibiotic retention by *S. aureus* may be restricted to fewer types of AGs, or possibly to just gentamicin. Gram-positive bacteria lack an OM. As such, the identity of the *S. aureus* gentamicin reservoir is presently unknown. Experiments with a labeled derivative of gentamicin may provide further insight into the subcellular location of the gentamicin reservoir of this pathogen. The inclusion of other pathogens in these studies, such as *S. pneumoniae*, can help ascertain whether the formation of such antibiotic reservoirs is conserved across multiple species of Gram-positive bacteria, or if it is unique to *S. aureus*.

Finally, as described in **Chapter II** and ref. (205), bacterial binding and retention of antibiotics following exposure appears to be specific to the AG class of antibiotics. AG antibiotics are polycationic and can therefore bind to negatively charged residues on the Gram-negative OM (217, 219). Colistin

is another cationic antibiotic relevant to the treatment of bacterial pneumonia, particularly MDR and XDR *A. baumannii*. Furthermore, like AG antibiotics, intravenous administration of colistin results in poor lung penetration (193), and treatment with inhaled colistin is therefore occasionally suggested in the treatment of Gram-negative pneumonia (6). Whether or not pathogenic bacteria bind and retain colistin following exposure similar to AG antibiotics remains to be determined. Further, it is presently unknown whether colistin synergizes with pulmonary surfactant to enhance killing of bacteria inside the lung. Expanding the studies described in **Chapter II** to include colistin may provide insight into the unique efficacy of colistin when administered directly to the lungs, and – like AGs – potentially expand its clinical utility.

Identify additional bacterial and host-derived factors that contribute to enhanced AG-mediated bacterial killing inside the lung.

Experiments described in **Chapter II** indicate that mice infected with AG-naïve *A. baumannii* and co-inoculated with AG-bound bacteria exhibit significantly lower bacterial burdens over the course of pneumonic infection compared to mice co-inoculated with AGs in solution. This finding implies that maximum AG-mediated bacterial killing inside the murine lung is achieved when AGs are bound to bacteria prior to inoculation. Therefore, in addition to pulmonary surfactant, additional bacterial and/or host factors may contribute to AG-mediated enhanced bacterial killing inside the lung. One example of such a bacterial product potentially contributing to this phenotype is OM vesicles (OMVs). OMVs are membrane-enclosed vesicles elaborated from the bacterial outer membrane, carry bacterial products such as lipids, outer membrane proteins, and nucleic acids, and affect both interbacterial and host-bacterial interactions (319). Exposure to antibiotics such as gentamicin increases the production of OMVs (320), but the extent to which they contribute to the killing of co-infecting bacteria in the experiments described in **Chapter II** remains to be elucidated. Isolation of bacterial OMVs requires ultracentrifugation at 150,000 × g (321), much faster than centrifugation speeds used to pellet bacteria in the experiments described in **Chapter II** (4,000 × g). Therefore, OMVs elaborated by AG-exposed

bacteria used in **Chapter II** are likely decanted along with the supernatant after centrifugation. However, this does not exclude a role for OMVs as they may continue to be elaborated by AG-exposed bacteria during pneumonic infection. To test the hypothesis that OMVs from AG-exposed bacteria contribute to AG-mediated enhanced bacterial killing inside the lung, one experiment would be to quantify OMVs in the supernatant of AG-exposed *A. baumannii* cultures and compare it to the concentration of OMVs in the supernatant of unexposed *A. baumannii* cultures. Both the quantity and the quality (e.g. size, shape) of *A. baumannii* OMVs can be assessed using a nanoparticle tracking analysis instrument (322). Additionally, to test the hypothesis that OMVs from AG-exposed bacteria contain AGs, AGs in OMV preparations from bacterial cultures can be quantified using an ELISA or LC-MS as described in **Chapter II**. Finally, to test the hypothesis that OMVs from AG-exposed bacteria enhance bacterial killing inside the murine lung, mice could be infected with AG-naïve *A. baumannii* and co-inoculated with a standardized amount of OMVs prepared from either AG-exposed *A. baumannii* cultures or unexposed *A. baumannii* cultures. The bacterial burdens of infected mice can be monitored over the course of infection as described in **Chapter II**.

The identification of additional host factors contributing to AG-mediated enhanced bacterial killing inside the lung is potentially technically challenging. However, one approach would be to infect mice with AG-naïve *A. baumannii* and co-inoculate them with AG-bound bacteria or bacteria unexposed to any antibiotics as described in **Chapter II**. Following infection, lungs from infected mice would be harvested, and total RNA extracted. Expression of host genes could then be compared between mice co-inoculated with AG-bound bacteria and mice co-inoculated with bacteria unexposed to any antibiotics using RNA sequencing technology. Of note, in the studies described in **Chapter II**, bacterial burdens were measured at 36 h.p.i. As differences in host gene transcription likely precede differences in bacterial burdens, lungs would need to be harvested earlier in the course of infection for this particular experiment. Host genes that may potentially be upregulated in mice co-inoculated with AG-bound bacteria include genes encoding antimicrobial peptides and immune signaling molecules.

Construct bacterial strains that differ based on the expression of CL but are otherwise isogenic.

Compared to *Ab* 17978 VU, there was an approximate two-fold increase in the abundance of CL in lipids extracted from *Ab* 17978 UN, suggesting that this strain overexpresses CL (**Chapter IV**). However, the effects of *A. baumannii* CL overexpression on pneumonia pathogenesis cannot be tested directly by comparing these two variants, as there are substantial, additional genetic differences between them (**Chapter III**). Integration of *clsC2* under the control of its native promoter into the chromosome of *Ab* 17978 VU (the variant that naturally lacks this gene) resulted in expression of *clsC2* that was even greater than expression of this gene in the *Ab* 17978 UN parental strain. However, expression of *clsC2* by *Ab* 17978 VU in this manner did not result in significant increases in CL abundance (**Chapter IV**). Congruently, the magnitude of phenotypes associated with CL-overexpression, such as bacterial uptake by macrophages, was substantially lower in *clsC2*-expressing strains derived from the *Ab* 17978 VU variant than in *Ab* 17978 UN. These findings suggest that expression of *clsC2* alone is insufficient to increase CL abundance in the *A. baumannii* cell envelope, and that additional elements present in *Ab* 17978 UN but absent in *Ab* 17978 VU likely play a role.

Inspection of the AbaAL44 accessory locus present in *Ab* 17978 UN but absent in *Ab* 17978 VU did not reveal any obvious candidate genes. However, several SNPs present in the genome of *Ab* 17978 UN may warrant further investigation. Two SNPs of potential interest include a SNP within *lptD* and a SNP within undecaprenyl pyrophosphate synthase (*uppS*). *A. baumannii lptD* is part of the LPS/LOS biosynthesis pathway (**Chapter I**). Regulation of bacterial lipid biosynthesis is complex, and CL and LPS/LOS are known to interact (135). Therefore, alterations in the functionality or expression of LPS/LOS biosynthesis pathway genes may affect CL synthesis, transport, or recycling. *uppS* is implicated in peptidoglycan synthesis, another component of the Gram-negative cell envelope (**Chapter I**). Preliminary studies from the Palmer laboratory (discussed here with permission) at the University of Illinois at Chicago suggest that deleting Mla pathway (discussed in **Chapter I**) genes in the background of the *Ab* 17978 UN *uppS* allele decreases bacterial resistance to membrane stress. Moreover, the colony morphology of these mutant strains resembles that of *Ab* 17978 UN Δ*clsC2*

(**Chapter III**). This suggests that, in *A. baumannii*, cell envelope gene mutations and the *Ab* 17978 UN *uppS* allele may be synergistically unfit. This raises the hypothesis that the *Ab* 17978 UN *uppS* and/or *lptD* alleles contribute to or permit increased cell envelope CL abundance, and/or render Δ*clsC2* mutants made in this background unfit. I intend to leverage this information to generate two *A. baumannii* strains where one strain overexpresses CL but is otherwise isogenic to the other strain. The Palmer laboratory has graciously provided me with the following strains: *Ab* 17978 VU(*uppS*^{UN}); *Ab* 17978 VU(*lptD*^{UN}); and *Ab* 17978 UN(*uppS*^{VU}). I am currently in the process of inserting *clsC2* under the control of its native promoter into the chromosomes of *Ab* 17978 VU(*uppS*^{UN}) and *Ab* 17978 VU(*lptD*^{UN}). In addition, I am in the process of constructing a marker-less *clsC2* deletion mutant in the background of *Ab* 17978 UN(*uppS*^{VU}). Once these strains are generated, I will measure the expression of *cls* genes during logarithmic growth phase and quantify CL abundance using the methods described in **Chapter IV**. If successful, such a set of strains can be utilized to address additional questions regarding the role of *A. baumannii* CL overexpression in pneumonia pathogenesis.

Determine the effects of bacterial CL overexpression on inflammation and lung injury in pneumonia.

In *Ab* 17978 UN, expression of *clsC2* is correlated with increased CL abundance and promotes bacterial resistance to osmotic and detergent stress. Additionally, *clsC2* expression by this strain promotes bacterial uptake and alters cytokine production by macrophages. Infection with *clsC2*-expressing *Ab* 17978 VU alters macrophage biology in a similar manner (**Chapters III** and **IV**). Further, mitochondrial CL is a direct agonist of the NLRP3 inflammasome (102), and patients with bacterial pneumonia exhibit increased levels of mitochondrial CL in their lungs (104). Pneumonic infection of mice with *clsC2*-expressing *Ab* 17978 UN also increases neutrophilic lung inflammation (**Chapter III**), which is an important driver of immune mediated lung injury in pneumonia (98). These findings suggest that variability in bacterial cell envelope CL content may be an underrecognized driver of inflammation and injury in pneumonia. Specifically, they raise the hypothesis that bacterial CL overexpression progresses pneumonia pathogenesis by increasing inflammation and lung injury (**Fig. 23**).

To test this hypothesis, I must first construct and phenotypically characterize the *A. baumannii* strains with differential CL abundance as described above. To expand my studies to include Gram-positive pathogens, I plan to request a set of *S. aureus* strains from the Peleg group at Monash University in Australia. These strains differ based on a single point mutation in *cls2*, resulting in an approximate two-fold increase in CL abundance, but are otherwise isogenic (315). To determine the effects of bacterial cell envelope CL content variability on inflammation during pneumonic infection, I would utilize the murine model of pneumonia previously described (**Chapters II** and **III**). Specifically, I would infect mice intranasally with the strains of *A. baumannii* and *S. aureus* described above. At multiple time points post-infection (e.g. 6, 12, 24, and 36 h.p.i.), mice would be euthanized, and samples (e.g. blood, organs, bronchoalveolar lavage fluid (BALF)) would be collected. To assess inflammation, I would measure the concentrations of multiple pro- and anti-inflammatory cytokines, as well as (neutrophil) chemokines, in serum and lung homogenates of infected mice using ELISAs. Based on previous data (**Chapters III** and **IV**), as well as the role of mitochondrial CL in NLRP3 inflammasome activation (102), I hypothesize that pneumonic infection with CL-overexpressing bacteria will lead to increases in the production of the pro-inflammatory cytokines IL-1β and IL-18 and the neutrophil chemokine KC. I also hypothesize that infection with these bacteria will lead to decreases in the production of the anti-inflammatory cytokines IL-10 and TGF- β. Since cytokines drive the recruitment of immune cells to the site of infection, I would also measure the relative abundance of multiple immune cell populations in serum, lung homogenates, and BALF of infected mice using flow cytometry and complete blood count studies. Based on data obtained with *clsC2*-expressing *Ab* 17978 UN, as well as the fact that IL-1β promotes neutrophilia (267), I hypothesize that infection with CL-overexpressing strain increases neutrophilic lung inflammation. To ascertain the effects of any differences in inflammation on bacterial burdens of infected mice, I would measure bacterial burdens of the lungs as well as extrapulmonary bacterial dissemination to the spleen of infected mice. Collectively, the results of these studies will determine the effects of differential bacterial cell envelope CL content on the host inflammatory response in experimental pneumonia.

To determine the effects of variable bacterial cell envelope CL content on lung injury, I would intranasally infect mice and collect samples at multiple time points post-infection as described above. Pulmonary edema as well as increased BALF concentrations of protein, lactate dehydrogenase, and hemoglobin are all markers of lung injury (323-325). Therefore, all of these parameters will be assayed by determining the ratio of wet to dry lung weight and using total protein (i.e. bicinchoninic acid assay (BCA assay)), lactate dehydrogenase, and hemoglobin quantification kits, respectively. Furthermore, lungs from a subset of mice will be harvested, fixed, stained with hematoxylin and eosin (H&E), and inspected for markers of lung injury, including immune cell infiltrate, compromised alveolar architecture, and hemorrhage, by an animal pathologist who is blinded to both hypothesis and treatment. Collectively, the results of these studies will establish the contribution of bacterial CL overexpression to lung injury during pneumonic infection.

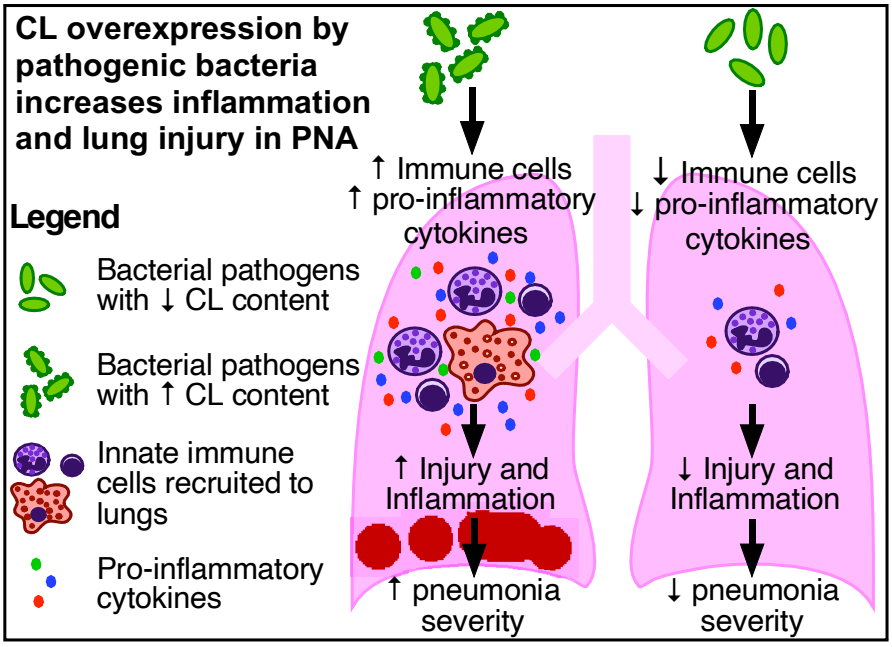

Figure 23. Central hypothesis regarding the effects of bacterial cell envelope CL content variability on pneumonia pathogenesis. PNA: pneumonia; CL: cardiolipin.

Determine the effects of bacterial CL overexpression on macrophage effector functions.

Bacterial CL differentially activates TLR4-mediated pro-inflammatory cytokine production depending on acyl chain saturation (125). Further, infection with *clsC2*-expressing *A. baumannii* augments bacterial uptake and the production of pro-inflammatory IL-1β by infected macrophages (**Chapters III** and **IV**), and mitochondrial CL is a direct agonist of the NLRP3 inflammasome, which also results in IL-1β production (102). These findings suggest that bacterial CL augments macrophage effector functions. To test the hypothesis that the increased bacterial uptake observed in macrophages infected with *clsC2*-expressing *A. baumannii* is due to CD36 scavenger receptor-mediated phagocytosis, I propose to infect BMDMs with the strains of *A. baumannii* and *S. aureus* described above and pharmacologically inhibit CD36 with salvionolic acid B (326). As a control, I would pharmacologically inhibit all phagocytosis with cytochalasin D (327). To corroborate the experiments with murine macrophages (i.e. BMDMs), I propose to repeat these studies with human macrophages derived from peripheral blood mononuclear cells (PBMCs). To assess differential intracellular killing of CL-overexpressing *A. baumannii* and *S. aureus* by macrophages, I will infect macrophages as described above and determine intra-macrophage bacterial survival by enumerating intracellular bacterial burdens at two separate time points post-infection using a gentamicin protection assay as described in **Chapter III**. The specific contributions of phagosome acidification and the respiratory burst to intracellular bacterial killing by infected macrophages will be interrogated by pharmacologically inhibiting these processes using Bafilomycin A or apocynin, respectively (328, 329). The results of these studies will elucidate the effects of CL overexpression by both Gram-negative and Gram-positive bacteria on multiple macrophage effector functions.

To test the hypothesis that CL-overexpressing bacteria augment NLRP3 inflammasome activation in infected macrophages, macrophages will be infected with bacteria as above and NLRP3 inflammasome activation will be assayed by measuring the production of IL-1β and IL-18 – two cytokines produced in response to NLRP3 inflammasome activation (102). As production of these cytokines can also be stimulated through alternative immune signaling pathways (91), the contribution

of the NLRP3 inflammasome will be interrogated directly through pharmacological inhibition with MCC950 (330). To corroborate these experiments, I propose to visualize NLRP3 inflammasome activation directly by utilizing a THP-1 macrophage cell line in which the ASC adaptor protein is fused to GFP such that it fluoresces upon NLRP3 inflammasome activation (331). To get a complete picture of differential cytokine production by macrophages infected with CL-overexpressing bacteria, I propose to use a 26-plex mouse cytokine and chemokine Luminex assay. The results of these studies will help determine how CL-overexpressing bacteria differentially activate inflammatory signaling pathways in macrophages. One can envision that similar studies of cytokine production and effector function activity might be conducted in other immune cell populations relevant to bacterial pneumonia pathogenesis such as neutrophils.

Assess variability in cell envelope CL content among respiratory isolates of pathogenic bacteria.

The accessory locus AbaAL44 described in **Chapter III** encompasses a *cls* gene: *clsC2*. Loci similar to AbaAL44 are present in at least 100 strains of *A. baumannii*, and *clsC2* expression is correlated with increased CL abundance in *Ab* 17978 UN (**Chapters III** and **IV**). In addition to *A. baumannii*, several other species of pathogenic bacteria vary in genomic *cls* gene content, including *P. aeruginosa* and *K. pneumoniae* (**Chapter IV**). These findings suggest that differential *cls* gene content and cell envelope CL abundance variability may be common among causative agents of bacterial pneumonia. Moreover, strains of *K. pneumoniae* harboring an additional *cls* gene have been associated with increased infection severity (317, 332). To establish cell envelope CL content variability among clinical isolates of pathogenic bacteria, our laboratory has procured over 1200 clinical respiratory isolates from Vanderbilt University Medical Center in collaboration with Dr. Jonathan Schmitz. This collection is comprised of multiple species of pathogenic bacteria including *A. baumannii*, *P. aeruginosa*, *S. aureus*, and *S. pneumoniae*. To screen for genomic *cls* gene content variability among *A. baumannii* clinical isolates, a preliminary approach would be to screen for the presence of *clsC2* using PCR with specific primers. Additionally, the fluorescent dye nonyl acridine orange (NAO), which

may be more specific for anionic lipids and CL in particular (116), could be employed to screen for differential CL abundance among these respiratory isolates. Specifically, with assistance from Dr. Benjamin Bratton at Vanderbilt University, I am currently in the process of designing a fluorescent microscopy-based approach. NAO bound to CL emits both a red and a green fluorescent signal (116). Therefore, the most prudent approach would be to calculate the ratiometric signal of red and green fluorescence emitted by NAO-stained bacteria. This ratiometric signal would then serve as a proxy for CL abundance. The two variants of *A. baumannii* 17978 described in this thesis with an approximate two-fold difference in CL abundance as confirmed by LC-MS/MS would serve as controls for these experiments. Of note, these fluorescent microscopy experiments would merely serve as a screening method. Any putative differences in CL abundance between isolates would need to be confirmed by LC-MS/MS as described in **Chapter IV**. The results of these studies will establish the variability of cell envelope CL content among pathogenic bacteria, and may bolster the clinical relevance of studying the contribution of bacterial CL to pneumonia pathogenesis.

Final remarks.

As described in this thesis, bacterial pneumonia remains a pervasive, global problem. To curb this problem, it must be approached from several angles. One such angle is to increase our mechanistic understanding of the molecular pathways at the host-microbe interface. Here, I have provided evidence to suggest that pathogenic bacteria such as *A. baumannii* modulate cell envelope lipid composition, affecting the interactions between bacteria and host cells. Additionally, the biophysical and biochemical properties of the Gram-negative cell envelope may be leveraged to improve treatment of bacterial pneumonia with (poly)cationic antimicrobials such as AGs and colistin. Continued interrogation of the microbe-host interface will further our mechanistic understanding of pneumonia pathogenesis. Doing so may also uncover novel therapeutic targets and maximize the efficacy of currently available antimicrobials. Combined, all of this may help improve clinical outcomes for many patients suffering from bacterial pneumonia.

REFERENCES

1. Centers for Disease Control and Prevention. 2017. Fast Stats - Pneumonia. https://www.cdc.gov/nchs/fastats/pneumonia.htm.
2. World Health Organization. 2021. Fact Sheets - Pneumonia. https://www.who.int/news-room/fact-sheets/detail/pneumonia.
3. World Health Organization. 2020. The top 10 causes of death. https://www.who.int/news-room/fact-sheets/detail/the-top-10-causes-of-death.
4. McAllister DA, Liu L, Shi T, Chu Y, Reed C, Burrows J, Adeloye D, Rudan I, Black RE, Campbell H, Nair H. 2019. Global, regional, and national estimates of pneumonia morbidity and mortality in children younger than 5 years between 2000 and 2015: a systematic analysis. Lancet Glob Health 7:e47-e57.
5. Lanks CW, Musani AI, Hsia DW. 2019. Community-acquired Pneumonia and Hospital-acquired Pneumonia. Med Clin North Am 103:487-501.
6. Kalil AC, Metersky ML, Klompas M, Muscedere J, Sweeney DA, Palmer LB, Napolitano LM, O'Grady NP, Bartlett JG, Carratalà J, El Solh AA, Ewig S, Fey PD, File TM, Restrepo MI, Roberts JA, Waterer GW, Cruse P, Knight SL, Brozek JL. 2016. Management of Adults With Hospital-acquired and Ventilator-associated Pneumonia: 2016 Clinical Practice Guidelines by the Infectious Diseases Society of America and the American Thoracic Society. Clin Infect Dis 63:e61-e111.
7. Modi AR, Kovacs CS. 2020. Hospital-acquired and ventilator-associated pneumonia: Diagnosis, management, and prevention. Cleve Clin J Med 87:633-639.
8. Musher DM, Abers MS, Bartlett JG. 2017. Evolving Understanding of the Causes of Pneumonia in Adults, With Special Attention to the Role of Pneumococcus. Clin Infect Dis 65:1736-1744.
9. Torres A, Cilloniz C, Niederman MS, Menéndez R, Chalmers JD, Wunderink RG, van der Poll T. 2021. Pneumonia. Nat Rev Dis Primers 7:25.
10. Said MA, Johnson HL, Nonyane BA, Deloria-Knoll M, O'Brien KL, Andreo F, Beovic B, Blanco S, Boersma WG, Boulware DR, Butler JC, Carratalà J, Chang FY, Charles PG, Diaz AA, Domínguez J, Ehara N, Endeman H, Falcó V, Falguera M, Fukushima K, Garcia-Vidal C, Genne D, Guchev IA, Gutierrez F, Hernes SS, Hoepelman AI, Hohenthal U, Johansson N, Kolek V, Kozlov RS, Lauderdale TL, Mareković I, Masiá M, Matta MA, Miró Ò, Murdoch DR, Nuermberger E, Paolini R, Perelló R, Snijders D, Plečko V, Sordé R, Strålin K, van der Eerden MM, Vila-Corcoles A, Watt JP, Team AAPBS. 2013. Estimating the burden of pneumococcal pneumonia among adults: a systematic review and meta-analysis of diagnostic techniques. PLoS One 8:e60273.
11. Lynch JP. 2001. Hospital-acquired pneumonia: risk factors, microbiology, and treatment. Chest 119:373S-384S.
12. Jones RN. 2010. Microbial etiologies of hospital-acquired bacterial pneumonia and ventilator-associated bacterial pneumonia. Clin Infect Dis 51 Suppl 1:S81-7.
13. Weber DJ, Rutala WA, Sickbert-Bennett EE, Samsa GP, Brown V, Niederman MS. 2007. Microbiology of ventilator-associated pneumonia compared with that of hospital-acquired pneumonia. Infect Control Hosp Epidemiol 28:825-31.
14. Hong HL, Hong SB, Ko GB, Huh JW, Sung H, Do KH, Kim SH, Lee SO, Kim MN, Jeong JY, Lim CM, Kim YS, Woo JH, Koh Y, Choi SH. 2014. Viral infection is not uncommon in adult patients with severe hospital-acquired pneumonia. PLoS One 9:e95865.
15. Fagon JY, Chastre J, Domart Y, Trouillet JL, Pierre J, Darne C, Gibert C. 1989. Nosocomial pneumonia in patients receiving continuous mechanical ventilation. Prospective analysis of 52 episodes with use of a protected specimen brush and quantitative culture techniques. Am Rev Respir Dis 139:877-84.

16. Lister PD, Wolter DJ, Hanson ND. 2009. Antibacterial-resistant *Pseudomonas aeruginosa*: clinical impact and complex regulation of chromosomally encoded resistance mechanisms. Clin Microbiol Rev 22:582-610.
17. Kyriakidis I, Vasileiou E, Pana ZD, Tragiannidis A. 2021. *Acinetobacter baumannii* Antibiotic Resistance Mechanisms. Pathogens 10.
18. Iwahara T, Ichiyama S, Nada T, Shimokata K, Nakashima N. 1994. Clinical and epidemiologic investigations of nosocomial pulmonary infections caused by methicillin-resistant *Staphylococcus aureus*. Chest 105:826-31.
19. Rello J, Torres A, Ricart M, Valles J, Gonzalez J, Artigas A, Rodriguez-Roisin R. 1994. Ventilator-associated pneumonia by *Staphylococcus aureus*. Comparison of methicillin-resistant and methicillin-sensitive episodes. Am J Respir Crit Care Med 150:1545-9.
20. Djordjevic ZM, Folic MM, Jankovic SM. 2017. Distribution and antibiotic susceptibility of pathogens isolated from adults with hospital-acquired and ventilator-associated pneumonia in intensive care unit. J Infect Public Health 10:740-744.
21. Giuliano KK, Baker D, Quinn B. 2018. The epidemiology of nonventilator hospital-acquired pneumonia in the United States. Am J Infect Control 46:322-327.
22. Herkel T, Uvizl R, Doubravska L, Adamus M, Gabrhelik T, Htoutou Sedlakova M, Kolar M, Hanulik V, Pudova V, Langova K, Zazula R, Rezac T, Moravec M, Cermak P, Sevcik P, Stasek J, Malaska J, Sevcikova A, Hanslianova M, Turek Z, Cerny V, Paterova P. 2016. Epidemiology of hospital-acquired pneumonia: Results of a Central European multicenter, prospective, observational study compared with data from the European region. Biomed Pap Med Fac Univ Palacky Olomouc Czech Repub 160:448-55.
23. Kharel S, Bist A, Mishra SK. 2021. Ventilator-associated pneumonia among ICU patients in WHO Southeast Asian region: A systematic review. PLoS One 16:e0247832.
24. Theilacker C, Sprenger R, Leverkus F, Walker J, Häckl D, von Eiff C, Schiffner-Rohe J. 2021. Population-based incidence and mortality of community-acquired pneumonia in Germany. PLoS One 16:e0253118.
25. Pessoa E, Bárbara C, Viegas L, Costa A, Rosa M, Nogueira P. 2020. Factors associated with in-hospital mortality from community-acquired pneumonia in Portugal: 2000-2014. BMC Pulm Med 20:18.
26. Metlay JP, Waterer GW, Long AC, Anzueto A, Brozek J, Crothers K, Cooley LA, Dean NC, Fine MJ, Flanders SA, Griffin MR, Metersky ML, Musher DM, Restrepo MI, Whitney CG. 2019. Diagnosis and Treatment of Adults with Community-acquired Pneumonia. An Official Clinical Practice Guideline of the American Thoracic Society and Infectious Diseases Society of America. Am J Respir Crit Care Med 200:e45-e67.
27. Krause KM, Serio AW, Kane TR, Connolly LE. 2016. Aminoglycosides: An Overview. Cold Spring Harb Perspect Med 6:a027029.
28. Poole K, Gilmour C, Farha MA, Mullen E, Lau CH, Brown ED. 2016. Potentiation of Aminoglycoside Activity in *Pseudomonas aeruginosa* by Targeting the AmgRS Envelope Stress-Responsive Two-Component System. Antimicrob Agents Chemother 60:3509-18.
29. Landman D, Kelly P, Bäcker M, Babu E, Shah N, Bratu S, Quale J. 2011. Antimicrobial activity of a novel aminoglycoside, ACHN-490, against *Acinetobacter baumannii* and *Pseudomonas aeruginosa* from New York City. J Antimicrob Chemother 66:332-4.
30. Panidis D, Markantonis SL, Boutzouka E, Karatzas S, Baltopoulos G. 2005. Penetration of gentamicin into the alveolar lining fluid of critically ill patients with ventilator-associated pneumonia. Chest 128:545-52.
31. Boselli E, Breilh D, Djabarouti S, Guillaume C, Rimmelé T, Gordien JB, Xuereb F, Saux MC, Allaouchiche B. 2007. Reliability of mini-bronchoalveolar lavage for the measurement of epithelial lining fluid concentrations of tobramycin in critically ill patients. Intensive Care Med 33:1519-23.

32. Mingeot-Leclercq MP, Tulkens PM. 1999. Aminoglycosides: nephrotoxicity. Antimicrob Agents Chemother 43:1003-12.
33. Dobie RA, Black FO, Pezsnecker SC, Stallings VL. 2006. Hearing loss in patients with vestibulotoxic reactions to gentamicin therapy. Arch Otolaryngol Head Neck Surg 132:253-7.
34. Leone M, Bouadma L, Bouhemad B, Brissaud O, Dauger S, Gibot S, Hraiech S, Jung B, Kipnis E, Launey Y, Luyt CE, Margetis D, Michel F, Mokart D, Montravers P, Monsel A, Nseir S, Pugin J, Roquilly A, Velly L, Zahar JR, Bruyère R, Chanques G. 2018. Hospital-acquired pneumonia in ICU. Anaesth Crit Care Pain Med 37:83-98.
35. Rogers GB, Hart CA, Mason JR, Hughes M, Walshaw MJ, Bruce KD. 2003. Bacterial diversity in cases of lung infection in cystic fibrosis patients: 16S ribosomal DNA (rDNA) length heterogeneity PCR and 16S rDNA terminal restriction fragment length polymorphism profiling. J Clin Microbiol 41:3548-58.
36. Ramsey BW, Dorkin HL, Eisenberg JD, Gibson RL, Harwood IR, Kravitz RM, Schidlow DV, Wilmott RW, Astley SJ, McBurnie MA. 1993. Efficacy of aerosolized tobramycin in patients with cystic fibrosis. N Engl J Med 328:1740-6.
37. Ramsey BW, Pepe MS, Quan JM, Otto KL, Montgomery AB, Williams-Warren J, Vasiljev-K M, Borowitz D, Bowman CM, Marshall BC, Marshall S, Smith AL. 1999. Intermittent administration of inhaled tobramycin in patients with cystic fibrosis. Cystic Fibrosis Inhaled Tobramycin Study Group. N Engl J Med 340:23-30.
38. Ratjen F, Munck A, Kho P, Angyalosi G, Group ES. 2010. Treatment of early *Pseudomonas aeruginosa* infection in patients with cystic fibrosis: the ELITE trial. Thorax 65:286-91.
39. Centers for Disease Control and Prevention. 2019. Antibiotic Resistance Threats in the United States, 2019. https://www.cdc.gov/drugresistance/biggest-threats.html.
40. Alcón A, Fàbregas N, Torres A. 2005. Pathophysiology of pneumonia. Clin Chest Med 26:39-46.
41. Peacock SJ, Foster TJ, Cameron BJ, Berendt AR. 1999. Bacterial fibronectin-binding proteins and endothelial cell surface fibronectin mediate adherence of *Staphylococcus aureus* to resting human endothelial cells. Microbiology (Reading) 145 (Pt 12):3477-3486.
42. Josse J, Laurent F, Diot A. 2017. Staphylococcal Adhesion and Host Cell Invasion: Fibronectin-Binding and Other Mechanisms. Front Microbiol 8:2433.
43. Alexander EH, Hudson MC. 2001. Factors influencing the internalization of *Staphylococcus aureus* and impacts on the course of infections in humans. Appl Microbiol Biotechnol 56:361-6.
44. Doig P, Todd T, Sastry PA, Lee KK, Hodges RS, Paranchych W, Irvin RT. 1988. Role of pili in adhesion of *Pseudomonas aeruginosa* to human respiratory epithelial cells. Infect Immun 56:1641-6.
45. Beaussart A, Baker AE, Kuchma SL, El-Kirat-Chatel S, O'Toole GA, Dufrêne YF. 2014. Nanoscale adhesion forces of *Pseudomonas aeruginosa* type IV Pili. ACS Nano 8:10723-33.
46. Brooks LRK, Mias GI. 2018. *Streptococcus pneumoniae's* Virulence and Host Immunity: Aging, Diagnostics, and Prevention. Front Immunol 9:1366.
47. Nelson AL, Roche AM, Gould JM, Chim K, Ratner AJ, Weiser JN. 2007. Capsule enhances pneumococcal colonization by limiting mucus-mediated clearance. Infect Immun 75:83-90.
48. Gilbert RJ, Jiménez JL, Chen S, Tickle IJ, Rossjohn J, Parker M, Andrew PW, Saibil HR. 1999. Two structural transitions in membrane pore formation by pneumolysin, the pore-forming toxin of *Streptococcus pneumoniae*. Cell 97:647-55.
49. Rai P, He F, Kwang J, Engelward BP, Chow VT. 2016. Pneumococcal Pneumolysin Induces DNA Damage and Cell Cycle Arrest. Sci Rep 6:22972.
50. Witzenrath M, Gutbier B, Hocke AC, Schmeck B, Hippenstiel S, Berger K, Mitchell TJ, de los Toyos JR, Rosseau S, Suttorp N, Schütte H. 2006. Role of pneumolysin for the development of acute lung injury in pneumococcal pneumonia. Crit Care Med 34:1947-54.

51. Rubins JB, Charboneau D, Paton JC, Mitchell TJ, Andrew PW, Janoff EN. 1995. Dual function of pneumolysin in the early pathogenesis of murine pneumococcal pneumonia. J Clin Invest 95:142-50.
52. Thay B, Wai SN, Oscarsson J. 2013. *Staphylococcus aureus* α-toxin-dependent induction of host cell death by membrane-derived vesicles. PLoS One 8:e54661.
53. Bartlett AH, Foster TJ, Hayashida A, Park PW. 2008. Alpha-toxin facilitates the generation of CXC chemokine gradients and stimulates neutrophil homing in *Staphylococcus aureus* pneumonia. J Infect Dis 198:1529-35.
54. Bubeck Wardenburg J, Schneewind O. 2008. Vaccine protection against *Staphylococcus aureus* pneumonia. J Exp Med 205:287-94.
55. Michalska M, Wolf P. 2015. *Pseudomonas* Exotoxin A: optimized by evolution for effective killing. Front Microbiol 6:963.
56. Jyot J, Balloy V, Jouvion G, Verma A, Touqui L, Huerre M, Chignard M, Ramphal R. 2011. Type II secretion system of *Pseudomonas aeruginosa*: in vivo evidence of a significant role in death due to lung infection. J Infect Dis 203:1369-77.
57. Sato H, Frank DW, Hillard CJ, Feix JB, Pankhaniya RR, Moriyama K, Finck-Barbançon V, Buchaklian A, Lei M, Long RM, Wiener-Kronish J, Sawa T. 2003. The mechanism of action of the *Pseudomonas aeruginosa*-encoded type III cytotoxin, ExoU. EMBO J 22:2959-69.
58. Howell HA, Logan LK, Hauser AR. 2013. Type III secretion of ExoU is critical during early *Pseudomonas aeruginosa* pneumonia. mBio 4:e00032-13.
59. Finck-Barbançon V, Goranson J, Zhu L, Sawa T, Wiener-Kronish JP, Fleiszig SM, Wu C, Mende-Mueller L, Frank DW. 1997. ExoU expression by *Pseudomonas aeruginosa* correlates with acute cytotoxicity and epithelial injury. Mol Microbiol 25:547-57.
60. Hauser AR, Cobb E, Bodi M, Mariscal D, Vallés J, Engel JN, Rello J. 2002. Type III protein secretion is associated with poor clinical outcomes in patients with ventilator-associated pneumonia caused by *Pseudomonas aeruginosa*. Crit Care Med 30:521-8.
61. Skaar EP, Humayun M, Bae T, DeBord KL, Schneewind O. 2004. Iron-source preference of *Staphylococcus aureus* infections. Science 305:1626-8.
62. Hammer ND, Skaar EP. 2011. Molecular mechanisms of *Staphylococcus aureus* iron acquisition. Annu Rev Microbiol 65:129-47.
63. Lawlor MS, O'connor C, Miller VL. 2007. Yersiniabactin is a virulence factor for *Klebsiella pneumoniae* during pulmonary infection. Infect Immun 75:1463-72.
64. Holden VI, Breen P, Houle S, Dozois CM, Bachman MA. 2016. *Klebsiella pneumoniae* Siderophores Induce Inflammation, Bacterial Dissemination, and HIF-1α Stabilization during Pneumonia. mBio 7.
65. Heiden SE, Hübner NO, Bohnert JA, Heidecke CD, Kramer A, Balau V, Gierer W, Schaefer S, Eckmanns T, Gatermann S, Eger E, Guenther S, Becker K, Schaufler K. 2020. A *Klebsiella pneumoniae* ST307 outbreak clone from Germany demonstrates features of extensive drug resistance, hypermucoviscosity, and enhanced iron acquisition. Genome Med 12:113.
66. Palmer LD, Skaar EP. 2016. Transition Metals and Virulence in Bacteria. Annu Rev Genet 50:67-91.
67. Hyams C, Camberlein E, Cohen JM, Bax K, Brown JS. 2010. The *Streptococcus pneumoniae* capsule inhibits complement activity and neutrophil phagocytosis by multiple mechanisms. Infect Immun 78:704-15.
68. Domenico P, Salo RJ, Cross AS, Cunha BA. 1994. Polysaccharide capsule-mediated resistance to opsonophagocytosis in *Klebsiella pneumoniae*. Infect Immun 62:4495-9.
69. Doorduijn DJ, Rooijakkers SH, van Schaik W, Bardoel BW. 2016. Complement resistance mechanisms of *Klebsiella pneumoniae*. Immunobiology 221:1102-9.
70. Talyansky Y, Nielsen TB, Yan J, Carlino-Macdonald U, Di Venanzio G, Chakravorty S, Ulhaq A, Feldman MF, Russo TA, Vinogradov E, Luna B, Wright MS, Adams MD, Spellberg B. 2021.

Capsule carbohydrate structure determines virulence in *Acinetobacter baumannii*. PLoS Pathog 17:e1009291.
71. Han S, Mallampalli RK. 2015. The Role of Surfactant in Lung Disease and Host Defense against Pulmonary Infections. Ann Am Thorac Soc 12:765-74.
72. Wu H, Kuzmenko A, Wan S, Schaffer L, Weiss A, Fisher JH, Kim KS, McCormack FX. 2003. Surfactant proteins A and D inhibit the growth of Gram-negative bacteria by increasing membrane permeability. J Clin Invest 111:1589-602.
73. Nkadi PO, Merritt TA, Pillers DA. 2009. An overview of pulmonary surfactant in the neonate: genetics, metabolism, and the role of surfactant in health and disease. Mol Genet Metab 97:95-101.
74. Radlinski LC, Rowe SE, Brzozowski R, Wilkinson AD, Huang R, Eswara P, Conlon BP. 2019. Chemical Induction of Aminoglycoside Uptake Overcomes Antibiotic Tolerance and Resistance in *Staphylococcus aureus*. Cell Chem Biol 26:1355-1364.e4.
75. Guillon A, Brea D, Morello E, Tang A, Jouan Y, Ramphal R, Korkmaz B, Perez-Cruz M, Trottein F, O'Callaghan RJ, Gosset P, Si-Tahar M. 2017. *Pseudomonas aeruginosa* proteolytically alters the interleukin 22-dependent lung mucosal defense. Virulence 8:810-820.
76. Malloy JL, Veldhuizen RA, Thibodeaux BA, O'Callaghan RJ, Wright JR. 2005. *Pseudomonas aeruginosa* protease IV degrades surfactant proteins and inhibits surfactant host defense and biophysical functions. Am J Physiol Lung Cell Mol Physiol 288:L409-18.
77. Kantyka T, Pyrc K, Gruca M, Smagur J, Plaza K, Guzik K, Zeglen S, Ochman M, Potempa J. 2013. *Staphylococcus aureus* proteases degrade lung surfactant protein A potentially impairing innate immunity of the lung. J Innate Immun 5:251-60.
78. Garvy BA, Harmsen AG. 1996. The importance of neutrophils in resistance to pneumococcal pneumonia in adult and neonatal mice. Inflammation 20:499-512.
79. Jeyaseelan S, Young SK, Yamamoto M, Arndt PG, Akira S, Kolls JK, Worthen GS. 2006. Toll/IL-1R domain-containing adaptor protein (TIRAP) is a critical mediator of antibacterial defense in the lung against *Klebsiella pneumoniae* but not *Pseudomonas aeruginosa*. J Immunol 177:538-47.
80. Robertson CM, Perrone EE, McConnell KW, Dunne WM, Boody B, Brahmbhatt T, Diacovo MJ, Van Rooijen N, Hogue LA, Cannon CL, Buchman TG, Hotchkiss RS, Coopersmith CM. 2008. Neutrophil depletion causes a fatal defect in murine pulmonary *Staphylococcus aureus* clearance. J Surg Res 150:278-85.
81. Limoli DH, Jones CJ, Wozniak DJ. 2015. Bacterial Extracellular Polysaccharides in Biofilm Formation and Function. Microbiol Spectr 3.
82. Thanabalasuriar A, Surewaard BG, Willson ME, Neupane AS, Stover CK, Warrener P, Wilson G, Keller AE, Sellman BR, DiGiandomenico A, Kubes P. 2017. Bispecific antibody targets multiple *Pseudomonas aeruginosa* evasion mechanisms in the lung vasculature. J Clin Invest 127:2249-2261.
83. de Jong NWM, van Kessel KPM, van Strijp JAG. 2019. Immune Evasion by *Staphylococcus aureus*. Microbiol Spectr 7.
84. Preston JA, Bewley MA, Marriott HM, McGarry Houghton A, Mohasin M, Jubrail J, Morris L, Stephenson YL, Cross S, Greaves DR, Craig RW, van Rooijen N, Bingle CD, Read RC, Mitchell TJ, Whyte MKB, Shapiro SD, Dockrell DH. 2019. Alveolar Macrophage Apoptosis-associated Bacterial Killing Helps Prevent Murine Pneumonia. Am J Respir Crit Care Med 200:84-97.
85. Dockrell DH, Marriott HM, Prince LR, Ridger VC, Ince PG, Hellewell PG, Whyte MK. 2003. Alveolar macrophage apoptosis contributes to pneumococcal clearance in a resolving model of pulmonary infection. J Immunol 171:5380-8.
86. Hashimoto S, Pittet JF, Hong K, Folkesson H, Bagby G, Kobzik L, Frevert C, Watanabe K, Tsurufuji S, Wiener-Kronish J. 1996. Depletion of alveolar macrophages decreases neutrophil chemotaxis to *Pseudomonas* airspace infections. Am J Physiol 270:L819-28.

87. Berenson CS, Kruzel RL, Eberhardt E, Sethi S. 2013. Phagocytic dysfunction of human alveolar macrophages and severity of chronic obstructive pulmonary disease. J Infect Dis 208:2036-45.
88. Bastaert F, Kheir S, Saint-Criq V, Villeret B, Dang PM, El-Benna J, Sirard JC, Voulhoux R, Sallenave JM. 2018. LasB Subverts Alveolar Macrophage Activity by Interfering With Bacterial Killing Through Downregulation of Innate Immune Defense, Reactive Oxygen Species Generation, and Complement Activation. Front Immunol 9:1675.
89. Medzhitov R, Preston-Hurlburt P, Kopp E, Stadlen A, Chen C, Ghosh S, Janeway CA. 1998. MyD88 is an adaptor protein in the hToll/IL-1 receptor family signaling pathways. Mol Cell 2:253-8.
90. Vinzing M, Eitel J, Lippmann J, Hocke AC, Zahlten J, Slevogt H, N'guessan PD, Günther S, Schmeck B, Hippenstiel S, Flieger A, Suttorp N, Opitz B. 2008. NAIP and Ipaf control *Legionella pneumophila* replication in human cells. J Immunol 180:6808-15.
91. Cohen TS, Prince AS. 2013. Activation of inflammasome signaling mediates pathology of acute *P. aeruginosa* pneumonia. J Clin Invest 123:1630-7.
92. Faure E, Mear JB, Faure K, Normand S, Couturier-Maillard A, Grandjean T, Balloy V, Ryffel B, Dessein R, Chignard M, Uyttenhove C, Guery B, Gosset P, Chamaillard M, Kipnis E. 2014. *Pseudomonas aeruginosa* type-3 secretion system dampens host defense by exploiting the NLRC4-coupled inflammasome. Am J Respir Crit Care Med 189:799-811.
93. Song N, Liu ZS, Xue W, Bai ZF, Wang QY, Dai J, Liu X, Huang YJ, Cai H, Zhan XY, Han QY, Wang H, Chen Y, Li HY, Li AL, Zhang XM, Zhou T, Li T. 2017. NLRP3 Phosphorylation Is an Essential Priming Event for Inflammasome Activation. Mol Cell 68:185-197.e6.
94. He Y, Hara H, Núñez G. 2016. Mechanism and Regulation of NLRP3 Inflammasome Activation. Trends Biochem Sci 41:1012-1021.
95. Patton LM, Saggart BS, Ahmed NK, Leff JA, Repine JE. 1995. Interleukin-1 beta-induced neutrophil recruitment and acute lung injury in hamsters. Inflammation 19:23-9.
96. Leung BP, Culshaw S, Gracie JA, Hunter D, Canetti CA, Campbell C, Cunha F, Liew FY, McInnes IB. 2001. A role for IL-18 in neutrophil activation. J Immunol 167:2879-86.
97. Liu T, Zhou Y, Li P, Duan JX, Liu YP, Sun GY, Wan L, Dong L, Fang X, Jiang JX, Guan CX. 2016. Blocking triggering receptor expressed on myeloid cells-1 attenuates lipopolysaccharide-induced acute lung injury via inhibiting NLRP3 inflammasome activation. Sci Rep 6:39473.
98. Amulic B, Cazalet C, Hayes GL, Metzler KD, Zychlinsky A. 2012. Neutrophil function: from mechanisms to disease. Annu Rev Immunol 30:459-89.
99. Dolinay T, Kim YS, Howrylak J, Hunninghake GM, An CH, Fredenburgh L, Massaro AF, Rogers A, Gazourian L, Nakahira K, Haspel JA, Landazury R, Eppanapally S, Christie JD, Meyer NJ, Ware LB, Christiani DC, Ryter SW, Baron RM, Choi AM. 2012. Inflammasome-regulated cytokines are critical mediators of acute lung injury. Am J Respir Crit Care Med 185:1225-34.
100. FitzGerald ES, Luz NF, Jamieson AM. 2020. Competitive Cell Death Interactions in Pulmonary Infection: Host Modulation Versus Pathogen Manipulation. Front Immunol 11:814.
101. Kagan VE, Tyurin VA, Jiang J, Tyurina YY, Ritov VB, Amoscato AA, Osipov AN, Belikova NA, Kapralov AA, Kini V, Vlasova II, Zhao Q, Zou M, Di P, Svistunenko DA, Kurnikov IV, Borisenko GG. 2005. Cytochrome c acts as a cardiolipin oxygenase required for release of proapoptotic factors. Nat Chem Biol 1:223-32.
102. Iyer SS, He Q, Janczy JR, Elliott EI, Zhong Z, Olivier AK, Sadler JJ, Knepper-Adrian V, Han R, Qiao L, Eisenbarth SC, Nauseef WM, Cassel SL, Sutterwala FS. 2013. Mitochondrial cardiolipin is required for Nlrp3 inflammasome activation. Immunity 39:311-323.
103. Sorice M, Circella A, Misasi R, Pittoni V, Garofalo T, Cirelli A, Pavan A, Pontieri GM, Valesini G. 2000. Cardiolipin on the surface of apoptotic cells as a possible trigger for antiphospholipids antibodies. Clin Exp Immunol 122:277-84.
104. Ray NB, Durairaj L, Chen BB, McVerry BJ, Ryan AJ, Donahoe M, Waltenbaugh AK, O'Donnell CP, Henderson FC, Etscheidt CA, McCoy DM, Agassandian M, Hayes-Rowan EC, Coon TA, Butler PL, Gakhar L, Mathur SN, Sieren JC, Tyurina YY, Kagan VE, McLennan G, Mallampalli

RK. 2010. Dynamic regulation of cardiolipin by the lipid pump Atp8b1 determines the severity of lung injury in experimental pneumonia. Nat Med 16:1120-1127.
105. Silhavy TJ, Kahne D, Walker S. 2010. The bacterial cell envelope. Cold Spring Harb Perspect Biol 2:a000414.
106. Furse S, Scott DJ. 2016. Three-Dimensional Distribution of Phospholipids in Gram Negative Bacteria. Biochemistry 55:4742-7.
107. Harding CM, Hennon SW, Feldman MF. 2018. Uncovering the mechanisms of *Acinetobacter baumannii* virulence. Nat Rev Microbiol 16:91-102.
108. Rojas ER, Billings G, Odermatt PD, Auer GK, Zhu L, Miguel A, Chang F, Weibel DB, Theriot JA, Huang KC. 2018. The outer membrane is an essential load-bearing element in Gram-negative bacteria. Nature 559:617-621.
109. Simpson BW, Nieckarz M, Pinedo V, McLean AB, Cava F, Trent MS. 2021. *Acinetobacter baumannii* Can Survive with an Outer Membrane Lacking Lipooligosaccharide Due to Structural Support from Elongasome Peptidoglycan Synthesis. mBio:e0309921.
110. Tomás JM, Ciurana B, Benedí VJ, Juarez A. 1988. Role of lipopolysaccharide and complement in susceptibility of *Escherichia coli* and *Salmonella typhimurium* to non-immune serum. J Gen Microbiol 134:1009-16.
111. Goebel EM, Wolfe DN, Elder K, Stibitz S, Harvill ET. 2008. O antigen protects *Bordetella parapertussis* from complement. Infect Immun 76:1774-80.
112. Maldonado RF, Sá-Correia I, Valvano MA. 2016. Lipopolysaccharide modification in Gram-negative bacteria during chronic infection. FEMS Microbiol Rev 40:480-93.
113. Liu T, Zhang L, Joo D, Sun SC. 2017. NF-κB signaling in inflammation. Signal Transduct Target Ther 2.
114. Hajjar AM, Ernst RK, Fortuno ES, Brasfield AS, Yam CS, Newlon LA, Kollmann TR, Miller SI, Wilson CB. 2012. Humanized TLR4/MD-2 mice reveal LPS recognition differentially impacts susceptibility to *Yersinia pestis* and *Salmonella enterica*. PLoS Pathog 8:e1002963.
115. Ernst RK, Yi EC, Guo L, Lim KB, Burns JL, Hackett M, Miller SI. 1999. Specific lipopolysaccharide found in cystic fibrosis airway *Pseudomonas aeruginosa*. Science 286:1561-5.
116. Mileykovskaya E, Dowhan W. 2000. Visualization of phospholipid domains in *Escherichia coli* by using the cardiolipin-specific fluorescent dye 10-N-nonyl acridine orange. J Bacteriol 182:1172-5.
117. Hsieh CW, Lin TY, Lai HM, Lin CC, Hsieh TS, Shih YL. 2010. Direct MinE-membrane interaction contributes to the proper localization of MinDE in *E. coli*. Mol Microbiol 75:499-512.
118. Arias-Cartin R, Grimaldi S, Arnoux P, Guigliarelli B, Magalon A. 2012. Cardiolipin binding in bacterial respiratory complexes: structural and functional implications. Biochim Biophys Acta 1817:1937-49.
119. Renner LD, Weibel DB. 2011. Cardiolipin microdomains localize to negatively curved regions of *Escherichia coli* membranes. Proc Natl Acad Sci U S A 108:6264-9.
120. Romantsov T, Helbig S, Culham DE, Gill C, Stalker L, Wood JM. 2007. Cardiolipin promotes polar localization of osmosensory transporter ProP in *Escherichia coli*. Mol Microbiol 64:1455-65.
121. Romantsov T, Guan Z, Wood JM. 2009. Cardiolipin and the osmotic stress responses of bacteria. Biochim Biophys Acta 1788:2092-100.
122. López GA, Heredia RM, Boeris PS, Lucchesi GI. 2016. Content of cardiolipin of the membrane and sensitivity to cationic surfactants in *Pseudomonas putida*. J Appl Microbiol 121:1004-14.
123. Wright SM, Hockey PM, Enhorning G, Strong P, Reid KB, Holgate ST, Djukanovic R, Postle AD. 2000. Altered airway surfactant phospholipid composition and reduced lung function in asthma. J Appl Physiol (1985) 89:1283-92.
124. Palmer LD, Minor KE, Mettlach JA, Rivera ES, Boyd KL, Caprioli RM, Spraggins JM, Dalebroux ZD, Skaar EP. 2020. Modulating Isoprenoid Biosynthesis Increases Lipooligosaccharides and

Restores *Acinetobacter baumannii* Resistance to Host and Antibiotic Stress. Cell Rep 32:108129.
125. Pizzuto M, Lonez C, Baroja-Mazo A, Martínez-Banaclocha H, Tourlomousis P, Gangloff M, Pelegrin P, Ruysschaert JM, Gay NJ, Bryant CE. 2019. Saturation of acyl chains converts cardiolipin from an antagonist to an activator of Toll-like receptor-4. Cell Mol Life Sci 76:3667-3678.
126. El Rayes J, Rodríguez-Alonso R, Collet JF. 2021. Lipoproteins in Gram-negative bacteria: new insights into their biogenesis, subcellular targeting and functional roles. Curr Opin Microbiol 61:25-34.
127. Fito-Boncompte L, Chapalain A, Bouffartigues E, Chaker H, Lesouhaitier O, Gicquel G, Bazire A, Madi A, Connil N, Véron W, Taupin L, Toussaint B, Cornelis P, Wei Q, Shioya K, Déziel E, Feuilloley MG, Orange N, Dufour A, Chevalier S. 2011. Full virulence of *Pseudomonas aeruginosa* requires OprF. Infect Immun 79:1176-86.
128. Qadi M, Lopez-Causapé C, Izquierdo-Rabassa S, Mateu Borrás M, Goldberg JB, Oliver A, Albertí S. 2016. Surfactant Protein A Recognizes Outer Membrane Protein OprH on *Pseudomonas aeruginosa* Isolates From Individuals With Chronic Infection. J Infect Dis 214:1449-1455.
129. Wolf AJ, Underhill DM. 2018. Peptidoglycan recognition by the innate immune system. Nat Rev Immunol 18:243-254.
130. Burkinshaw BJ, Deng W, Lameignère E, Wasney GA, Zhu H, Worrall LJ, Finlay BB, Strynadka NC. 2015. Structural analysis of a specialized type III secretion system peptidoglycan-cleaving enzyme. J Biol Chem 290:10406-17.
131. Symmons MF, Bokma E, Koronakis E, Hughes C, Koronakis V. 2009. The assembled structure of a complete tripartite bacterial multidrug efflux pump. Proc Natl Acad Sci U S A 106:7173-8.
132. Klein K, Sonnabend MS, Frank L, Leibiger K, Franz-Wachtel M, Macek B, Trunk T, Leo JC, Autenrieth IB, Schütz M, Bohn E. 2019. Deprivation of the Periplasmic Chaperone SurA Reduces Virulence and Restores Antibiotic Susceptibility of Multidrug-Resistant *Pseudomonas aeruginosa*. Front Microbiol 10:100.
133. Bogdanov M, Pyrshev K, Yesylevskyy S, Ryabichko S, Boiko V, Ivanchenko P, Kiyamova R, Guan Z, Ramseyer C, Dowhan W. 2020. Phospholipid distribution in the cytoplasmic membrane of Gram-negative bacteria is highly asymmetric, dynamic, and cell shape-dependent. Sci Adv 6:eaaz6333.
134. Arias-Cartin R, Grimaldi S, Pommier J, Lanciano P, Schaefer C, Arnoux P, Giordano G, Guigliarelli B, Magalon A. 2011. Cardiolipin-based respiratory complex activation in bacteria. Proc Natl Acad Sci U S A 108:7781-6.
135. Douglass MV, Cléon F, Trent MS. 2021. Cardiolipin aids in lipopolysaccharide transport to the gram-negative outer membrane. Proc Natl Acad Sci U S A 118.
136. Tan BK, Bogdanov M, Zhao J, Dowhan W, Raetz CR, Guan Z. 2012. Discovery of a cardiolipin synthase utilizing phosphatidylethanolamine and phosphatidylglycerol as substrates. Proc Natl Acad Sci U S A 109:16504-9.
137. Balasubramanian K, Maeda A, Lee JS, Mohammadyani D, Dar HH, Jiang JF, St Croix CM, Watkins S, Tyurin VA, Tyurina YY, Klöditz K, Polimova A, Kapralova VI, Xiong Z, Ray P, Klein-Seetharaman J, Mallampalli RK, Bayir H, Fadeel B, Kagan VE. 2015. Dichotomous roles for externalized cardiolipin in extracellular signaling: Promotion of phagocytosis and attenuation of innate immunity. Sci Signal 8:ra95.
138. Van Rhijn I, van Berlo T, Hilmenyuk T, Cheng TY, Wolf BJ, Tatituri RV, Uldrich AP, Napolitani G, Cerundolo V, Altman JD, Willemsen P, Huang S, Rossjohn J, Besra GS, Brenner MB, Godfrey DI, Moody DB. 2016. Human autoreactive T cells recognize CD1b and phospholipids. Proc Natl Acad Sci U S A 113:380-5.
139. Van den Berg B, Clemons WM, Collinson I, Modis Y, Hartmann E, Harrison SC, Rapoport TA. 2004. X-ray structure of a protein-conducting channel. Nature 427:36-44.

140. Shrivastava R, Chng SS. 2019. Lipid trafficking across the Gram-negative cell envelope. J Biol Chem 294:14175-14184.
141. Abellón-Ruiz J, Kaptan SS, Baslé A, Claudi B, Bumann D, Kleinekathöfer U, van den Berg B. 2017. Structural basis for maintenance of bacterial outer membrane lipid asymmetry. Nat Microbiol 2:1616-1623.
142. Narita S, Tokuda H. 2007. Amino acids at positions 3 and 4 determine the membrane specificity of *Pseudomonas aeruginosa* lipoproteins. J Biol Chem 282:13372-8.
143. Li XZ, Nikaido H, Poole K. 1995. Role of mexA-mexB-oprM in antibiotic efflux in *Pseudomonas aeruginosa*. Antimicrob Agents Chemother 39:1948-53.
144. Antunes LC, Visca P, Towner KJ. 2014. *Acinetobacter baumannii*: evolution of a global pathogen. Pathog Dis 71:292-301.
145. Dijkshoorn L, Nemec A, Seifert H. 2007. An increasing threat in hospitals: multidrug-resistant *Acinetobacter baumannii*. Nat Rev Microbiol 5:939-51.
146. Fournier PE, Richet H. 2006. The epidemiology and control of *Acinetobacter baumannii* in health care facilities. Clin Infect Dis 42:692-9.
147. Munoz-Price LS, Arheart K, Nordmann P, Boulanger AE, Cleary T, Alvarez R, Pizano L, Namias N, Kett DH, Poirel L. 2013. Eighteen years of experience with *Acinetobacter baumannii* in a tertiary care hospital. Crit Care Med 41:2733-42.
148. Vincent JL, Sakr Y, Singer M, Martin-Loeches I, Machado FR, Marshall JC, Finfer S, Pelosi P, Brazzi L, Aditianingsih D, Timsit JF, Du B, Wittebole X, Máca J, Kannan S, Gorordo-Delsol LA, De Waele JJ, Mehta Y, Bonten MJM, Khanna AK, Kollef M, Human M, Angus DC, Investigators EI. 2020. Prevalence and Outcomes of Infection Among Patients in Intensive Care Units in 2017. JAMA 323:1478-1487.
149. Chen MZ, Hsueh PR, Lee LN, Yu CJ, Yang PC, Luh KT. 2001. Severe community-acquired pneumonia due to *Acinetobacter baumannii*. Chest 120:1072-7.
150. Davis JS, McMillan M, Swaminathan A, Kelly JA, Piera KE, Baird RW, Currie BJ, Anstey NM. 2014. A 16-year prospective study of community-onset bacteremic *Acinetobacter* pneumonia: low mortality with appropriate initial empirical antibiotic protocols. Chest 146:1038-1045.
151. Inchai J, Pothirat C, Bumroongkit C, Limsukon A, Khositsakulchai W, Liwsrisakun C. 2015. Prognostic factors associated with mortality of drug-resistant *Acinetobacter baumannii* ventilator-associated pneumonia. J Intensive Care 3:9.
152. Eberle BM, Schnüriger B, Putty B, Barmparas G, Kobayashi L, Inaba K, Belzberg H, Demetriades D. 2010. The impact of *Acinetobacter baumannii* infections on outcome in trauma patients: a matched cohort study. Crit Care Med 38:2133-8.
153. Garnacho J, Sole-Violan J, Sa-Borges M, Diaz E, Rello J. 2003. Clinical impact of pneumonia caused by *Acinetobacter baumannii* in intubated patients: a matched cohort study. Crit Care Med 31:2478-82.
154. Villegas MV, Hartstein AI. 2003. *Acinetobacter* outbreaks, 1977-2000. Infect Control Hosp Epidemiol 24:284-95.
155. Monem S, Furmanek-Blaszk B, Łupkowska A, Kuczyńska-Wiśnik D, Stojowska-Swędrzyńska K, Laskowska E. 2020. Mechanisms Protecting *Acinetobacter baumannii* against Multiple Stresses Triggered by the Host Immune Response, Antibiotics and Outside-Host Environment. Int J Mol Sci 21.
156. Russo TA, Luke NR, Beanan JM, Olson R, Sauberan SL, MacDonald U, Schultz LW, Umland TC, Campagnari AA. 2010. The K1 capsular polysaccharide of *Acinetobacter baumannii* strain 307-0294 is a major virulence factor. Infect Immun 78:3993-4000.
157. Geisinger E, Isberg RR. 2015. Antibiotic modulation of capsular exopolysaccharide and virulence in *Acinetobacter baumannii*. PLoS Pathog 11:e1004691.
158. Koeleman JG, van der Bijl MW, Stoof J, Vandenbroucke-Grauls CM, Savelkoul PH. 2001. Antibiotic resistance is a major risk factor for epidemic behavior of *Acinetobacter baumannii*. Infect Control Hosp Epidemiol 22:284-8.

159. Tipton KA, Chin CY, Farokhyfar M, Weiss DS, Rather PN. 2018. Role of Capsule in Resistance to Disinfectants, Host Antimicrobials, and Desiccation in *Acinetobacter baumannii*. Antimicrob Agents Chemother 62.
160. Weber BS, Harding CM, Feldman MF. 2015. Pathogenic *Acinetobacter*: from the Cell Surface to Infinity and Beyond. J Bacteriol 198:880-7.
161. Boll JM, Tucker AT, Klein DR, Beltran AM, Brodbelt JS, Davies BW, Trent MS. 2015. Reinforcing Lipid A Acylation on the Cell Surface of *Acinetobacter baumannii* Promotes Cationic Antimicrobial Peptide Resistance and Desiccation Survival. mBio 6:e00478-15.
162. Erridge C, Moncayo-Nieto OL, Morgan R, Young M, Poxton IR. 2007. *Acinetobacter baumannii* lipopolysaccharides are potent stimulators of human monocyte activation via Toll-like receptor 4 signalling. J Med Microbiol 56:165-171.
163. Wong D, Nielsen TB, Bonomo RA, Pantapalangkoor P, Luna B, Spellberg B. 2017. Clinical and Pathophysiological Overview of *Acinetobacter* Infections: a Century of Challenges. Clin Microbiol Rev 30:409-447.
164. Lin L, Tan B, Pantapalangkoor P, Ho T, Baquir B, Tomaras A, Montgomery JI, Reilly U, Barbacci EG, Hujer K, Bonomo RA, Fernandez L, Hancock RE, Adams MD, French SW, Buslon VS, Spellberg B. 2012. Inhibition of LpxC protects mice from resistant *Acinetobacter baumannii* by modulating inflammation and enhancing phagocytosis. mBio 3.
165. Beceiro A, Moreno A, Fernández N, Vallejo JA, Aranda J, Adler B, Harper M, Boyce JD, Bou G. 2014. Biological cost of different mechanisms of colistin resistance and their impact on virulence in *Acinetobacter baumannii*. Antimicrob Agents Chemother 58:518-26.
166. Powers MJ, Trent MS. 2018. Expanding the paradigm for the outer membrane: *Acinetobacter baumannii* in the absence of endotoxin. Mol Microbiol 107:47-56.
167. Moffatt JH, Harper M, Harrison P, Hale JD, Vinogradov E, Seemann T, Henry R, Crane B, St Michael F, Cox AD, Adler B, Nation RL, Li J, Boyce JD. 2010. Colistin resistance in *Acinetobacter baumannii* is mediated by complete loss of lipopolysaccharide production. Antimicrob Agents Chemother 54:4971-7.
168. Sánchez-Encinales V, Álvarez-Marín R, Pachón-Ibáñez ME, Fernández-Cuenca F, Pascual A, Garnacho-Montero J, Martínez-Martínez L, Vila J, Tomás MM, Cisneros JM, Bou G, Rodríguez-Baño J, Pachón J, Smani Y. 2017. Overproduction of Outer Membrane Protein A by *Acinetobacter baumannii* as a Risk Factor for Nosocomial Pneumonia, Bacteremia, and Mortality Rate Increase. J Infect Dis 215:966-974.
169. Farrow JM, Wells G, Pesci EC. 2018. Desiccation tolerance in *Acinetobacter baumannii* is mediated by the two-component response regulator BfmR. PLoS One 13:e0205638.
170. Kyrpides NC, Hugenholtz P, Eisen JA, Woyke T, Göker M, Parker CT, Amann R, Beck BJ, Chain PS, Chun J, Colwell RR, Danchin A, Dawyndt P, Dedeurwaerdere T, DeLong EF, Detter JC, De Vos P, Donohue TJ, Dong XZ, Ehrlich DS, Fraser C, Gibbs R, Gilbert J, Gilna P, Glöckner FO, Jansson JK, Keasling JD, Knight R, Labeda D, Lapidus A, Lee JS, Li WJ, Ma J, Markowitz V, Moore ER, Morrison M, Meyer F, Nelson KE, Ohkuma M, Ouzounis CA, Pace N, Parkhill J, Qin N, Rossello-Mora R, Sikorski J, Smith D, Sogin M, Stevens R, Stingl U, Suzuki K, et al. 2014. Genomic encyclopedia of bacteria and archaea: sequencing a myriad of type strains. PLoS Biol 12:e1001920.
171. Antunes LC, Imperi F, Carattoli A, Visca P. 2011. Deciphering the multifactorial nature of *Acinetobacter baumannii* pathogenicity. PLoS One 6:e22674.
172. Hugh R, Reese R. 1968. A comparison of 120 strains of *Bacterium anitratum* Schaub and Hauber with the type strain of this species. International Journal of Systematic and Evolutionary Microbiology 18:1-3.
173. Jacobs AC, Thompson MG, Black CC, Kessler JL, Clark LP, McQueary CN, Gancz HY, Corey BW, Moon JK, Si Y, Owen MT, Hallock JD, Kwak YI, Summers A, Li CZ, Rasko DA, Penwell WF, Honnold CL, Wise MC, Waterman PE, Lesho EP, Stewart RL, Actis LA, Palys TJ, Craft DW,

Zurawski DV. 2014. AB5075, a Highly Virulent Isolate of *Acinetobacter baumannii*, as a Model Strain for the Evaluation of Pathogenesis and Antimicrobial Treatments. mBio 5:e01076-14.
174. McGann P, Courvalin P, Snesrud E, Clifford RJ, Yoon EJ, Onmus-Leone F, Ong AC, Kwak YI, Grillot-Courvalin C, Lesho E, Waterman PE. 2014. Amplification of aminoglycoside resistance gene aphA1 in *Acinetobacter baumannii* results in tobramycin therapy failure. mBio 5:e00915.
175. Pogue JM, Mann T, Barber KE, Kaye KS. 2013. Carbapenem-resistant *Acinetobacter baumannii*: epidemiology, surveillance and management. Expert Rev Anti Infect Ther 11:383-93.
176. Dickstein Y, Lellouche J, Ben Dalak Amar M, Schwartz D, Nutman A, Daitch V, Yahav D, Leibovici L, Skiada A, Antoniadou A, Daikos GL, Andini R, Zampino R, Durante-Mangoni E, Mouton JW, Friberg LE, Dishon Benattar Y, Bitterman R, Neuberger A, Carmeli Y, Paul M, Group AS. 2019. Treatment Outcomes of Colistin- and Carbapenem-resistant *Acinetobacter baumannii* Infections: An Exploratory Subgroup Analysis of a Randomized Clinical Trial. Clin Infect Dis 69:769-776.
177. Hsueh PR, Teng LJ, Chen CY, Chen WH, Yu CJ, Ho SW, Luh KT. 2002. Pandrug-resistant *Acinetobacter baumannii* causing nosocomial infections in a university hospital, Taiwan. Emerg Infect Dis 8:827-32.
178. Nowak J, Zander E, Stefanik D, Higgins PG, Roca I, Vila J, McConnell MJ, Cisneros JM, Seifert H, WP4 MWG. 2017. High incidence of pandrug-resistant *Acinetobacter baumannii* isolates collected from patients with ventilator-associated pneumonia in Greece, Italy and Spain as part of the MagicBullet clinical trial. J Antimicrob Chemother 72:3277-3282.
179. Traglia G, Chiem K, Quinn B, Fernandez JS, Montaña S, Almuzara M, Mussi MA, Tolmasky ME, Iriarte A, Centrón D, Ramírez MS. 2018. Genome sequence analysis of an extensively drug-resistant *Acinetobacter baumannii* indigo-pigmented strain depicts evidence of increase genome plasticity. Sci Rep 8:16961.
180. Liu F, Zhu Y, Yi Y, Lu N, Zhu B, Hu Y. 2014. Comparative genomic analysis of *Acinetobacter baumannii* clinical isolates reveals extensive genomic variation and diverse antibiotic resistance determinants. BMC Genomics 15:1163.
181. Wright MS, Haft DH, Harkins DM, Perez F, Hujer KM, Bajaksouzian S, Benard MF, Jacobs MR, Bonomo RA, Adams MD. 2014. New insights into dissemination and variation of the health care-associated pathogen *Acinetobacter baumannii* from genomic analysis. mBio 5:e00963-13.
182. Adams MD, Wright MS, Karichu JK, Venepally P, Fouts DE, Chan AP, Richter SS, Jacobs MR, Bonomo RA. 2019. Rapid Replacement of *Acinetobacter baumannii* Strains Accompanied by Changes in Lipooligosaccharide Loci and Resistance Gene Repertoire. MBio 10.
183. Jaidane N, Naas T, Mansour W, Radhia BB, Jerbi S, Boujaafar N, Bouallegue O, Bonnin RA. 2018. Genomic analysis of in vivo acquired resistance to colistin and rifampicin in *Acinetobacter baumannii*. Int J Antimicrob Agents 51:266-269.
184. Turton JF, Ward ME, Woodford N, Kaufmann ME, Pike R, Livermore DM, Pitt TL. 2006. The role of ISAba1 in expression of OXA carbapenemase genes in *Acinetobacter baumannii*. FEMS Microbiol Lett 258:72-7.
185. Abdi SN, Ghotaslou R, Ganbarov K, Mobed A, Tanomand A, Yousefi M, Asgharzadeh M, Kafil HS. 2020. *Acinetobacter baumanni* Efflux Pumps and Antibiotic Resistance. Infect Drug Resist 13:423-434.
186. Magnet S, Courvalin P, Lambert T. 2001. Resistance-nodulation-cell division-type efflux pump involved in aminoglycoside resistance in *Acinetobacter baumannii* strain BM4454. Antimicrob Agents Chemother 45:3375-80.
187. Marchand I, Damier-Piolle L, Courvalin P, Lambert T. 2004. Expression of the RND-type efflux pump AdeABC in *Acinetobacter baumannii* is regulated by the AdeRS two-component system. Antimicrob Agents Chemother 48:3298-304.

188. Yoon EJ, Courvalin P, Grillot-Courvalin C. 2013. RND-type efflux pumps in multidrug-resistant clinical isolates of *Acinetobacter baumannii*: major role for AdeABC overexpression and AdeRS mutations. Antimicrob Agents Chemother 57:2989-95.
189. Sumyk M, Himpich S, Foong WE, Herrmann A, Pos KM, Tam HK. 2021. Binding of Tetracyclines to *Acinetobacter baumannii* TetR Involves Two Arginines as Specificity Determinants. Front Microbiol 12:711158.
190. Adams MD, Nickel GC, Bajaksouzian S, Lavender H, Murthy AR, Jacobs MR, Bonomo RA. 2009. Resistance to colistin in *Acinetobacter baumannii* associated with mutations in the PmrAB two-component system. Antimicrob Agents Chemother 53:3628-34.
191. Pelletier MR, Casella LG, Jones JW, Adams MD, Zurawski DV, Hazlett KR, Doi Y, Ernst RK. 2013. Unique structural modifications are present in the lipopolysaccharide from colistin-resistant strains of *Acinetobacter baumannii*. Antimicrob Agents Chemother 57:4831-40.
192. Penwell WF, Shapiro AB, Giacobbe RA, Gu RF, Gao N, Thresher J, McLaughlin RE, Huband MD, DeJonge BL, Ehmann DE, Miller AA. 2015. Molecular mechanisms of sulbactam antibacterial activity and resistance determinants in *Acinetobacter baumannii*. Antimicrob Agents Chemother 59:1680-9.
193. Imberti R, Cusato M, Villani P, Carnevale L, Iotti GA, Langer M, Regazzi M. 2010. Steady-state pharmacokinetics and BAL concentration of colistin in critically Ill patients after IV colistin methanesulfonate administration. Chest 138:1333-9.
194. Ni W, Shao X, Di X, Cui J, Wang R, Liu Y. 2015. In vitro synergy of polymyxins with other antibiotics for *Acinetobacter baumannii*: a systematic review and meta-analysis. Int J Antimicrob Agents 45:8-18.
195. Klockgether J, Munder A, Neugebauer J, Davenport CF, Stanke F, Larbig KD, Heeb S, Schöck U, Pohl TM, Wiehlmann L, Tümmler B. 2010. Genome diversity of *Pseudomonas aeruginosa* PAO1 laboratory strains. J Bacteriol 192:1113-21.
196. Monteford J, Bilverstone TW, Ingle P, Philip S, Kuehne SA, Minton NP. 2021. What's a SNP between friends: The lineage of *Clostridioides difficile* R20291 can effect research outcomes. Anaerobe:102422.
197. Lopalco P, Stahl J, Annese C, Averhoff B, Corcelli A. 2017. Identification of unique cardiolipin and monolysocardiolipin species in *Acinetobacter baumannii*. Sci Rep 7:2972.
198. Buskirk SW, Lafontaine ER. 2014. *Moraxella catarrhalis* expresses a cardiolipin synthase that impacts adherence to human epithelial cells. J Bacteriol 196:107-20.
199. Koprivnjak T, Zhang D, Ernst CM, Peschel A, Nauseef WM, Weiss JP. 2011. Characterization of *Staphylococcus aureus* cardiolipin synthases 1 and 2 and their contribution to accumulation of cardiolipin in stationary phase and within phagocytes. J Bacteriol 193:4134-42.
200. Ferriols-Lisart R, Alós-Almiñana M. 1996. Effectiveness and safety of once-daily aminoglycosides: a meta-analysis. Am J Health Syst Pharm 53:1141-50.
201. Bhatt J, Jahnke N, Smyth AR. 2019. Once-daily versus multiple-daily dosing with intravenous aminoglycosides for cystic fibrosis. Cochrane Database Syst Rev 9:CD002009.
202. Serio AW, Keepers T, Andrews L, Krause KM. 2018. Aminoglycoside Revival: Review of a Historically Important Class of Antimicrobials Undergoing Rejuvenation. EcoSal Plus 8:10.1128/ecosalplus.ESP-0002-2018. https://doi.org/10.1128/ecosalplus.ESP-0002-2018.
203. Dellit TH, Owens RC, McGowan JE, Gerding DN, Weinstein RA, Burke JP, Huskins WC, Paterson DL, Fishman NO, Carpenter CF, Brennan PJ, Billeter M, Hooton TM, America IDSo, America SfHEo. 2007. Infectious Diseases Society of America and the Society for Healthcare Epidemiology of America guidelines for developing an institutional program to enhance antimicrobial stewardship. Clin Infect Dis 44:159-77.
204. Paul M, Benuri-Silbiger I, Soares-Weiser K, Leibovici L. 2004. Beta lactam monotherapy versus beta lactam-aminoglycoside combination therapy for sepsis in immunocompetent patients: systematic review and meta-analysis of randomised trials. BMJ 328:668.

205. Hood-Pishchany MI, Pham L, Wijers CD, Burns WJ, Boyd KL, Palmer LD, Skaar EP, Noto MJ. 2020. Broad-spectrum suppression of bacterial pneumonia by aminoglycoside-propagated *Acinetobacter baumannii*. PLoS Pathog 16:e1008374.
206. Wijers CDM, Pham L, Menon S, Boyd KL, Noel HR, Skaar EP, Gaddy JA, Palmer LD, Noto MJ. 2021. Identification of Two Variants of *Acinetobacter baumannii* Strain ATCC 17978 with Distinct Genotypes and Phenotypes. Infect Immun 89:e0045421.
207. Hood MI, Becker KW, Roux CM, Dunman PM, Skaar EP. 2013. genetic determinants of intrinsic colistin tolerance in *Acinetobacter baumannii*. Infect Immun 81:542-51.
208. Weber BS, Miyata ST, Iwashkiw JA, Mortensen BL, Skaar EP, Pukatzki S, Feldman MF. 2013. Genomic and functional analysis of the type VI secretion system in *Acinetobacter*. PLoS One 8:e55142.
209. Shih PC, Huang CT. 2002. Effects of quorum-sensing deficiency on *Pseudomonas aeruginosa* biofilm formation and antibiotic resistance. J Antimicrob Chemother 49:309-14.
210. Karkhoff-Schweizer RR, Schweizer HP. 1994. Utilization of a mini-Dlac transposable element to create an alpha-complementation and regulated expression system for cloning in *Pseudomonas aeruginosa*. Gene 140:7-15.
211. Bakker-Woudenberg IA, van den Berg JC, Vree TB, Baars AM, Michel MF. 1985. Relevance of serum protein binding of cefoxitin and cefazolin to their activities against *Klebsiella pneumoniae* pneumonia in rats. Antimicrob Agents Chemother 28:654-9.
212. Kennedy AD, Otto M, Braughton KR, Whitney AR, Chen L, Mathema B, Mediavilla JR, Byrne KA, Parkins LD, Tenover FC, Kreiswirth BN, Musser JM, DeLeo FR. 2008. Epidemic community-associated methicillin-resistant *Staphylococcus aureus*: recent clonal expansion and diversification. Proc Natl Acad Sci U S A 105:1327-32.
213. Spiliotis M. 2012. Inverse fusion PCR cloning. PLoS One 7:e35407.
214. Itoh Y, Haas D. 1985. Cloning vectors derived from the *Pseudomonas* plasmid pVS1. Gene 36:27-36.
215. Dorsey CW, Tomaras AP, Actis LA. 2006. Sequence and organization of pMAC, an *Acinetobacter baumannii* plasmid harboring genes involved in organic peroxide resistance. Plasmid 56:112-23.
216. Hood MI, Mortensen BL, Moore JL, Zhang Y, Kehl-Fie TE, Sugitani N, Chazin WJ, Caprioli RM, Skaar EP. 2012. Identification of an *Acinetobacter baumannii* zinc acquisition system that facilitates resistance to calprotectin-mediated zinc sequestration. PLoS Pathog 8:e1003068.
217. John T, Thomas T, Abel B, Wood BR, Chalmers DK, Martin LL. 2017. How kanamycin A interacts with bacterial and mammalian mimetic membranes. Biochim Biophys Acta Biomembr 1859:2242-2252.
218. Rivera M, Hancock RE, Sawyer JG, Haug A, McGroarty EJ. 1988. Enhanced binding of polycationic antibiotics to lipopolysaccharide from an aminoglycoside-supersusceptible, *tolA* mutant strain of *Pseudomonas aeruginosa*. Antimicrob Agents Chemother 32:649-55.
219. Taber HW, Mueller JP, Miller PF, Arrow AS. 1987. Bacterial uptake of aminoglycoside antibiotics. Microbiol Rev 51:439-57.
220. Hancock RE, Raffle VJ, Nicas TI. 1981. Involvement of the outer membrane in gentamicin and streptomycin uptake and killing in *Pseudomonas aeruginosa*. Antimicrob Agents Chemother 19:777-85.
221. Hancock RE. 1981. Aminoglycoside uptake and mode of action--with special reference to streptomycin and gentamicin. I. Antagonists and mutants. J Antimicrob Chemother 8:249-76.
222. Davis BD. 1987. Mechanism of bactericidal action of aminoglycosides. Microbiol Rev 51:341-50.
223. Fraimow HS, Greenman JB, Leviton IM, Dougherty TJ, Miller MH. 1991. Tobramycin uptake in *Escherichia coli* is driven by either electrical potential or ATP. J Bacteriol 173:2800-8.
224. Sistrunk JR, Nickerson KP, Chanin RB, Rasko DA, Faherty CS. 2016. Survival of the Fittest: How Bacterial Pathogens Utilize Bile To Enhance Infection. Clin Microbiol Rev 29:819-36.

225. Sabeti Azad M, Okuda M, Cyrenne M, Bourge M, Heck MP, Yoshizawa S, Fourmy D. 2020. Fluorescent Aminoglycoside Antibiotics and Methods for Accurately Monitoring Uptake by Bacteria. ACS Infect Dis 6:1008-1017.
226. Isaksson B, Nilsson L, Maller R, Sörén L. 1988. Postantibiotic effect of aminoglycosides on gram-negative bacteria evaluated by a new method. J Antimicrob Chemother 22:23-33.
227. Ramirez-Ronda CH, Holmes RK, Sanford JP. 1975. Effects of divalent cations on binding of aminoglycoside antibiotics to human serum proteins and to bacteria. Antimicrob Agents Chemother 7:239-45.
228. Llano-Sotelo B, Azucena EF, Kotra LP, Mobashery S, Chow CS. 2002. Aminoglycosides modified by resistance enzymes display diminished binding to the bacterial ribosomal aminoacyl-tRNA site. Chem Biol 9:455-63.
229. Bruni GN, Kralj JM. 2020. Membrane voltage dysregulation driven by metabolic dysfunction underlies bactericidal activity of aminoglycosides. Elife 9:e58706.
230. Vidal L, Gafter-Gvili A, Borok S, Fraser A, Leibovici L, Paul M. 2007. Efficacy and safety of aminoglycoside monotherapy: systematic review and meta-analysis of randomized controlled trials. J Antimicrob Chemother 60:247-57.
231. Gudiol F, Pallarés R, Ariza X, Fernández-Viladrich P, Rufi G, Liñares J. 1986. Comparative clinical evaluation of aztreonam versus aminoglycosides in gram-negative septicaemia. J Antimicrob Chemother 17:661-71.
232. Bliziotis IA, Petrosillo N, Michalopoulos A, Samonis G, Falagas ME. 2011. Impact of definitive therapy with beta-lactam monotherapy or combination with an aminoglycoside or a quinolone for *Pseudomonas aeruginosa* bacteremia. PLoS One 6:e26470.
233. Zhao J, Schloss PD, Kalikin LM, Carmody LA, Foster BK, Petrosino JF, Cavalcoli JD, VanDevanter DR, Murray S, Li JZ, Young VB, LiPuma JJ. 2012. Decade-long bacterial community dynamics in cystic fibrosis airways. Proc Natl Acad Sci U S A 109:5809-14.
234. Khanolkar RA, Clark ST, Wang PW, Hwang DM, Yau YCW, Waters VJ, Guttman DS. 2020. Ecological Succession of Polymicrobial Communities in the Cystic Fibrosis Airways. mSystems 5:e00809-20.
235. Flynn JM, Cameron LC, Wiggen TD, Dunitz JM, Harcombe WR, Hunter RC. 2020. Disruption of Cross-Feeding Inhibits Pathogen Growth in the Sputa of Patients with Cystic Fibrosis. mSphere 5:e00343-20.
236. Clark ST, Diaz Caballero J, Cheang M, Coburn B, Wang PW, Donaldson SL, Zhang Y, Liu M, Keshavjee S, Yau YC, Waters VJ, Elizabeth Tullis D, Guttman DS, Hwang DM. 2015. Phenotypic diversity within a *Pseudomonas aeruginosa* population infecting an adult with cystic fibrosis. Sci Rep 5:10932.
237. Foweraker JE, Laughton CR, Brown DF, Bilton D. 2005. Phenotypic variability of *Pseudomonas aeruginosa* in sputa from patients with acute infective exacerbation of cystic fibrosis and its impact on the validity of antimicrobial susceptibility testing. J Antimicrob Chemother 55:921-7.
238. Bridges JP, Ikegami M, Brilli LL, Chen X, Mason RJ, Shannon JM. 2010. LPCAT1 regulates surfactant phospholipid synthesis and is required for transitioning to air breathing in mice. J Clin Invest 120:1736-48.
239. Kanafani ZA, Zahreddine N, Tayyar R, Sfeir J, Araj GF, Matar GM, Kanj SS. 2018. Multi-drug resistant *Acinetobacter* species: a seven-year experience from a tertiary care center in Lebanon. Antimicrob Resist Infect Control 7:9.
240. Anderson SE, Sherman EX, Weiss DS, Rather PN. 2018. Aminoglycoside Heteroresistance in *Acinetobacter baumannii* AB5075. mSphere 3.
241. Tada T, Miyoshi-Akiyama T, Shimada K, Shimojima M, Kirikae T. 2014. Dissemination of 16S rRNA methylase ArmA-producing *Acinetobacter baumannii* and emergence of OXA-72 carbapenemase coproducers in Japan. Antimicrob Agents Chemother 58:2916-20.

242. Hsu LY, Apisarnthanarak A, Khan E, Suwantarat N, Ghafur A, Tambyah PA. 2017. Carbapenem-Resistant *Acinetobacter baumannii* and Enterobacteriaceae in South and Southeast Asia. Clin Microbiol Rev 30:1-22.
243. Evans BA, Hamouda A, Amyes SG. 2013. The rise of carbapenem-resistant *Acinetobacter baumannii*. Curr Pharm Des 19:223-38.
244. Tacconelli E, Carrara E, Savoldi A, Harbarth S, Mendelson M, Monnet DL, Pulcini C, Kahlmeter G, Kluytmans J, Carmeli Y, Ouellette M, Outterson K, Patel J, Cavaleri M, Cox EM, Houchens CR, Grayson ML, Hansen P, Singh N, Theuretzbacher U, Magrini N, Group WPPLW. 2018. Discovery, research, and development of new antibiotics: the WHO priority list of antibiotic-resistant bacteria and tuberculosis. Lancet Infect Dis 18:318-327.
245. Park YK, Jung SI, Park KH, Cheong HS, Peck KR, Song JH, Ko KS. 2009. Independent emergence of colistin-resistant *Acinetobacter* spp. isolates from Korea. Diagn Microbiol Infect Dis 64:43-51.
246. Trebosc V, Gartenmann S, Tötzl M, Lucchini V, Schellhorn B, Pieren M, Lociuro S, Gitzinger M, Tigges M, Bumann D, Kemmer C. 2019. Dissecting Colistin Resistance Mechanisms in Extensively Drug-Resistant Acinetobacter baumannii Clinical Isolates. mBio 10.
247. Li J, Nation RL, Turnidge JD, Milne RW, Coulthard K, Rayner CR, Paterson DL. 2006. Colistin: the re-emerging antibiotic for multidrug-resistant Gram-negative bacterial infections. Lancet Infect Dis 6:589-601.
248. Xie R, Zhang XD, Zhao Q, Peng B, Zheng J. 2018. Analysis of global prevalence of antibiotic resistance in *Acinetobacter baumannii* infections disclosed a faster increase in OECD countries. Emerg Microbes Infect 7:31.
249. Wright MS, Iovleva A, Jacobs MR, Bonomo RA, Adams MD. 2016. Genome dynamics of multidrug-resistant *Acinetobacter baumannii* during infection and treatment. Genome Med 8:26.
250. Boone RL, Whitehead B, Avery TM, Lu J, Francis JD, Guevara MA, Moore RE, Chambers SA, Doster RS, Manning SD, Townsend SD, Dent L, Marshall D, Gaddy JA, Damo SM. 2021. Analysis of virulence phenotypes and antibiotic resistance in clinical strains of *Acinetobacter baumannii* isolated in Nashville, Tennessee. BMC Microbiol 21:21.
251. Wang N, Ozer EA, Mandel MJ, Hauser AR. 2014. Genome-wide identification of *Acinetobacter baumannii* genes necessary for persistence in the lung. MBio 5:e01163-14.
252. Sato Y, Unno Y, Kawakami S, Ubagai T, Ono Y. 2017. Virulence characteristics of *Acinetobacter baumannii* clinical isolates vary with the expression levels of omps. J Med Microbiol 66:203-212.
253. Ramirez MS, Penwell WF, Traglia GM, Zimbler DL, Gaddy JA, Nikolaidis N, Arivett BA, Adams MD, Bonomo RA, Actis LA, Tolmasky ME. 2019. Identification of Potential Virulence Factors in the Model Strain *Acinetobacter baumannii* A118. Front Microbiol 10:1599.
254. Hesse LE, Lonergan ZR, Beavers WN, Skaar EP. 2019. The *Acinetobacter baumannii* Znu System Overcomes Host-Imposed Nutrient Zinc Limitation. Infect Immun 87.
255. Lonergan ZR, Nairn BL, Wang J, Hsu YP, Hesse LE, Beavers WN, Chazin WJ, Trinidad JC, VanNieuwenhze MS, Giedroc DP, Skaar EP. 2019. An *Acinetobacter baumannii*, Zinc-Regulated Peptidase Maintains Cell Wall Integrity during Immune-Mediated Nutrient Sequestration. Cell Rep 26:2009-2018.e6.
256. Wood CR, Ohneck EJ, Edelmann RE, Actis LA. 2018. A Light-Regulated Type I Pilus Contributes to *Acinetobacter baumannii* Biofilm, Motility, and Virulence Functions. Infect Immun 86.
257. Williams CL, Neu HM, Alamneh YA, Reddinger RM, Jacobs AC, Singh S, Abu-Taleb R, Michel SLJ, Zurawski DV, Merrell DS. 2020. Characterization of *Acinetobacter baumannii* Copper Resistance Reveals a Role in Virulence. Front Microbiol 11:16.
258. Dobrindt U, Hacker J. 2001. Whole genome plasticity in pathogenic bacteria. Curr Opin Microbiol 4:550-7.
259. Imperi F, Antunes LC, Blom J, Villa L, Iacono M, Visca P, Carattoli A. 2011. The genomics of *Acinetobacter baumannii*: insights into genome plasticity, antimicrobial resistance and pathogenicity. IUBMB Life 63:1068-74.

260. Weber BS, Ly PM, Irwin JN, Pukatzki S, Feldman MF. 2015. A multidrug resistance plasmid contains the molecular switch for type VI secretion in *Acinetobacter baumannii*. Proc Natl Acad Sci U S A 112:9442-7.
261. Kim J, Lee JY, Lee H, Choi JY, Kim DH, Wi YM, Peck KR, Ko KS. 2017. Microbiological features and clinical impact of the type VI secretion system (T6SS) in *Acinetobacter baumannii* isolates causing bacteremia. Virulence 8:1378-1389.
262. Jensen T, Tellgren-Roth C, Redl S, Maury J, Jacobsen SAB, Pedersen LE, Nielsen AT. 2019. Genome-wide systematic identification of methyltransferase recognition and modification patterns. Nat Commun 10:3311.
263. Smith MG, Gianoulis TA, Pukatzki S, Mekalanos JJ, Ornston LN, Gerstein M, Snyder M. 2007. New insights into *Acinetobacter baumannii* pathogenesis revealed by high-density pyrosequencing and transposon mutagenesis. Genes Dev 21:601-14.
264. Breslow JM, Meissler JJ, Hartzell RR, Spence PB, Truant A, Gaughan J, Eisenstein TK. 2011. Innate immune responses to systemic *Acinetobacter baumannii* infection in mice: neutrophils, but not interleukin-17, mediate host resistance. Infect Immun 79:3317-27.
265. van Faassen H, KuoLee R, Harris G, Zhao X, Conlan JW, Chen W. 2007. Neutrophils play an important role in host resistance to respiratory infection with *Acinetobacter baumannii* in mice. Infect Immun 75:5597-608.
266. Qiu H, KuoLee R, Harris G, Chen W. 2009. High susceptibility to respiratory *Acinetobacter baumannii* infection in A/J mice is associated with a delay in early pulmonary recruitment of neutrophils. Microbes Infect 11:946-55.
267. Mahmutovic Persson I, Menzel M, Ramu S, Cerps S, Akbarshahi H, Uller L. 2018. IL-1β mediates lung neutrophilia and IL-33 expression in a mouse model of viral-induced asthma exacerbation. Respir Res 19:16.
268. Miller LS, Pietras EM, Uricchio LH, Hirano K, Rao S, Lin H, O'Connell RM, Iwakura Y, Cheung AL, Cheng G, Modlin RL. 2007. Inflammasome-mediated production of IL-1beta is required for neutrophil recruitment against *Staphylococcus aureus* in vivo. J Immunol 179:6933-42.
269. Biondo C, Mancuso G, Midiri A, Signorino G, Domina M, Lanza Cariccio V, Mohammadi N, Venza M, Venza I, Teti G, Beninati C. 2014. The interleukin-1β/CXCL1/2/neutrophil axis mediates host protection against group B streptococcal infection. Infect Immun 82:4508-17.
270. Mantovani A, Dinarello CA, Molgora M, Garlanda C. 2019. Interleukin-1 and Related Cytokines in the Regulation of Inflammation and Immunity. Immunity 50:778-795.
271. Andrade EB, Alves J, Madureira P, Oliveira L, Ribeiro A, Cordeiro-da-Silva A, Correia-Neves M, Trieu-Cuot P, Ferreira P. 2013. TLR2-induced IL-10 production impairs neutrophil recruitment to infected tissues during neonatal bacterial sepsis. J Immunol 191:4759-68.
272. Sun L, Guo RF, Newstead MW, Standiford TJ, Macariola DR, Shanley TP. 2009. Effect of IL-10 on neutrophil recruitment and survival after *Pseudomonas aeruginosa* challenge. Am J Respir Cell Mol Biol 41:76-84.
273. Tucker AT, Nowicki EM, Boll JM, Knauf GA, Burdis NC, Trent MS, Davies BW. 2014. Defining gene-phenotype relationships in *Acinetobacter baumannii* through one-step chromosomal gene inactivation. MBio 5:e01313-14.
274. Avalos Vizcarra I, Hosseini V, Kollmannsberger P, Meier S, Weber SS, Arnoldini M, Ackermann M, Vogel V. 2016. How type 1 fimbriae help *Escherichia coli* to evade extracellular antibiotics. Sci Rep 6:18109.
275. Lo AW, Van de Water K, Gane PJ, Chan AW, Steadman D, Stevens K, Selwood DL, Waksman G, Remaut H. 2014. Suppression of type 1 pilus assembly in uropathogenic *Escherichia coli* by chemical inhibition of subunit polymerization. J Antimicrob Chemother 69:1017-26.
276. Martinez JJ, Mulvey MA, Schilling JD, Pinkner JS, Hultgren SJ. 2000. Type 1 pilus-mediated bacterial invasion of bladder epithelial cells. EMBO J 19:2803-12.
277. Sarkar S, Vagenas D, Schembri MA, Totsika M. 2016. Biofilm formation by multidrug resistant *Escherichia coli* ST131 is dependent on type 1 fimbriae and assay conditions. Pathog Dis 74.

278. Imlay JA. 2013. The molecular mechanisms and physiological consequences of oxidative stress: lessons from a model bacterium. Nat Rev Microbiol 11:443-54.
279. Wan B, Zhang Q, Ni J, Li S, Wen D, Li J, Xiao H, He P, Ou HY, Tao J, Teng Q, Lu J, Wu W, Yao YF. 2017. Type VI secretion system contributes to Enterohemorrhagic *Escherichia coli* virulence by secreting catalase against host reactive oxygen species (ROS). PLoS Pathog 13:e1006246.
280. Goulart CL, Barbosa LC, Bisch PM, von Krüger WMA. 2016. Catalases and PhoB/PhoR system independently contribute to oxidative stress resistance in *Vibrio cholerae* O1. Microbiology 162:1955-1962.
281. El-Benna J, Hurtado-Nedelec M, Marzaioli V, Marie JC, Gougerot-Pocidalo MA, Dang PM. 2016. Priming of the neutrophil respiratory burst: role in host defense and inflammation. Immunol Rev 273:180-93.
282. Nguyen GT, Green ER, Mecsas J. 2017. Neutrophils to the ROScue: Mechanisms of NADPH Oxidase Activation and Bacterial Resistance. Front Cell Infect Microbiol 7:373.
283. Tropp BE. 1997. Cardiolipin synthase from *Escherichia coli*. Biochim Biophys Acta 1348:192-200.
284. Rowlett VW, Mallampalli VKPS, Karlstaedt A, Dowhan W, Taegtmeyer H, Margolin W, Vitrac H. 2017. Impact of Membrane Phospholipid Alterations in *Escherichia coli* on Cellular Function and Bacterial Stress Adaptation. J Bacteriol 199.
285. López CS, Alice AF, Heras H, Rivas EA, Sánchez-Rivas C. 2006. Role of anionic phospholipids in the adaptation of *Bacillus subtilis* to high salinity. Microbiology 152:605-16.
286. Sahl JW, Gillece JD, Schupp JM, Waddell VG, Driebe EM, Engelthaler DM, Keim P. 2013. Evolution of a pathogen: a comparative genomics analysis identifies a genetic pathway to pathogenesis in *Acinetobacter*. PLoS One 8:e54287.
287. Juttukonda LJ, Green ER, Lonergan ZR, Heffern MC, Chang CJ, Skaar EP. 2019. OxyR Regulates the Transcriptional Response to Hydrogen Peroxide. Infect Immun 87.
288. Chakraborty K, Raundhal M, Chen BB, Morse C, Tyurina YY, Khare A, Oriss TB, Huff R, Lee JS, St Croix CM, Watkins S, Mallampalli RK, Kagan VE, Ray A, Ray P. 2017. The mito-DAMP cardiolipin blocks IL-10 production causing persistent inflammation during bacterial pneumonia. Nat Commun 8:13944.
289. Garg M, Johri S, Sagar S, Mundhada A, Agrawal A, Ray P, Chakraborty K. 2021. Cardiolipin-mediated PPARγ S112 phosphorylation impairs IL-10 production and inflammation resolution during bacterial pneumonia. Cell Rep 34:108736.
290. Saraiva M, O'Garra A. 2010. The regulation of IL-10 production by immune cells. Nat Rev Immunol 10:170-81.
291. Moreira LO, El Kasmi KC, Smith AM, Finkelstein D, Fillon S, Kim YG, Núñez G, Tuomanen E, Murray PJ. 2008. The TLR2-MyD88-NOD2-RIPK2 signalling axis regulates a balanced pro-inflammatory and IL-10-mediated anti-inflammatory cytokine response to Gram-positive cell walls. Cell Microbiol 10:2067-77.
292. Castro F, Cardoso AP, Gonçalves RM, Serre K, Oliveira MJ. 2018. Interferon-Gamma at the Crossroads of Tumor Immune Surveillance or Evasion. Front Immunol 9:847.
293. Darwich L, Coma G, Peña R, Bellido R, Blanco EJ, Este JA, Borras FE, Clotet B, Ruiz L, Rosell A, Andreo F, Parkhouse RM, Bofill M. 2009. Secretion of interferon-gamma by human macrophages demonstrated at the single-cell level after costimulation with interleukin (IL)-12 plus IL-18. Immunology 126:386-93.
294. Robinson CM, O'Dee D, Hamilton T, Nau GJ. 2010. Cytokines involved in interferon-gamma production by human macrophages. J Innate Immun 2:56-65.
295. Sun D, Crowell SA, Harding CM, De Silva PM, Harrison A, Fernando DM, Mason KM, Santana E, Loewen PC, Kumar A, Liu Y. 2016. KatG and KatE confer *Acinetobacter* resistance to hydrogen peroxide but sensitize bacteria to killing by phagocytic respiratory burst. Life Sci 148:31-40.

296. Wright MS, Mountain S, Beeri K, Adams MD. 2017. Assessment of Insertion Sequence Mobilization as an Adaptive Response to Oxidative Stress in *Acinetobacter baumannii* Using IS-seq. J Bacteriol 199.
297. Pfefferle K, Lopalco P, Breisch J, Siemund A, Corcelli A, Averhoff B. 2020. In vivo synthesis of monolysocardiolipin and cardiolipin by *Acinetobacter baumannii* phospholipase D and effect on cationic antimicrobial peptide resistance. Environ Microbiol.
298. Boyd KJ, Alder NN, May ER. 2018. Molecular Dynamics Analysis of Cardiolipin and Monolysocardiolipin on Bilayer Properties. Biophys J 114:2116-2127.
299. Powers MJ, Simpson BW, Trent MS. 2020. The Mla pathway in *Acinetobacter baumannii* has no demonstrable role in anterograde lipid transport. Elife 9.
300. Deatherage DE, Barrick JE. 2014. Identification of mutations in laboratory-evolved microbes from next-generation sequencing data using breseq. Methods Mol Biol 1151:165-88.
301. Barrick JE, Colburn G, Deatherage DE, Traverse CC, Strand MD, Borges JJ, Knoester DB, Reba A, Meyer AG. 2014. Identifying structural variation in haploid microbial genomes from short-read resequencing data using breseq. BMC Genomics 15:1039.
302. Kumar A, Dalton C, Cortez-Cordova J, Schweizer HP. 2010. Mini-Tn7 vectors as genetic tools for single copy gene cloning in *Acinetobacter baumannii*. J Microbiol Methods 82:296-300.
303. Jacobs AC, Hood I, Boyd KL, Olson PD, Morrison JM, Carson S, Sayood K, Iwen PC, Skaar EP, Dunman PM. 2010. Inactivation of phospholipase D diminishes *Acinetobacter baumannii* pathogenesis. Infect Immun 78:1952-62.
304. Gaddy JA, Tomaras AP, Actis LA. 2009. The *Acinetobacter baumannii* 19606 OmpA protein plays a role in biofilm formation on abiotic surfaces and in the interaction of this pathogen with eukaryotic cells. Infect Immun 77:3150-60.
305. Greene SE, Hibbing ME, Janetka J, Chen SL, Hultgren SJ. 2015. Human Urine Decreases Function and Expression of Type 1 Pili in Uropathogenic *Escherichia coli*. mBio 6:e00820.
306. Álvarez-Fraga L, Pérez A, Rumbo-Feal S, Merino M, Vallejo JA, Ohneck EJ, Edelmann RE, Beceiro A, Vázquez-Ucha JC, Valle J, Actis LA, Bou G, Poza M. 2016. Analysis of the role of the LH92_11085 gene of a biofilm hyper-producing *Acinetobacter baumannii* strain on biofilm formation and attachment to eukaryotic cells. Virulence 7:443-55.
307. Amend SR, Valkenburg KC, Pienta KJ. 2016. Murine Hind Limb Long Bone Dissection and Bone Marrow Isolation. J Vis Exp.
308. Zhang X, Goncalves R, Mosser DM. 2008. The isolation and characterization of murine macrophages. Curr Protoc Immunol Chapter 14:Unit 14.1.
309. Misharin AV, Morales-Nebreda L, Mutlu GM, Budinger GR, Perlman H. 2013. Flow cytometric analysis of macrophages and dendritic cell subsets in the mouse lung. Am J Respir Cell Mol Biol 49:503-10.
310. Mulvey MA, Schilling JD, Hultgren SJ. 2001. Establishment of a persistent *Escherichia coli* reservoir during the acute phase of a bladder infection. Infect Immun 69:4572-9.
311. Rosen DA, Pinkner JS, Jones JM, Walker JN, Clegg S, Hultgren SJ. 2008. Utilization of an intracellular bacterial community pathway in *Klebsiella pneumoniae* urinary tract infection and the effects of FimK on type 1 pilus expression. Infect Immun 76:3337-45.
312. Hunger M, Schmucker R, Kishan V, Hillen W. 1990. Analysis and nucleotide sequence of an origin of DNA replication in *Acinetobacter calcoaceticus* and its use for *Escherichia coli* shuttle plasmids. Gene 87:45-51.
313. Carruthers MD, Nicholson PA, Tracy EN, Munson RS. 2013. *Acinetobacter baumannii* utilizes a type VI secretion system for bacterial competition. PLoS One 8:e59388.
314. Hiraoka S, Matsuzaki H, Shibuya I. 1993. Active increase in cardiolipin synthesis in the stationary growth phase and its physiological significance in *Escherichia coli*. FEBS Lett 336:221-4.
315. Jiang JH, Bhuiyan MS, Shen HH, Cameron DR, Rupasinghe TWT, Wu CM, Le Brun AP, Kostoulias X, Domene C, Fulcher AJ, McConville MJ, Howden BP, Lieschke GJ, Peleg AY. 2019.

Antibiotic resistance and host immune evasion in *Staphylococcus aureus* mediated by a metabolic adaptation. Proc Natl Acad Sci U S A 116:3722-3727.
316. Cao F, Tian X, Li Z, Lv Y, Han J, Zhuang R, Cheng B, Gong Y, Ying B, Jin S, Gao Y. 2020. Suppression of NLRP3 Inflammasome by Erythropoietin via the EPOR/JAK2/STAT3 Pathway Contributes to Attenuation of Acute Lung Injury in Mice. Front Pharmacol 11:306.
317. Lery LM, Frangeul L, Tomas A, Passet V, Almeida AS, Bialek-Davenet S, Barbe V, Bengoechea JA, Sansonetti P, Brisse S, Tournebize R. 2014. Comparative analysis of *Klebsiella pneumoniae* genomes identifies a phospholipase D family protein as a novel virulence factor. BMC Biol 12:41.
318. Folch J, Lees M, Sloane Stanley GH. 1957. A simple method for the isolation and purification of total lipides from animal tissues. J Biol Chem 226:497-509.
319. Jan AT. 2017. Outer Membrane Vesicles (OMVs) of Gram-negative Bacteria: A Perspective Update. Front Microbiol 8:1053.
320. Kadurugamuwa JL, Beveridge TJ. 1995. Virulence factors are released from *Pseudomonas aeruginosa* in association with membrane vesicles during normal growth and exposure to gentamicin: a novel mechanism of enzyme secretion. J Bacteriol 177:3998-4008.
321. Jun SH, Lee JH, Kim BR, Kim SI, Park TI, Lee JC, Lee YC. 2013. *Acinetobacter baumannii* outer membrane vesicles elicit a potent innate immune response via membrane proteins. PLoS One 8:e71751.
322. Kim SY, Kim MH, Kim SI, Son JH, Kim S, Lee YC, Shin M, Oh MH, Lee JC. 2019. The sensor kinase BfmS controls production of outer membrane vesicles in *Acinetobacter baumannii*. BMC Microbiol 19:301.
323. Ehrentraut H, Weisheit CK, Frede S, Hilbert T. 2019. Inducing Acute Lung Injury in Mice by Direct Intratracheal Lipopolysaccharide Instillation. J Vis Exp.
324. Mizgerd JP. 2018. Inflammation and Pneumonia: Why Are Some More Susceptible than Others? Clin Chest Med 39:669-676.
325. Tatsumi K, Antoniak S, Subramaniam S, Gondouin B, Neidich SD, Beck MA, Mickelson J, Monroe DM, Bastarache JA, Mackman N. 2016. Anticoagulation increases alveolar hemorrhage in mice infected with influenza A. Physiol Rep 4.
326. Yang J, Park KW, Cho S. 2018. Inhibition of the CD36 receptor reduces visceral fat accumulation and improves insulin resistance in obese mice carrying the BDNF-. J Biol Chem 293:13338-13348.
327. Elliott JA, Winn WC. 1986. Treatment of alveolar macrophages with cytochalasin D inhibits uptake and subsequent growth of Legionella pneumophila. Infect Immun 51:31-6.
328. Ip WK, Sokolovska A, Charriere GM, Boyer L, Dejardin S, Cappillino MP, Yantosca LM, Takahashi K, Moore KJ, Lacy-Hulbert A, Stuart LM. 2010. Phagocytosis and phagosome acidification are required for pathogen processing and MyD88-dependent responses to *Staphylococcus aureus*. J Immunol 184:7071-81.
329. Altenhöfer S, Radermacher KA, Kleikers PW, Wingler K, Schmidt HH. 2015. Evolution of NADPH Oxidase Inhibitors: Selectivity and Mechanisms for Target Engagement. Antioxid Redox Signal 23:406-27.
330. Zahid A, Li B, Kombe AJK, Jin T, Tao J. 2019. Pharmacological Inhibitors of the NLRP3 Inflammasome. Front Immunol 10:2538.
331. Hoss F, Rodriguez-Alcazar JF, Latz E. 2017. Assembly and regulation of ASC specks. Cell Mol Life Sci 74:1211-1229.
332. Decré D, Verdet C, Emirian A, Le Gourrierec T, Petit JC, Offenstadt G, Maury E, Brisse S, Arlet G. 2011. Emerging severe and fatal infections due to *Klebsiella pneumoniae* in two university hospitals in France. J Clin Microbiol 49:3012-4.